ANUL XLIV **1999**

S T U D I A
UNIVERSITATIS BABEŞ-BOLYAI
PHYSICA
2

Editorial Office: 3400 CLUJ-NAPOCA, Gh. Bilaşcu no. 24 ♦ Phone:064-40.53.52

S U M A R - C O N T E N T S

Solid State Physics

Theoretical Physics

Biophysics

STUDIA UNIVERSITATIS BABEŞ-BOLYAI, PHYSICA, XLIV, 2, 1999

EPR AND MAGNETIC SUSCEPTIBILITY INVESTIGATIONS OF IRON CONTAININGTeO_2-B_2O_3-SrF_2 AND TeO_2-B_2O_3-SrO GLASSES

I. ARDELEAN*, M. PETEANU*, V. SIMON*, F. CIORCAS*, R. CICEO-LUCACEL*, S. SIMON*

ABSTRACT. Iron ions were used as probes to explore the structural and magnetic properties of $70TeO_2 \cdot 25B_2O_3 \cdot 5SrF_2$ and $70TeO_2 \cdot 25B_2O_3 \cdot 5SrO$ vitreous matrices. The distribution of Fe^{3+} ions on different structural aggregates was revealed by means of EPR, as depending on Fe_2O_3 concentration. Strongly distorted octahedral sites were detected for the isolated paramagnetic ions, and also clusters of iron ions especially at high Fe_2O_3 content of samples. Magnetic susceptibility measurements evidenced both dipole-dipole and superexchange type interactions involving iron ions. Mixed valence states of iron were also detected. The effects of the network-modifier change (SrF_2 to SrO) on the relative ratio of Fe^{3+} and Fe^{2+} valence states, and the type and strength of interactions involving them, was revealed.

1. Introduction

Structural investigation of glasses performed by means of EPR of transition metal ions may use Fe^{3+} ($3d^5$, $^6S_{5/2}$) ions as paramagnetic probes. There are several site symmetries appropriate to split the ground state level of Fe^{3+} ion into three doublets, the EPR absorption spectra being characterized by the $g \approx 4.3$ resonance line arising from the isotropic transition inside one of the Kramers doublets [1-5]. Resonance lines at $g \approx 2.0$ may also occur, due to ions distributed in clusters which interact by superexchange coupling [6-8].

Useful information about the valence states and interactions involving the iron ions in vitreous systems were obtained by means of magnetic measurements. The temperature dependence of the magnetic susceptibility indicates an antiferromagnetic interaction between iron ions in

* Faculty of Physics, "Babeş-Bolyai" University, 3400 Cluj-Napoca, Romania

phosphate [9, 10] borate [11, 12], lead-tellurite [13] or lead-bismuthate [14] oxide glasses. The presence of both Fe^{2+} and Fe^{3+} ionic species was also evidenced. The antiferromagnetic behaviour depends on the concentration range of iron, the glass matrix structure [15], the preparation conditions [16] and consequently on the Fe^{3+}/Fe^{2+} ratio [17].

Tellurite-borate vitreous systems [18] and binary tellurite oxide systems containing transition metal ions [19] were investigated in detail due to their interesting properties having number of applications in microelectronics. These are optical glasses with high refraction index (n>2) and a good IR transmission, being suitable as laser and opto-acoustical materials. Tellurite systems containing Fe_2O_3 were studied for revealing their electrical properties as well as the structural ones [20-23]. A new vitreous matrix, i.e. $70TeO_2 \cdot 25B_2O_3 \cdot 5SrF_2$, containing Fe_2O_3, was chosen by us to obtain more information on tellurite glass systems. The Te^{4+} ions may be three- or four-fold coordinated by oxygen in function of the matrix composition, by adequate adding of the network-modifier. Besides the non-conventional network-former, TeO_2, used in preparing the studied matrix, SrF_2 as non-conventional network-modifier would confer more structural stability, high density, great polarizability. It is also possible that transition ions, in our case iron ions, enter the matrix in both network-former and network-modifier sites [24, 25] giving the possibility to obtain homogeneous glasses up to high iron ions concentration. Composition change effects upon the iron ions distribution on various structural aggregates and valence states and also upon the type and strength of interactions involving these ions, were studied by replacing SrF_2 with SrO.

This paper aims to present our results concerning iron containing TeO_2-B_2O_3-SrF_2 and TeO_2-B_2O_3-SrO glasses, studied by means of EPR and magnetic susceptibility measurements.

2. Results and discussion

Sample preparation

Two series of glasses, corresponding to the systems $xFe_2O_3 \cdot (100-x)[70TeO_2 \cdot 25B_2O_3 \cdot 5SrF_2]$ and $xFe_2O_3 \cdot (100-x)[70TeO_2 \cdot 25B_2O_3 \cdot 5SrO]$ were prepared by using reagent grade purity compounds: TeO_2, H_3BO_3, SrF_2, SrO and Fe_2O_3. The melting was performed in electric furnace, at 1000^oC, during 10 min. Sintered alumina crucibles were used. The quenching was done at room temperature, by pouring the molten material on stainless-steel plates.

Typical glasses were obtained up to x = 20 mol % Fe_2O_3 for both systems. Their structure was studied by means of X-ray diffraction. Only the

samples whose XRD patterns did not show any crystalline phase were selected for further investigation.

Electron paramagnetic resonance data

EPR measurements were performed at room temperature, using a JEOL-type spectrometer, in the X frequency band and 100 kHz field modulation.

EPR absorption spectra, corresponding to Fe^{3+} paramagnetic ions, were obtained. Their structure mainly consists in resonance lines centered at $g \approx 4.3$ and $g \approx 2.0$ values, and depends on the Fe^{3+} ions concentration (Fig. 1). The evolution of the resonance lines when increasing the iron content of samples was followed by using the concentration dependence of their EPR parameters, namely the peak-to-peak linewidth ΔH and the lineintensity approximated as $I = I \cdot (\Delta H)^2$, where I denotes the height of the

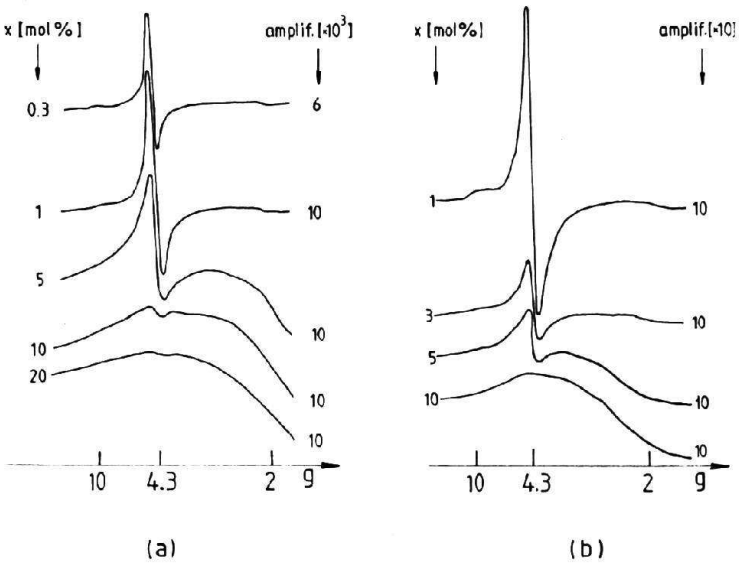

Fig. 1. Concentration dependence of the EPR absorption spectra for: (a) samples of the system with SrF_2; (b) samples of the system with SrO.

The detected EPR absorption spectra (Fig. 1) show resonance lines centered at g ≈ 4.3 and g ≈ 2.0 values, their relative intensity depending on concentration. The line at g ≈ 4.3 is due to Fe^{3+} ions in sites subjected to strong crystal field effects, when the zero field splitting is high enough to avoid transitions between the energy levels of different doublets, so that transitions may be induced only between sublevels inside the doublets. This occurs for ionic vicinities of strongly distorted (tetragonally or rhombically) octahedral symmetry [1-4]. The composition range for which Fe^{3+} ions enter the matrix in such vicinities, i.e. structural units of defined

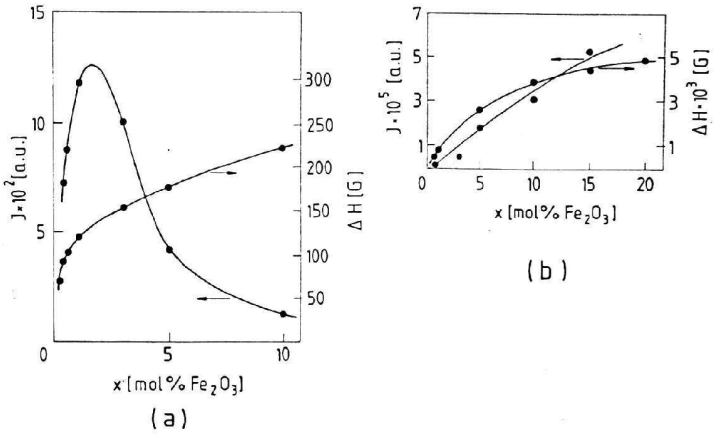

Fig. 2. Concentration dependence of the EPR parameters for: (a) the g ≈ 4.3 resonance line; (b) the g ≈ 2.0 resonance line corresponding to glasses of the system with SrF_2

symmetry, is relatively narrow. According to Figs. 2a and 3a the corresponding line intensity increases up to x ≅ 1 mol % Fe_2O_3 and abruptly decreases thereafter. The linewidth evolution shows the line broadening within 0.3 ≤ x ≤ 10 mol % due to dipole-dipole interactions between the Fe^{3+} ions. For samples containing x > 1 mol % Fe_2O_3 the increasing of ΔH is progressively attenuated due to the diminished number of ions involved in such interactions (see the corresponding lineintensity decreasing).

The resonance lines at g ≈ 2.0 were detected within 1 ≤ x ≤ 20 mol % Fe_2O_3 and may be attributed to Fe^{3+} ions associated in clusters [6-8]. The lineintensity increases with the iron content of sample revealing the high capacity of the investigated matrices to favor iron cluster aggregation. The increasing does not follow linearly the values of x (mol %) (Figs. 2b

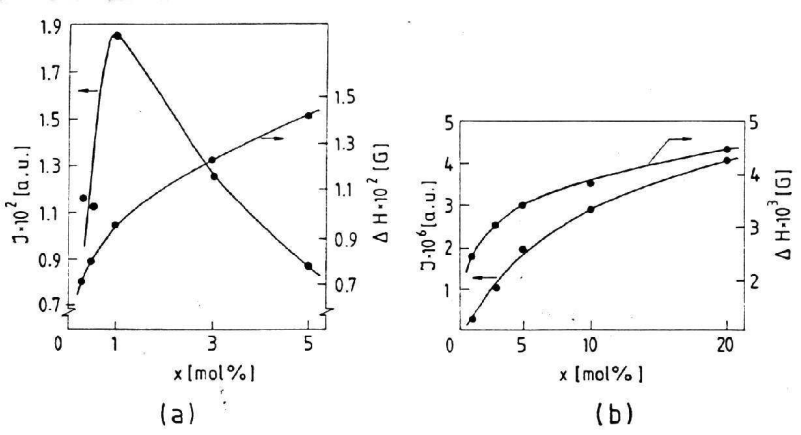

Fig. 3. Concentration dependence of the EPR parameters for: (a) the g ≈ 4.3 resonance line; (b) the g ≈ 2.0 resonance line corresponding to glasses of the system with SrO

and 3b). This suggests another valence states of iron ions, most probably (2+), which also enter the matrix during the doping process. Without giving rise to EPR absorption (at least at room temperature) these ionic species may influence the Fe^{3+} absorption lines when involved in interactions. There are differences in the I = f(x) dependences for glasses of the two systems, revealing changes of the involved Fe^{3+} ions concentration at different stages of doping. The slope change of the curve occurs at about 5 mol % Fe_2O_3 for samples of the system with SrF_2 and it is a more marked one than that corresponding to samples of the system with SrO, where the intensity attenuates only after 10 mol % Fe_2O_3. The width of the g ≈ 2.0 line also depends on concentration. The ΔH = f(x) dependence reflects the competition between the broadening mechanisms (dipole-dipole interactions, interactions between ions in multivalent states, the increased disordering of the matrix structure) and the narrowing ones (superexchange interactions). The prevalence of one type of mechanism or another is function of the iron content of the sample.

EPR absorption data reflect the structural changes in the investigated vitreous matrices when increasing the iron content. At low Fe_2O_3 concentration there are structural aggregates of well defined symmetry, involving Fe^{3+} as isolated ions, interacting only by means of dipole-dipole mechanisms. The short concentration range where the g ≈ 4.3 absorptions were detected proves the reduced capacity of the vitreous

system in accepting Fe^{3+} in structural units of a certain symmetry, due to its peculiar structure [27, 28]. In tellurite glasses Fe^{3+} was already detected as involved in almost planar distorted tetrahedra, the site symmetry being sufficiently low to explain the $g \approx 4.3$ absorptions [28]. The site symmetry is not stable when iron accumulates in the matrix and for $x > 1$ mol % Fe_2O_3 cluster formation is favored and progressively concern all iron ions further entering the matrix. Being involved in the TeO_2 "sublattice" of the glass, the isolated Fe^{3+} ions seem to be not affected by the $SrF_2 \rightarrow SrO$ substitution, whereas those implied in clusters are more vulnerable.

Magnetic susceptibility data

Magnetic susceptibility measurements where performed using a Faraday-type balance in the 80-300 K temperature range. For a correct estimation of the magnetic susceptibility values, corrections due to the diamagnetism of samples were taken into account.

The temperature dependence of the reciprocal magnetic susceptibility of samples is given in Fig. 4. Samples of system with SrF_2

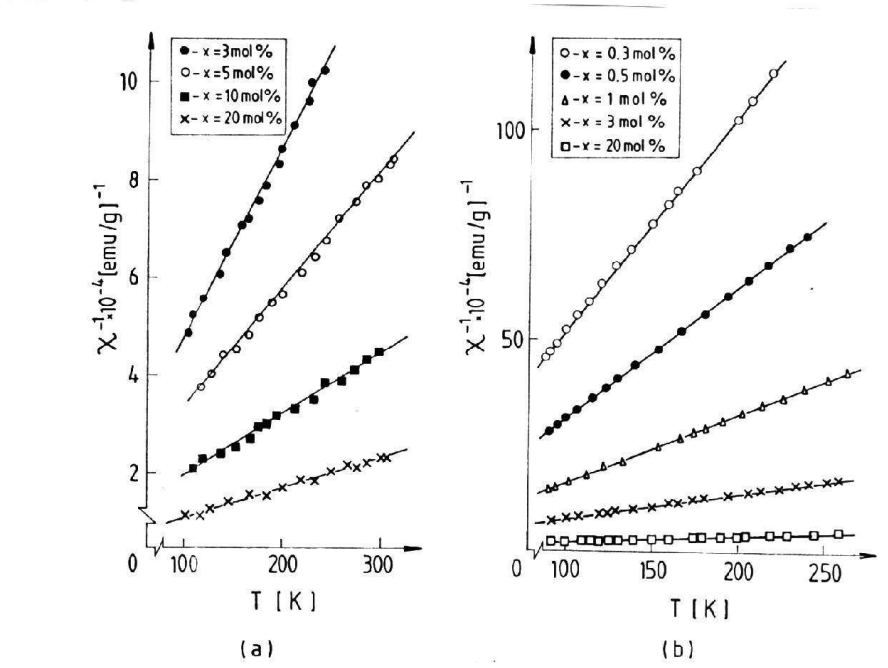

Fig. 4. Temperature dependence of the reciprocal magnetic susceptibility corresponding (a) to samples of system with SrF_2; (b) to glasses of system with SrO.

containing $x \leq 3$ mol % Fe_2O_3 show a Curie-type behaviour. For $x > 3$ mol % Fe_2O_3 a Curie-Weiss type behaviour, with negative paramagnetic Curie temperature, θ_p, was revealed. The absolute values of θ_p increase when increases the iron content of samples.

Samples of system with SrO show this change of behaviour at concentrations of about 1 mol % Fe_2O_3. By using the $1/\chi = f(T)$ dependences the values of the molar Curie constant were estimated. For samples of both systems these values increase with the Fe_2O_3 content.

For samples where the experimental values of the molar Curie constant, C_M, and the effective magnetic moment estimated as $\mu_{exp} = 2.827 (C_M/2x)^{1/2}$ per iron ion, were lower than the expected ones assuming that all iron ions are in Fe^{3+} valence state and higher than those characteristic for Fe^{2+} ions, we suppose both Fe^{2+} and Fe^{3+} ions to be present. In paramagnetic salts and glasses [26] the magnetic moment values of iron ions are very close to those corresponding to the free ion states: $\mu_{Fe^{3+}} = 5.90\mu_B$; $\mu_{Fe^{2+}} = 4.92\mu_B$. Consequently, the molar fractions of these ions were estimated, in first approximation, as result of:

$$\begin{cases} x(\mu_{exp})^2 = x_1(\mu_{Fe^{3+}})^2 + x_2(\mu_{Fe^{2+}})^2 \\ x = x_1 + x_2 \end{cases}$$

where x is the iron content of the sample, and x_1, x_2 represent the molar fractions of Fe^{3+} and Fe^{2+} ions, respectively. The obtained values are given in Table 1.

The magnetic susceptibility data agree well with the EPR results and complete them. Thus for samples of system with SrF_2 with $x \leq 3$ mol % Fe_2O_3 the temperature dependence of the reciprocal magnetic susceptibility show a Curie-type behaviour (Fig. 4a), characteristic for isolated ions, involved only in dipolar interactions. For concentration $x > 3$ mol % Fe_2O_3 the behaviour is of a Curie-Weiss type, with negative paramagnetic temperature θ_p, suggesting antiferromagnetically coupled ions by means of superexchange interactions. These interactions are narrowing mechanisms of the EPR absorption line and explain the slope change of the $\Delta H = f(x)$ curve (Fig. 2b) at about x = 3 mol % and the further attenuation of the ΔH values of $g \approx 2.0$ resonance line. For samples of system with SrO the change of behaviour in the $1/\chi = f(T)$ dependence occurs at lower concentrations, at about x = 1 mol % Fe_2O_3 (Fig. 4b). Consequently, the resonance line due to clusters of iron ions, at $g \approx 2.0$, show a slower increasing of ΔH (Fig. 3b) than those corresponding to samples of system with SrF_2 due to the superexchange narrowing effects which act earlier than in the previously considered system.

In glasses there is short-range structural ordering. Therefore interactions have a local impact, and a mictomagnetic type ordering may take place [29].

The progressive accumulation of Fe^{2+} ions in the matrix during the increase of iron content may explain the I = f(x) dependences in Figs. 2b and 3b because the EPR absorption is due only to Fe^{3+} species. According to the estimated values of molar fractions of Fe^{3+} and Fe^{2+} ions (Table 1), these values increase for both iron valence states when the Fe_2O_3 content of samples increases, but the concentration range involving Fe^{3+} ions as prevailing species is different in the two

Table 1. Molar fractions of Fe^{3+} and Fe^{2+} ions in glasses of the systems Fe_2O_3-TeO_2-B_2O_3-SrF_2 and Fe_2O_3-TeO_2-B_2O_3-SrO

x [mol %]	system with SrF_2		system with SrO	
	x_1 [mol % $Fe_2^{3+}O_3$]	x_2 [mol % $Fe_2^{2+}O_3$]	x_1 [mol % $Fe_2^{3+}O_3$]	x_2 [mol % $Fe_2^{2+}O_3$]
0.3	0.2	0.1	0.30	-
0.5	0.32	0.18	0.50	-
1.0	0.6	0.4	0.83	0.13
3.0	1.6	1.4	2.20	0.80
5.0	2.4	2.6	3.20	1.80
10	3.9	6.1	4.70	5.30
20	7.3	12.7	7.00	13.0

investigated systems. In samples of system with SrF_2 the x_1 exceed the x_2 values for concentrations up to 3 mol % Fe_2O_3 whereas in samples of system with SrO the Fe^{3+} ions change their part as preponderant species as about 10 mol % Fe_2O_3. The composition of matrix with SrF_2 is more favorable to Fe^{2+} ions concentration increasing than that of matrix with SrO and consequently, the intensity of the $g \approx 2.0$ resonance line achieves its increasing at lower concentrations in samples of system with SrF_2 than those corresponding to system with SrO.

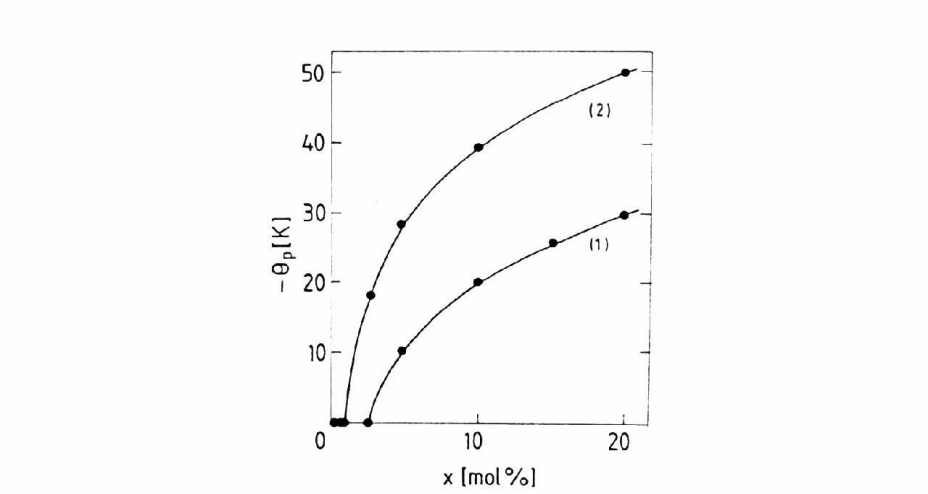

Fig. 5. Concentration dependence of the paramagnetic Curie temperature, for samples of systems with SrF_2 and with SrO.

According to Fig. 5 the paramagnetic Curie temperature absolute values increase with the iron content increasing. This behaviour results as effect of intensifying the magnetic interactions involving iron ions. For samples of system with SrF_2 the $|\theta_p|$ values increase for x > 3 mol Fe_2O_3 up to 30 K, whereas the samples of system with SrO show an increasing of the absolute values of paramagnetic Curie temperature for x > 1 mol % Fe_2O_3 up to 50 K. Samples of system with SrO more rich in Fe^{3+} ions, show superexchange-type interactions within a larger concentration range than those of system with SrF_2, and also stronger interactions than the corresponding ones in the system with SrF_2.

As result of these data we may consider the magnetic properties of the investigated systems as being the result of interactions involving both Fe^{3+} and Fe^{2+} ions. These may occur within the simple pairs of ions: Fe^{3+} - Fe^{3+}; Fe^{2+} - Fe^{2+}, and also in the mixed pairs, Fe^{3+} - Fe^{2+}. Interactions between ions in mixed valence states are broadening mechanisms of the EPR absorption line, while the superexchange interactions between ions of the same valence state are narrowing mechanisms. Consequently the linewidth, ΔH, of the $g \approx 2.0$ resonance line is a result of both types of interactions, acting simultaneously but having various prevalence in function of the Fe_2O_3 concentration.

3. Conclusions

Homogeneous, stable glasses of the systems $xFe_2O_3 \cdot (100-x)[70TeO_2 \cdot 25B_2O_3 \cdot 5SrF_2]$ and $xFe_2O_3 \cdot (100-x)[70TeO_2 \cdot 25B_2O_3 \cdot 5SrO]$ were obtained up to x = 20 mol %.

For all the investigated glasses, EPR absorption spectra due to Fe^{3+} ($3d^5$; $^6S_{5/2}$) paramagnetic ions, were detected. The structure of the EPR spectra significantly depends on the Fe^{3+} ions concentration of the sample. As rising concentration, structural changes from isolated ions in sites of strongly distorted octahedral symmetry to ions which participate to dipole-dipole interactions and those associated in clusters, were evidenced. Cluster aggregates become progressively preponderant in glasses of the system with SrF_2 containing $x > 3$ mol % Fe_2O_3 and $x \geq 1$ mol % Fe_2O_3 in glasses of system with SrO.

The type of interactions involving iron ions and their valence states were determined by means of magnetic susceptibility measurements. For samples of system with SrF_2 containing $x \leq 3$ mol % Fe_2O_3 the dipole-dipole type interactions are characteristic, while for $x > 3$ mol % Fe_2O_3 antiferromagnetically coupled pairs of ions, connected by means of superexchange type interactions were detected. In samples of system with SrO this change of behaviour was revealed at about 1 mol % Fe_2O_3. Mixed valence states of ions were revealed by the evolution of the EPR parameters of absorption lines when increasing concentration, and also by magnetic measurements data. Fe^{2+} ionic species simultaneously present with the Fe^{3+} ones explain the magnetic properties of the investigated glasses as being due to interactions of ions connected in Fe^{3+} - Fe^{3+}; Fe^{2+} - Fe^{2+} and Fe^{3+} - Fe^{2+} pairs, inside the clusters. The matrix of system with SrF_2 is more favorable to Fe^{2+} ions accumulation during samples preparation. The matrix of system with SrO favors the Fe^{3+} ions formation, clusters rise at lower concentrations of Fe_2O_3 and the interactions between ions are stronger than those corresponding to system with SrF_2.

REFERENCES

1. H. H. Wickman, M. P. Klein and D. A. Shirley, J. Chem. Phys. 42, 2113 (1965).
2. D. Loveridge and S. Parke, Phys. Chem. Glasses 12, 19 (1971).
3. M. Ya. Shcherbakova and V. E. Istomin, Phys. Stat. Solidi (b) 67, 461 (1975).
4. V. Cerny, B. Petrova and M. Fumar, J. Non-Cryst. Solids 125, 17 (1990).
5. J. L. Rao, A. Muraly and E. D. Rao, J. Non-Cryst. Solids 202, 215 (1996).
6. D. W. Moon, M. J. M. Aitken, R. K. McCrone and G. S. Cieloszky, Phys. Chem. Glasses 16, 91 (1975).
7. E. Burzo and I. Ardelean, Phys. Status Solidi (b) 87, K137 (1978).
8. M. Peteanu, L. Cociu and I. Ardelean, J. Mat. Sci. Technol. 10, 97 (1994).
9. L. K. Wilson, E. J. Friebele and D. L. Kinser, Proc. Int. Symp. Amorphous Magnetism, Plenum Press, New York, 1975, p. 65.
10. B. Kumar and C. H. Chen, J. Appl. Phys. 75, 6760 (1994).
11. E. Burzo and I. Ardelean, Phys. Chem. Glasses 20, 15 (1979).
12. I. Ardelean, Gh. Ilonca, O. Cozar and Gh. Muresan, Studia Univ. Babes-Bolyai, Physica 2, 37 (1989).
13. I. Ardelean, Gh. Ilonca, M. Peteanu and I. Luca, Studia Univ. Babes-Bolyai, Physica 1, 65 (1979).
14. I. Ardelean, Gh. Ilonca, O. Cozar, V. Simon, and S. Filip, Mat. Lett. 21, 321 (1994).
15. E. Burzo, I. Ardelean and I. Ursu, J. Mat. Sci. 15, 5781 (1980).
16. E. Burzo, I. Ursu, D. Ungur and I. Ardelean, Mat. Res. Bull. 15, 1273 (1980).
17. B. Kumar, C. H. Chen and S. Liu, Phys. Chem. Glasses, 38, 45 (1992).
18. M. A. Bursukova, E. P. Kashchieva and Y. B. Dimitriev, J. Non-Cryst. Solids 192-193, 40 (1995).
19. V. S. Kozhoukharov, M. P. Marinov and G. Grigorova, J. Non-Cryst. Solids 28, 429 (1978).
20. V. S. Kozhoukharov and M. P. Marinov, Compt. Rend. Akad. Bulg. Sci. 26, 343 (1973).
21. I. Ardelean, M. Peteanu, V. Simon and F. Ciorcas, Studia Univ. Babes-Bolyai, Physica XLII with SrO, 3 (1997).
22. I. Ardelean, M. Peteanu, S. Filip, V. Simon and G. Györffy, Solid State Commun. 102 (4), 341 (1997).
23. Hong-Hua Qui, H. Mori, H. Sakata and T. Hirayama, J. Ceram. Soc. Jpn. 103, 32 (1995).
24. D. L. Griscom, Glass Science and Technology 48, 151 (1990).
25. P. J. Bray and A. H. Silver, Modern Aspects of the Vitreous State, vol. I, Butterworth, London 1960.

STUDIA UNIVERSITATIS BABEŞ-BOLYAI, PHYSICA, XLIV, 2, 1999

ROLE OF DEFECTS AND SUBSTITUTIONS ON SOME PHYSICAL PROPERTIES OF COMPLEX LEAD-PEROVSKITES CERAMICS, $Pb_2B'B''O_6$

I. BARBUR*, I. ARDELEAN*, A. VERES*, V. TIMAR*, G. BORODI**

ABSTRACT. In this contribution, the influence of defects created in Pb_2MgWO_6 by preparation conditions or by gamma irradiation on structural, electric and magnetic properties are presented. Also, the role of substitutions on some physical properties in $Pb_2B'WO_6$ (B' = Mg, Mn, Fe, Cd, Co, Zn, Ni, Cu) is discussed.

INTRODUCTION

Lead perovskites of the general composition $Pb_2B'B''O_6$ (B': Mg, Zn, Ni, Fe, Mn, B'': W, Nb, Ta, Mo) are characterized by very good dielectric and electrostrictive properties [1], and form a large groups of compounds possessing either ferroelectric (FE) or antiferroelectric (AFE) phase transitions.

Lead magnesium tungstate (Pb_2MgWO_6), hereafter designated PMW is a compound of $A_2^{2+}B^{2+}W^{6+}O_3$ type with B-site ordered perovskite-type structure, in which the two kinds of ions (Mg^{2}_{+} and W^{6+}) regularly occupy octahedral positions [2]. The dielectric properties of PMW have been widely investigated in both the single-crystal and ceramic forms [3]. The main feature of the dielectric properties of PMW, common to all of the above compounds was a broad maximum of the dielectric constant. At around 38^oC PMW undergoes a phase transition, from the rhombic paraelectric to the orthorhombic antiferroelectric state with a well-defined superstructure [4]. In all compounds of $A_2^{2+}B^{2+}B^{6+}O_6$-type an ordered distribution of the B^{2+} and B^{6+} ions is observed when a large difference exists in either charges or ionic radii [5].

* "Babes-Bolyai" University, Faculty of Physics, Cluj-Napoca, Romania
** Institute of Isotopic and Molecular Technologies, 3400 Cluj-Napoca, Romania

In the present work, the influence of defects created in PMW by preparation conditions or by gamma irradiation and also the role of substitution on the structural, electric and magnetic properties is studied.

EXPERIMENTAL

The polycrystalline samples of Pb_2MgWO_6, $Pb_2Mg_{1-X}Mn_XWO_6$, $Pb_2Mg_{1-X}Fe_XWO_6$ and $Pb_2MgW_{1-X}V_XO_6$, were prepared by reacting corresponding stoechiometric proportions of PbO, H_2WO_4, $Mg(NO_3)_2 \cdot 6H_2O$, $MnCO_3$, Fe_2O_3 and V_2O_5. The mixture was calcinated at 700^{o}C for 4 hours and sintered at 1000^{o}C for 2 hours. All the samples were prepared in air. The EPR spectra were recorded using a modified JEOL-type spectrometer in X-band (9. 4 GHz) and 100 KHz field modulation. The dielectric permitivity was measured in the temperature range 300-400 K at 1 KHz using a digital automatic bridge. The magnetic susceptibility measurements were realized using a Faraday-type balance in the temperature range 80-300 K.

1. RESULTS AND DISCUSSION

a). Paramagnetic centers in Pb_2MgWO_6. Using electron paramagnetic resonance (EPR) method, a paramagnetic center was detected in PMW [6]. The preparation conditions of the samples created by air atmosphere and high temperature may lead to the change of valence of the component ions associated with oxygen diffusion in the sample, and the creation of oxygen vacancies, which are stabilized mainly in the form of F-centers.

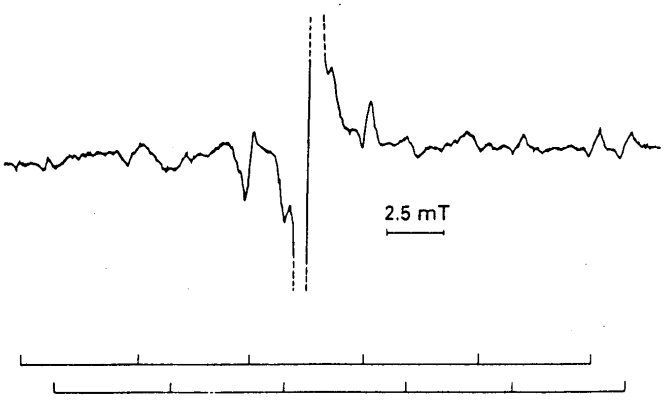

Fig. 1. The EPR spectrum detected in PMW sample.

The EPR spectrum of such center detected in PMW consists of a central intense narrow line centered at g = 1. 9818 and two sextets of small lines equally spaced and not so well resolved (Fig. 1). The central line of the EPR spectrum can be described as due to a system with S = ½ and g-factor of
1. 9818±0. 004. The two sextets are due to the isotropic hyperfine interactions of the unpaired electron with a nucleus of spin 5/2 in two non-equivalent positions. Only one nucleus (^{25}Mg) in PMW has I = 5/2. So, magnesium ions are involved in our paramagnetic center. The measured valence of the hyperfine interaction constant was A = 147 MHz, which is appropriate to the value typical for Mg^{+} (100 MHz). Since magnesium enters PMW as Mg^{2+} ion, we can conclude that in our case the preparation conditions of the samples may lead to the change of valence of the Mg ion associated with oxygen diffusion in the samples. A similar defect was detected in X-irradiated CaO [7] and recently in MgO [8].

b). Influence of gamma irradiation on structural and electric properties of PMW. The PMW samples were irradiated in air, at room temperature with a dose of 32Gy/hour from a ^{60}Co-gamma source. The X-ray diffraction measurements were performed on a DRON-2 – type diffractometer using a CrK_{α} radiation.

The X-ray diffraction for unirradiated PMW (Fig. 2a) confirm earlier tetragonal structure having the cell parameters: a = c = (16. 08±0. 01) Å, b = (15. 88±0. 01) Å and $\beta = 90^{o}$ [9]. The most intense diffraction lines are indexed as single perovskite structure, and lines of lower intensity as suprastructure lines [10].

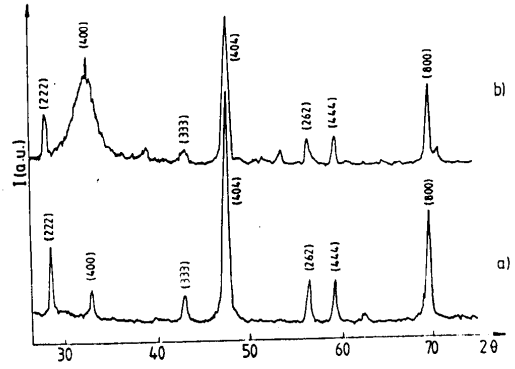

Fig. 2. The X-ray diffraction patterns for unirradiated (a) and irradiated (b), PMW samples.

For irradiated PMW sample the diffraction lines are similar to that of unirradiated one, but the (400) Bragg reflection is very broadening (Fig, 2b). Such behaviour can be explained by decreasing of domain size, as a consequence of gamma irradiation and also may be connected with unisotropic displacement of atoms parallel to cell axis and the presence of the antiphase domain [11].

The gamma irradiation influences the temperature dependence of the dielectric constant [12]. For unirradiated PMW sample, a dielectric anomaly at 38°C related to antiferroelectric transition is observed [Fig. 3].

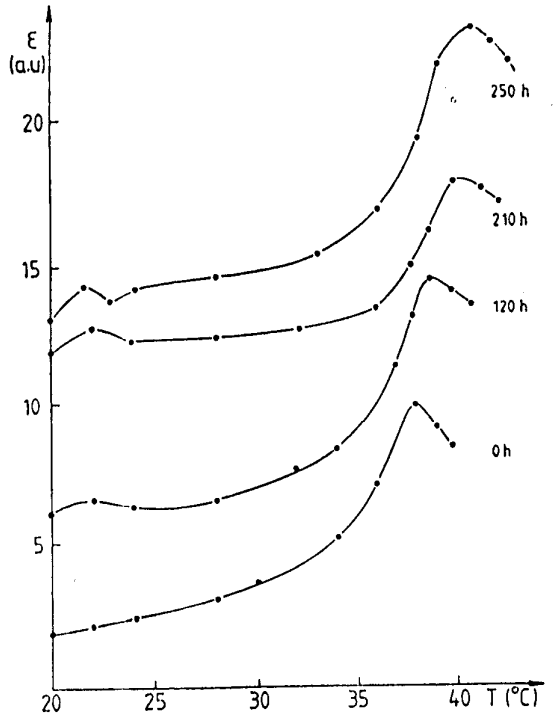

Fig. 3. The temperature dependence of the dielectric constant for different gamma-dose (time of exposure).

As the gamma-dose increases (time of exposure) transition becomes more diffuse and a small increases of the transition temperature is observed (Fig. 4). Also, a small anomaly can be noticed at about 22°C.

The above observations can be explained taking into account that gamma irradiation of PMW produces damage center which introduce a lattice strain. When the strain reaches a critical level the domains are subdivided into smaller domains [11]. This assumption is consistent with the broadening of (400) Bragg reflection observed by us in X-ray diffraction measurements.

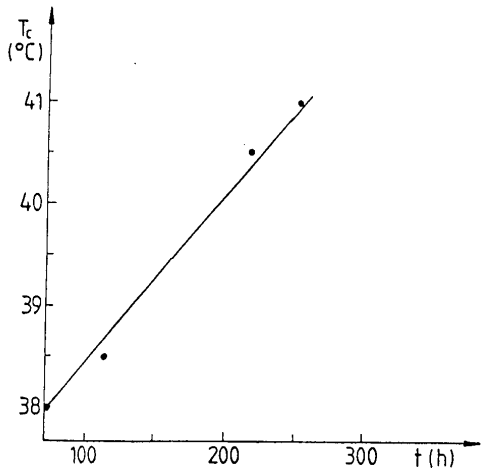

Fig. 4. T_c versus gamma-dose (time of expose) for PMW sample.

c). Substitution influence on structure and dielectric properties of $Pb_2B'B''O_6$ complex perovskites. By Mn and Fe substitution for Mg in Pb_2MgWO_6 compound, a change in lattice parameters is observed. With Mn content increases in $Pb_2Mg_{1-X}Mn_XWO_6$ a small increases of the lattice parameters take place. This phenomenon can be explained by the difference in the ionic radii of Mn^{2+} and Mg^{2+}. $\left[R_{(Mn^{2+})} = 0.080\ \text{nm}\right]$, $\left[R_{(Mg^{2+})} = 0.063\ \text{nm}\right]$.

For $Pb_2Mg_{1-X}Fe_XWO_6$ samples the intensity of the lines decreases with increases of x as a consequence of the increases of the lattice defects.

For both substitution, the a, c and b lattice parameters become closer in value with increases of x.

Dielectric anomaly at T_c (38^oC) related to antiferroelectric transition in Pb_2MgWO_6 is affected by Mn or Fe substitution for Mg. Addition of Mn increases T_c up to 150^oC which is the transition temperature for Pb_2MnWO_6 (Fig. 4). The Curie temperature increases linearly with Mn contents, and

this behaviour is a common property for complex systems that involve a ferroelectric or antiferroelectric transition [5].

The temperature dependence of the dielectric constant for $Pb_2Mg_{1-x}Fe_xWO_6$ ($0 < x \leq 0.1$) is shown in Fig. 5. As it is seen from Fig. 5, the T_c decreases when the concentration of Fe increases. For Pb_2FeWO_6 the transition temperature is -75^oC [5].

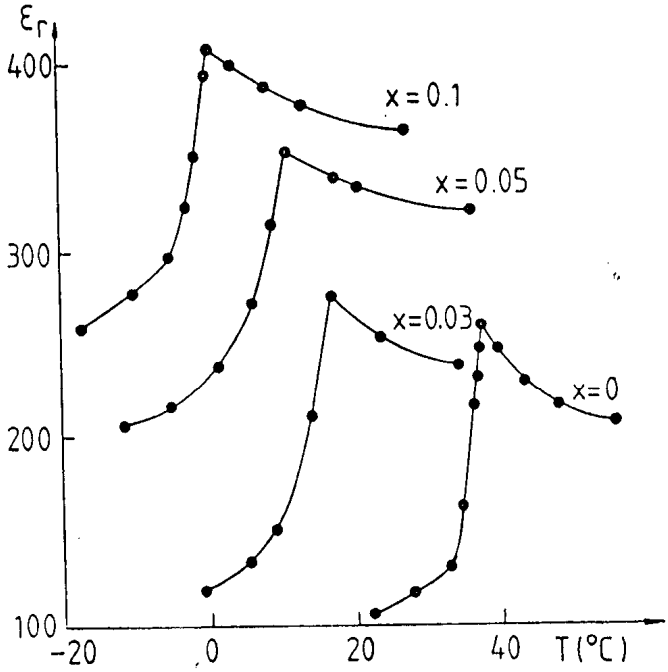

Fig. 5. Dielectric constant versus temperature for different x in $Pb_2Mg_{1-x}Fe_xWO_6$

Our results and those obtained by other authors indicate that existence of superstructure and antiferroelectric or ferroelectric transition in $Pb_2B'WO_6$ perovskite family depend on some characteristics of B' ions.

The Table 1 contents some physical data for $Pb_2B'WO_6$ family (B' = Mg, Cd, Zn, Mn, Na, Fe, Cu); transition temperature - T_c; antiferroelectric (AFE), or ferroelectric (FE) transition, ionic radii of B' ion – $R_{B'}$ and unit cell edge a', a cubic cell which represent the same volume allowed in the unit cell for a molecule.

Table 1. Some physical data for $Pb_2B'WO_6$ family of compounds

B'	Tc (^oC)	Transition	$R_{B'}$ (Å)	a' (Å)
Mg^{2+}	38	AFE	0. 74	4. 05
Cd^{2+}	420	AFE	0. 97	4. 133
Co^{2+}	32	AFE	0. 73	3. 999
Zn^{2+}	130	AFE	0. 74	
Mn^{2+}	150	AFE	0. 80	4. 052
Ni^{2+}	17	AFE	0. 69	
Fe^{2+}	7	AFE?	0. 63	4. 015
Mn^{2+}			0. 67	4. 052
Cu^{2+}		?	0. 72	4. 04

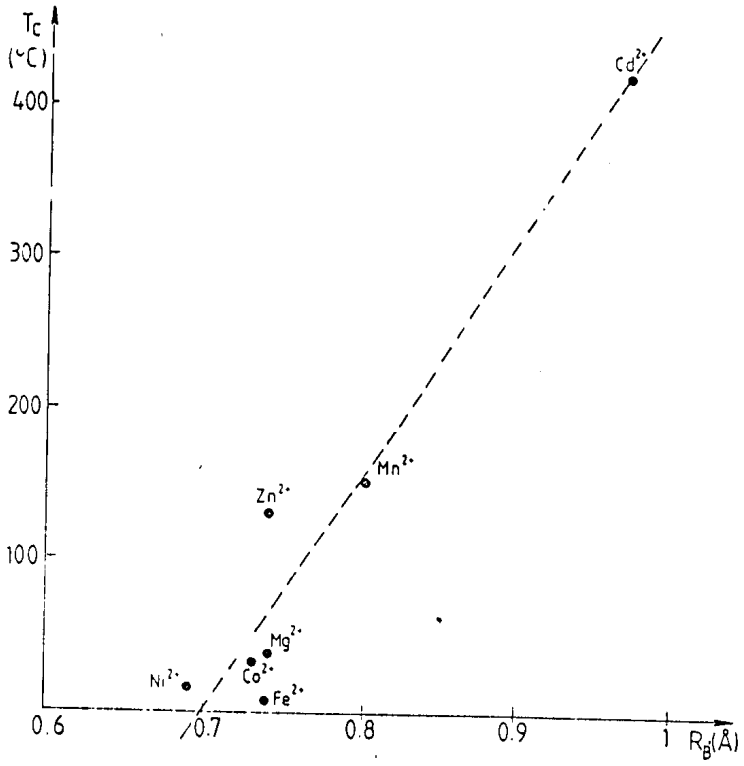

Fig. 6. T_c versus $R_{B'}$ for $Pb_2B'WO_6$ family.

As is it seems from Table 1, the transition temperature T_c depends on ionic radii $R_{B'}$. Fig. 6 shows the dependence of T_c on ionic radii of B', for B" = Mg^{2+}, Cd^{2+}, Co^{2+}, Zn^{2+}, Mn^{2+}, Ni^{2+}, Fe^{2+}, Mn^{3+} and Cu^{2+}. It may be noticed, that T_c depends linear on $R_{B'}$.

The deviation from linearity for Zn^{2+}, Ni^{2+} and Fe^{2+} ions may be due to the existence of small amount of Zn^{1+}, Ni^{3+} and Fe^{3+} in sample composition. Our EPR measurements confirm existence of Fe^{3+} in $Pb_2Mg_{1-x}Fe_xWO_6$ samples.

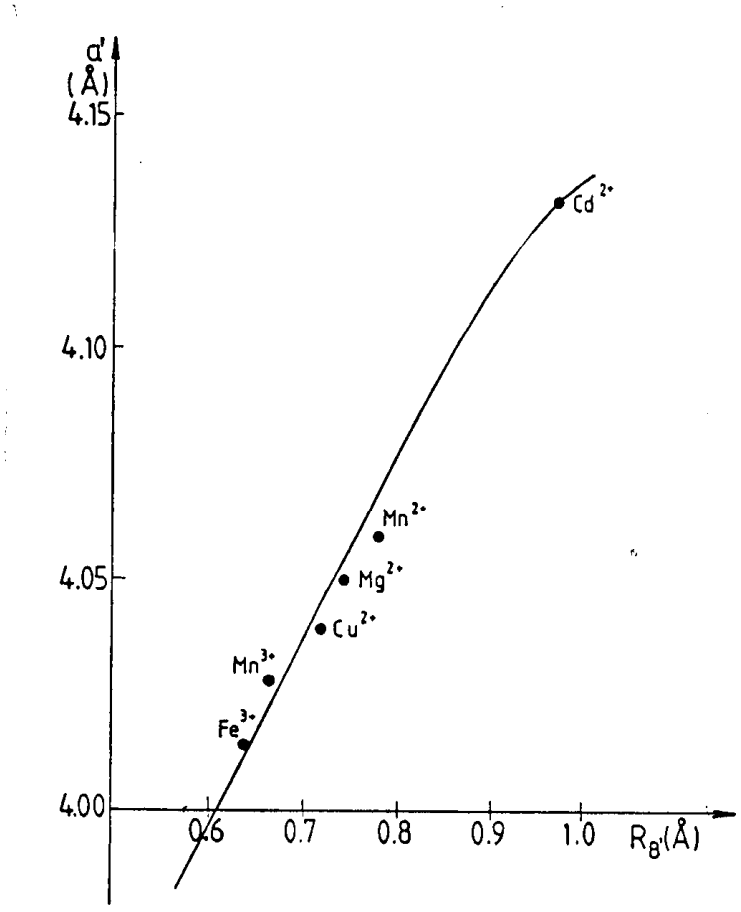

Fig. 7. The unit cell edge a' versus $R_{B'}$ for $Pb_2B'WO_6$ family.

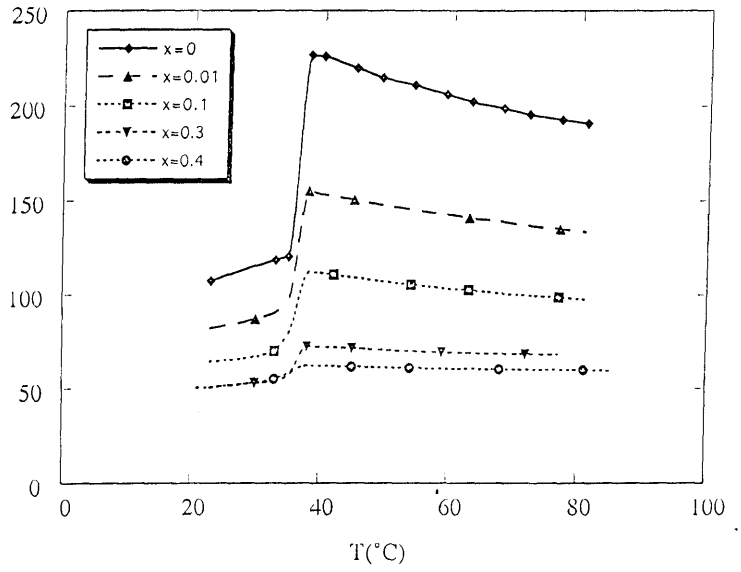

Fig. 8. Dielectric constant ε versus temperature for different x in $Pb_2MgW_{1-x}V_xO_6$.

The influence of the ionic radii of B' ion on symmetry and existence of superstructure is more evidenced by the dependence of a' (a'= $\sqrt[3]{V_o}$) on ionic radii $R_{B'}$ (Fig. 7). The deviation from linearity of this dependence for large value of $R_{B'}$ (Cd^{2+}) may be due to the appearance of a parasitic pyroclore phase for large $R_{B'}$, phenomenon which is more evidenced in case of $Ba_2B'B''O_6$ and $SrB'B''O_6$ families of compounds [13].

It is interesting to notice the influence of B'' substitution in $Pb_2B'B''O_6$ compound. For this purpose we have performed structural and dielectric measurements on $Pb_2MgW_{1-X}V_XO_6$ compound (PMWV) [14]. The antiferroelectricity and B site ordering is proved for $0 \leq x \leq 0.4$ but a decreases of the intensity of the X-ray diffraction lines with increases of x is observed. Also a broadening of the lines is noticed as a consequence of the increases of the lattice defects.

Addition of vanadium not affects the antiferroelectric temperature (Fig. 8). However, with increases of the vanadium content, transition Becomes more diffuse due to the, crystallite-size modification and increases of the lattice defects.

CONCLUSIONS

Using EPR method, a paramagnetic center was detected in Pb_2MgWO_6 as a consequence of preparation condition of the samples.

Gamma irradiation of the Pb_2MgWO_6 sample leads to broadening of (400) Bragg reflection line and increases antiferroelectric transition temperature with increases of gamma dose.

The effect of Mn and Fe substitution for Mg in Pb_2MgWO_6 is decreases of the intensity of diffraction lines and lattice parameters become closer in value. The T_c shifts upward (for Mn addition and downward (for Fe addition).

The antiferroelectric transition temperature depends linearly on ionic radii, $R_{B'}$ in Pb_2MgWO_6 family. Also, a linear increasing of the unit cell edge a' with ionic radii $R_{B'}$ is observed.

REFERENCES

1. T. R. Shrout, A. Hallyial, Am. Ceram. Soc. Bull. 66, 704 (1987)
2. G. A. Smolenskii, A. I. Agranovskaia, V. A. Isupov, Fiz. Tverd. Tela 1, 990 (1959).
3. N. N. Krainik, A. I. Agranovskaia, Fiz. Tverd. Tela 2, 70 (196O).
4. A. I. Zaslavskii, M. F. Bruzhina, Sov. Phys. Crystallogr. 7, 709 (1962).
5. F. S. Galasso, Perovskites and high T_c –superconductors (Gordon and Breach, New York, 1990).
6. I. Barbur, I. Ardelean, J. Mat. Sci. Lett. 12, 1747 (1993).
7. V. M. Orera, M. L. Sanjnan, P. J. Alonso, J. Phys. C: Solid. St. Phys. 19, 4763 (1986).
8. A. S. Novick, MRS Bull. 38 (Nov. 1991).
9. I. Barbur, I. Ardelean, G. Borodi, A. Veres, Mater. Lett. 28, 175 (1996).
10. W. K. Chao, H. J. Kim, J. H. Yung et al. , Jpn. J. Appl. Phys. 32, 4249 (1993).
11. A. I. Burkhanov, A. V. Shilnikov, S. U. Shishlov, Ferroelectrics 186, 145 (1996).
12. I. Barbur, I. Ardelean, G. Borodi, A. Veres, In press to Ferroelectrics Letters, vol. 26, No. 3/4, 1999.
13. E. G. Fesenko, V. S. Filipyev, M. F. Kupriyanov, Izv. Akad. Nauk, SSSR, Ser. Phys. 28, 669 (1964).
14. I. Barbur, I. Ardelean, Gh. Borodi, A. Veres, V. Timar, Ferroelectric Letters 23, 69 (1997).

MAGNETIC BEHAVIOUR OF COBALT IN PSEUDOBINARY RARE-EARTH COMPOUNDS

E. BURZO*

ABSTRACT. Magnetic measurements were performed on $Dy_xZr_{1-x}Co_2$ compounds in the temperature range 4.2 - 700 K and external fields up to 7T. $ZrCo_2$ shows a nearly temperature independent paramagnetism. For $x \geq 0.2$ the compounds are ferrimagnetically ordered. The cobalt moments at 4.2 K are strongly dependent on composition. As a function of exchange field a metamagnetic transition of cobalt moments is evidenced at $H_{exch} \cong 60$ T. The effective moments are little dependent on composition. The magnetic behaviour of cobalt in analysed in spin fluctuation model.

1. Introduction

The RCo_2 compounds, where R is a rare-earth, Y or Zr, crystall cubic C15 - type structure. In this lattice the R and Co atoms occu only one type of site. Since of high symmetry of lattice, the study e compounds may give useful information on the magnetic behavi nstituent atoms [1].

Previously, the magnetic behaviour of $DyCo_2$ [2,3] and $ZrCo_2$ pounds was analysed in a large temperature range. The magne eptibility of $ZrCo_2$ increases slightly up to ~ 90 K and then decrease om temperature. The χ values do not change in the temperature ran - 600 K and then increase slowly up to 800 K. The changes in χ valu relatively small and of the order of 10 %. The $DyCo_2$ compound i magnet. The cobalt moment determined at 4.2 K is $M_{Co} \cong 1\mu_B$. er temperatures than 450 K, the reciprocal susceptibilities follow r temperature dependence. The effective cobalt moment determin

= 9 - 10), at T < 15 K, follows a T^2 dependence. The χ values increa
have maxima at a temperature T_{max} and then decrease. For T > T*
T* is a characteristic temperature, Curie - Weiss type dependence
shown. The effective cobalt moments are close to that of Co
considering only spin contribution. This behaviour is typical for a
which shows spin fluctuations. In case of $ZrCo_2$, as above mentione
the incipient features of spin fluctuation type behaviour can be s
evidenced by a small maximum and a decrease of χ values up to
These features can be correlated with a smaller Stoner ex
enhancement factor (s = 5 - 6) as compared to YCo_2 or $LuCo_2$.

When Zr is gradually substituted by a magnetic rare - ea
exchange interactions will increase and it is expected that the m
behaviour of cobalt will be changed both in ordered and param
state. In order to analyse this matter we studied $Dy_XZr_{1-X}Co_2$ syste

Experimental

The $Dy_XZr_{1-X}Co_2$ compounds were prepared by induction
of constituent elements in water cooled copper boat in purifie
atmosphere. Then, the samples were thermally treated for ten days
C and rapidly cooled. The X - ray analysis shows the presence of o
phase. The composition dependence of the lattice parameters
approximately a Vegard type law - Table 1.

Table 1. Magnetic properties of $Dy_XZr_{1-X}Co_2$

Composition (x)	1.0	0.8	0.7	0.6	0.4
Lattice constant (Å)	7.195	7.140	7.120	7.104	7.017
Saturation magnetization at 4.2 K (μ_B/f.u.)	6.80	5.34	4.96	4.50	2.80
Curie constant, C (emuK/f.u.)	16.28	13.20	11.92	10.40	7.70
M_{eff}(μ_B/Co atom)	3.02	2.83	2.92	2.83	2.91
Curie temperature, T_C (K)	135	113.2	85	56.5	40

00 K and fields up to 7 T. The spontaneous magnetizations, etermined from magnetization isotherms according to approach ion law $M = M_S (1-a/H) + \chi_0 H$. We denoted by χ_0 a field independ tibility and a is the coefficient of magnetic hardness. In agnetic range, the magnetic susceptibilities, χ, were determined fr eld dependencies according to the relation $\chi_m = \chi + c\, M_S/H$, olating the measured values χ_m to $H^{-1} \rightarrow 0$ [6]. By c is denote ned impurity content and M_S is the saturation magnetization y. By this method any possible alteration of magnetic susceptib sult of the presence of small quantities of magnetic ordered phase , is avoided. For all compounds the estimated impurity conten is smaller than 0.1 %.

Experimental results

The thermal variations of spontaneous magnetizations are plotte

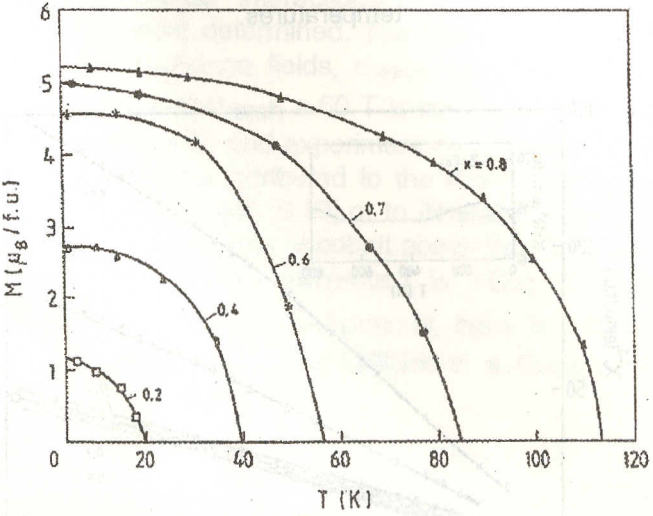

Fig.1. Thermal variations of spontaneous magnetizations.

diffraction measurements [7] or magnetic studies [2] in $DyCo_2$. The M
decrease rapidly in the composition range $0.6 \leq x \leq 0.8$ - Fig. 2.

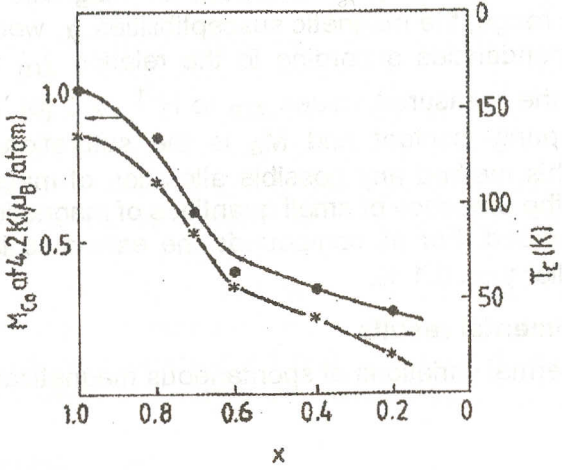

Fig. 2. Composition dependencies of the cobalt moments at 4.2 K and temperatures.

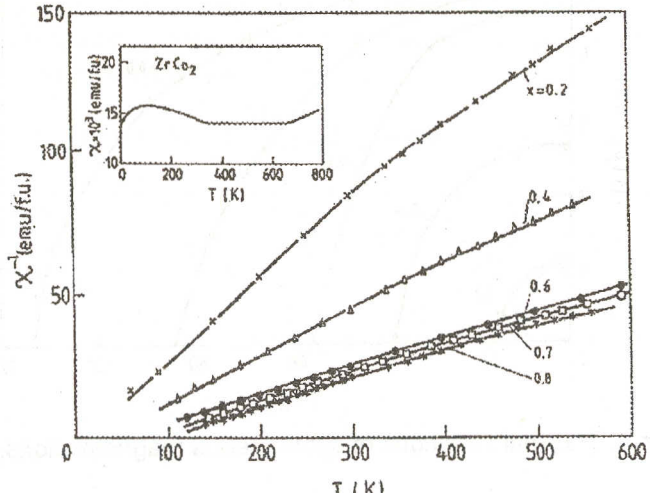

The same type dependence is evidenced also for the Cu temperatures.

The temperature dependencies of the reciprocal susceptibilities a plotted in Fig. 3. A downward curvature of χ^{-1} vs T values is evidenced temperatures above T_C, followed by linear variations at higher temperatu than ~ 400 K. These features are similar to that observed in $DyCo_2$ [2,8]. W note that above ~ 600 K a small increase of χ values for compounds hav composition $x \leq 0.8$ is observed, this behaviour being probably connected w the change of susceptibility, evidenced in $ZrCo_2$, at the same temperature-F 3 inset. From the linear part of χ^{-1} vs T we determined the Curie constants, and the contributions of cobalt atoms to C values. The effective cob moments are little dependent on composition and around 3 μ_B, close to t value determined previously in $DyCo_2$ [8] - Table 1.

Discussion

The composition dependence of cobalt moments, at 4.2 K, can attributed only to the variation of exchange interactions. In order to analy this matter the exchange interactions coefficients inside and betwe magnetic sublattices were determined. The dependence of cobalt moment 4.2 K, M_{Co}, on the exchange fields, H_{exch}, is plotted in Fig. 4. A sudd increase in M_{Co} values at $H_{exch} \cong 60$ T is evidenced. The above behavio was previously proposed [9] and experimentally reported [10-12] in rare-ea cobalt compounds and was attributed to the shift of spin-up and spin-dow cobalt bands by exchange field [9,10] or to itinerant electron metamagnetis [11, 12]. The magnetic behaviour of cobalt above the Curie temperatures ma be analysed parallel with that evidenced in YCo_2 or $LuCo_2$. As abov mentioned, in RCo_2 (R = Y, Lu) compounds, there is a transition from a T dependence of the magnetic susceptibilities to a Curie - Weiss behavio above a characteristic temperature T*.

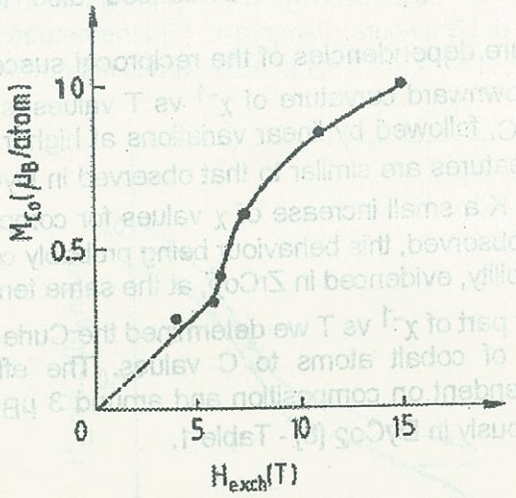

Fig. 4. The dependence of cobalt moment at 4.2 K on the exchange fields.

The effective cobalt moments were close to that of Co^{2+} ion considering only the spin contribution, M_{eff} = 3.87 μ_B. In these strong exchange enhancement paramagnets, the wave number dependent susceptibility χ_q, has a large enhancement due to electron - electron interaction for small q values. For these q values, χ_q increases until the average amplitude of local spin fluctuations $\left\langle S_{loc}^2 \right\rangle = 3k_B T \sum_q \chi_q$ reaches an upper limit determined by the charge neutrality condition at temperatures above a characteristic value T* [5]. A similar behaviour is expected for cobalt in $Dy_XZr_{1-X}Co_2$ system. The specific heat measurements on $DyCo_2$ [13] show that the magnetic entropy corresponding to cobalt moment at 4.2 K with S = 1/2 (M_{Co} = 1 μ_B), of 5.76 J/mol K cannot be observed at temperatures close but above T_C. This is an indication that cobalt behaves similar as observed in YCo_2 or $LuCo_2$ at low temperatures.

We mentioned above that the exchange enhancement factor, s, for magnetic susceptibility of $ZrCo_2$ is not high enough that this system behaves as a spin fluctuation one. When substituting Zr by Dy, due to the increase of the exchange interactions, there is a gradual increase of s values, these approaching to those evidenced in strongly exchange enhanced paramagnets. Consequently, a similar behaviour as that

observed for YCo_2 or $LuCo_2$, at $T > T_{max}$, is expected. The susceptibilitie
will decrease above T_C and for $T > T^*$ the χ vs T is supposed to follow
Curie - Weiss type dependence, as experimentally observed at $T \geq 400$
Unlike YCo_2 or $LuCo_2$ the effective cobalt moments are smaller than th
value characteristic for Co^{2+} ion considering only the spin contributio
Two opposite mechanisms may be invoked to explain this behaviour. Th
first is a gradual quenching of spin fluctuations by internal fields as the D
content increases. This, type behaviour was reported in RCo_2 compound
and is evidenced by a decrease a effective cobalt moments whe
increasing the exchange fields [3]. For compounds with low Dy content, th
exchange enhancement factor of cobalt susceptibility is belived to be no
high enough to behave as a saturated spin fluctuation system and to attai
the expected $\langle S^2_{loc} \rangle$ value. Consequently the effective cobalt moment ma
be lower than that expected from charge neutrality condition. We note tha
this situation was evidenced in $LaNi_{5-X}Cu_X$ system [14]. Thus, th
tendency for approaching to the saturation of $\langle S^2_{loc} \rangle$ value, whe
increasing exchange interactions is counterbalanced by gradual quenchin
of spin fluctuations. Consequently, we expect only small variations of th
effective cobalt moments along the series.

Finally, we conclude that the magnetic behaviour of cobalt i
$Dy_XZr_{1-X}Co_2$ system, both at 4.2 K and above Curie temperature i
strongly influenced by the exchange interactions.

REFERENCES

1. E. Burzo, A. Chelkowski and H. R. Kirchmayr, Landolt Börnstei
   Handbuch, vol. 19d2, Springer-Verlag, 1990.
2. E. Burzo, Int. J. Magn. 3, 161 (1972).
3. E. Burzo and R. Lemaire, Solid State Commun. 84, 1145 (1992).
4. E. Burzo, E. Gratz and V. Pop, J. Magn. Magn. Mat. 123, 159 (1993).
5. T. Moriya, J. Magn. Magn. Mat. 14, 1 (1979); 100, 261 (1991).
6. L. F. Bates, Modern Magnetism, Cambridge University Press, Cambrige, 195
   p. 133.
7. R. M. Moon, W. C. Koehler, J. Farrell, J. Appl. Phys. 36, 978 (1965).
8. E. Burzo, Phys. Rev. B6 2882 (1972).
9. E. Burzo, Rev. Roum. Phys 23, 689 (1978): J. Less Common Met. 77, 25
   (1981).

10.E.Burzo, N. Plugaru, I.Creanga and M.Van, J. Less Common Met. 155, 281 (1980).
11.N. N. Duc, T. D. Hien, P. E. Bromer and J. J. Franse, J. Magn. Magn. Mater. 104 - 107, 1252 (1992).
12.E. Burzo, J. Magn. Magn. Mat. 140 - 144, 2013 (1995).
13.N. Pillmayr, C. Schmutzer, E. Gratz, G. Hilscher and V. Sechovsky, J. Magn. Magn. Mat. 70, 162 (1987).
14.E. Burzo, S. Chiuzbaian, L. Ghioncel, M. Neumann : J. Phys.: Solid State (submitted for publication).

STUDIA UNIVERSITATIS BABEŞ-BOLYAI, PHYSICA, XLIV, 2, 1999

X - RAY PHOTOELECTRON SPECTROSCOPY AND MAGNETISM OF $GdNi_{5-X}Al_X$ INTERMETALLIC COMPUNDS

M. COLDEA*, M. NEUMANN, D. TODORAN*, M. DEMETER**, R. TETEAN*, V. POP*, S. CHIUZBAIAN****

ABSTRACT. X-Ray photoelectron spectroscopy (XPS) and magnetic susceptibility of $GdNi_5$, $GdNi_4Al$, $GdNi_2Al_3$ and $GdNiAl_4$ are reported. The magnetic state of Ni 3d - electrons strongly depends on the crystallographic structure of the compounds, showing spin fluctuations in $GdNi_5$ and $GdNi_4Al$, a similar behavior with that of metallic Ni in $GdNi_2Al_3$ and a filled 3d - band in $GdNiAl_4$.

INTRODUCTION

In the $GdNi_{5-X}Al_X$ series are reported four intermetallic compounds with different crystallographic structures [1]. The compounds $GdNi_5$ and $GdNi_4Al$ are isostructural and crystallize in the hexagonal $CaCu_5$ structure type with the lattice parameters a = 0.490nm, c = 0.397nm and a = 0.4969nm, c = 0.4048nm, respectively. The crystallographic structure of $GdNi_2Al_3$ is more complicated, namely a modulated $CaCu_5$ structure type (Pearson symbol hP$*$) with the lattice parameters a = 0.9043nm and c = 0.4103nm and two formula unit per unit cell, which has a volume almost double in comparison with those of $GdNi_5$ and $GdNi_4Al$. The compound $GdNiAl_4$ crystallizes in the orthorhombic $YNiAl_4$ structure type with the lattice parameters a = 0.4087nm, b = 1.530nm and c = 0.669nm.

The magnetic properties of $GdNi_5$ were studied earlier in the temperature range 4.2K - 290K [2]. This compound is a ferromagnet with T_c = 32K and a magnetic moment $\mu = 6.2\mu_B$/f.u. Ni is not magnetic but a negative 3d - band polarization of $0.16\mu_B$/Ni is induced by the interactions with the Gd spins. An effective magnetic moment of $7.7\mu_B$/f.u. was determined from the Curie constant in the paramagnetic state. This value is smaller than that of the free Gd^{3+} ion ($7.94\mu_B$). On the other hand, the superimposed susceptibility of $GdNi_5$ measured in high fields [2] and the values of the susceptibilities measured in the isostructural compounds YNi_5 [2,3] and YNi_4Al [4] showed that these compounds are exchange -

* "Babes-Bolyai" University, Faculty of Physics, 3400 Cluj - Napoca, Romania
** Universität Osnabrück, Fachbereich Physik, 49069 Osnabrück, Germany

enhanced Pauli paramagnets. The earlier studies on exchange - enhanced Pauli paramagnets revealed the importance of performing magnetic measurements in a large temperature range in order to understand the magnetic behavior of the investigated compounds [5].

The X - Ray photoelectron spectroscopy has been proved to be of central importance for understanding the magnetic properties and the elctronic structure of the rare - earth transition metal compounds.

The aim of this paper is to study by using magnetic measurements and XPS technique the influence of partially replacing of Ni by Al on the magnetic state of the Ni 3d - electrons in $GdNi_{5-X}Al_X$.

EXPERIMENTAL

The investigated compounds $GdNi_5$, $GdNi_4Al$, $GdNi_2Al_3$ and $GdNiAl_4$ were prepared by argon arc melting. The samples were melted repeatedly (four times) in the same atmosphere to ensure homogeneity. The weight losses of the final materials were found to be less than 1%. The purity of the starting materials was 99.9% for Gd and Ni and 99.99% for Al. X - ray powder diffraction measurements showed that all compounds are single phases with the expected structure types. The lattice parameters agree with those reported in [1].

The magnetic susceptibility was measured between 90K and 900K with a Weiss - Forrer magnetic balance with a sensitivity of 10^{-8} emu/g. The magnetization of $GdNi_2Al_3$ was measured at 4.2K in high magnetic fields between 6T and 9T with a vibrating magnetometer.

The XPS spectra were recorded using a PHI 5600ci ESCA spectrometer with a monochromatized Al K_α radiation (h v= 1486.6eV) at room temperature. The pressure in the ultrahigh - vacuum chamber was about 5 x 10^{-9} mbar during the measurements. Sample cleanliness was checked by monitoring oxygen and carbon 1s levels.

RESULTS AND DISCUSSION

The temperature dependence of the reciprocal susceptibilities for $GdNi_5$ and $GdNi_4Al$ are shown in Fig. 1. The $1/\chi$ (T) curves for both compounds show two linear portions with a change in the slope at about 700K for $GdNi_5$ and 450K for $GdNi_4Al$. The effective magnetic moments determined from the Curie constants for the two temperature ranges are as follows: μ_{eff} = 7.6 μ_B/f.u. and 8.85 μ_B/f.u for $GdNi_5$ and μ_{eff} = 7.88 μ_B/f.u and 8.72 μ_B/f.u for $GdNi_4Al$. The first values of the effective magnetic moments for the two compounds show that the Ni atoms do not carry localized magnetic moments. In the rare-earth transition metal compounds, the transition metal atoms form a 3d band, hybridized with the 5d states. As in

all RNi5 compounds, Ni is not magnetic because of charge transfer of R 5d electrons to the Ni 3d band.

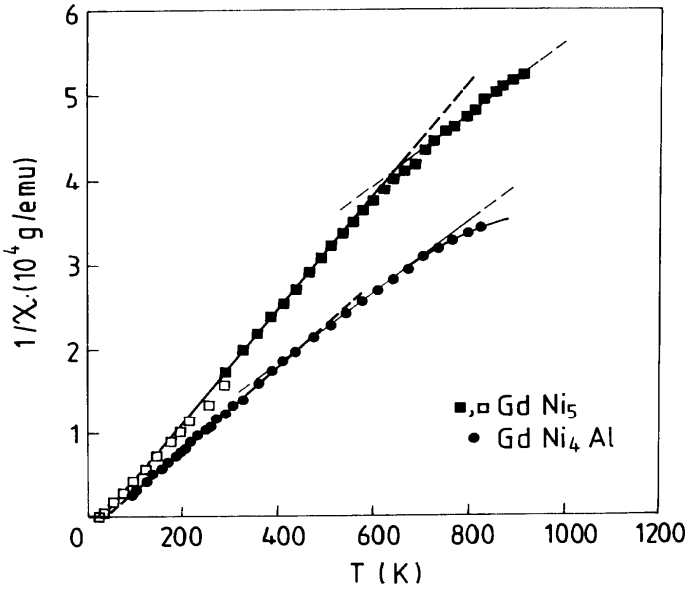

Fig. 1. Thermal variations of the reciprocal susceptibility for $GdNi_5$ and $GdNi_4Al$. Open squares are data taken from Ref. [2].

The deficit magnetic moment in $GdNi_5$ is related mainly to the negative polarization of the Ni 3d band which persists also in the paramagnetic state. This is not the case for the $GdNi_4Al$ compound. On the other hand, from the Curie constants of $GdNi_5$ for T > 700 K and of $GdNi_4Al$ for T > 450 K a value of about 1.76 μ_B/Ni is deduced which is very close to that of the free Ni^+ ion (1.73 μ_B, $3d^9$ configuration). We may explain the contribution of the Ni atoms to the measured susceptibility for the two compounds in a similar way as for the reference compounds YNi_5 [3] and YNi_4Al [4]. In the paramagnetic state, the average amplitude of the local spin fluctuations $\langle S_L^2 \rangle = 3k_BT\sum_q\chi_q$ (where χ_q is the wave-number dependent susceptibility) increases with temperature until it reaches an upper limit determined by the charge neutrality condition [5]. The temperature dependence of χ is the result of the increase in the local moments with increasing temperature. The amplitude $\langle S_L^2 \rangle$ of thermally longitudinal spin fluctuations saturates at

a certain temperature T^*(700 K for $GdNi_5$ and 450 K for $GdNi_4Al$), above which the susceptibility is governed by local moment-type fluctuations and therefore a Curie -Weiss behavior is observed. The $\chi(T)$ curves for the investigated compounds may also be explained by considering the position of the Fermi level in a region, where the density of states show a positive curvature, as confirmed by the band structure calculations for YNi_5 [6].

The valence bands of $GdNi_5$, $GdNi_4Al$ and of the isostructural compounds YNi_5 and YNi_4Al are shown in Fig. 2. These arise mainly

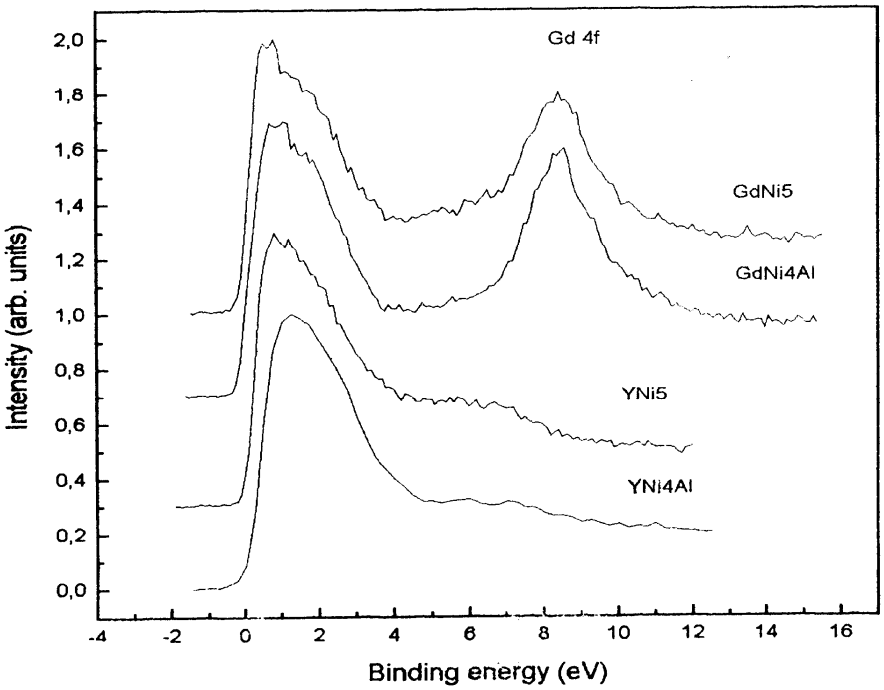

Fig. 2. XPS valence bands of $GdNi_5$, $GdNi_4Al$, $YNi_5$and YNi_4Al

from the Ni 3d electrons which are close to the onset of ferromagnetism. The 3d states are hybridized with 4d (in YNi5 and YNi_4Al) or 5d (in $GdNi_5$ and $GdNi_4Al$) states. The occupied part of the valence bands are over 4eV wide. The 6-eV satellite structure observed in all these compounds, similarly as in Ni metal, may be attributed to the Ni - $3d^8$ final state [7]. One can see also a marked feature near the maximum of the valence bands of $GdNi_5$ and $GdNi_4Al$. This may be explained as a partial quenching of the spin fluctuations by the strong magnetic moments of Gd atoms.

Furthermore, the substitution of Ni by Al leads to an increase of the localization of the Ni 3d electrons, reflected by an energy shift of the valence band maximum to higher binding energies, namely from 0.82 eV to 1.26 eV. This is also supported by the different values of the saturation temperature of the spin fluctuations T^* obtained for $GdNi_5$ and $GdNi_4Al$.

The temperature dependence of the reciprocal susceptibility for $GdNi_2Al_3$ is shown in Fig. 3. The susceptibility obeys a Curie - Weiss

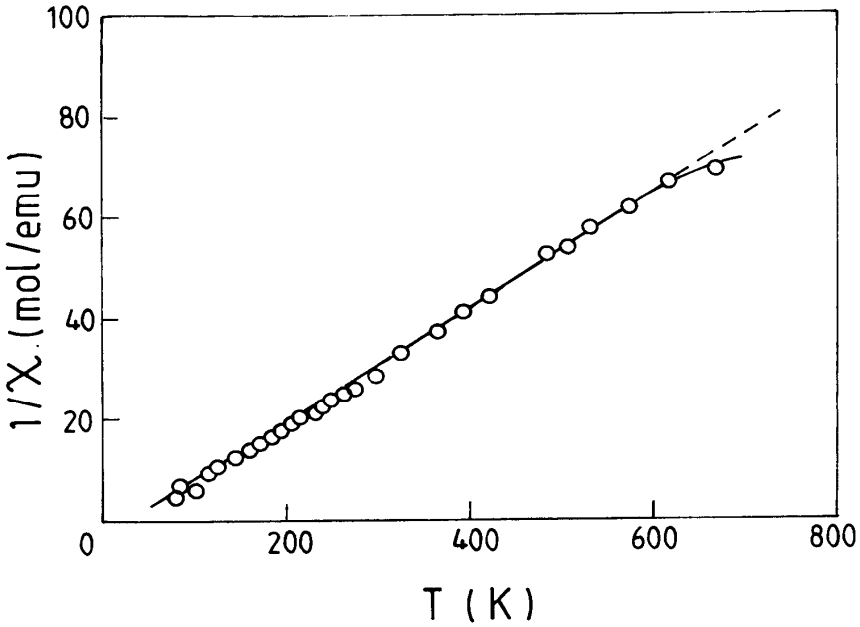

Fig. 3. Thermal variation of the reciprocal susceptibility for $GdNi_2Al_3$

law modified by a temperature - independent part X_0 ,accordind to

$$X = C/(T - \Theta) + X_0$$

with the paramagnetic Curie temperature $\Theta = 37K$ and $X_0 = 14 \times 10^{-4}$ emu/mol. The effective magnetic moment per Ni atom determined from the Curie constant is $\mu_{Ni} = 1.74\mu_B$, taking for the effective magnetic moment per Gd atom the value for the free Gd^{3+} ion. The effective Ni moment in $GdNi_2Al_3$ is close to that of Ni^+ ion, considering only the spin contribution, and to the value found in Ni metal ($1.64\mu_B$). This means that the magnetic state of Ni

atoms in $GdNi_2Al_3$ is almost the same as in pure Ni. This conclusion is also supported by the values of the magnetization measured at 4.2K in the high magnetic fields up to 9T. The saturation magnetization was obtained by extrapolating 1 / B to zero and has the value $M_s = 5.9\mu_B$ /f.u. This value is smaller than the theoretical moment of $7.0\mu_B$ for free Gd^{3+} and suggests that the Ni atoms have a non - zero magnetic moment and the Ni sublattice moments couple antiparallel to the Gd moments. For this ferrimagnetic arrangement the magnetic moment per Ni atom in the ordered state is deduced to be $0.55\mu_B$, which is very close to that found in Ni metal ($0.6\mu_B$)

The valence bands of $GdNiAl_4$ and of pure Ni are shown in Fig. 4.

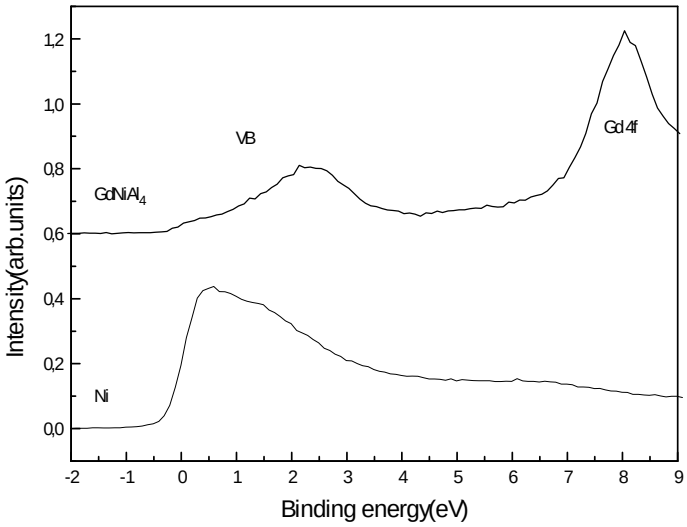

Fig. 4. Valence bands of $GdNiAl_4$ and of pure Ni

One can observe marked differences both in the shape and in the position of the valence band for the two materials. The density of states at the Fermi level in $GdNiAl_4$ is drastically reduced in comparison with pure Ni and the maximum of the valence band is shifted to higher binding energy, namely from 0.59eV in Ni to 2.3eV in $GdNiAl_4$. The states at the Fermi level have 3d and s - p character in Ni and $GdNiAl_4$, respectively. In d - band metals and alloys the 3d states are shifted gradually to higher binding energy with the increasing of the d - state occupancy and consequently a decreasing of the density of states at E_F occurs [8]. These results reveal the complete filling of Ni 3d - band by charge transfer of Gd 5d electrons and

the s - p character of the states at the Fermi level in $GdNiAl_4$. This conclusion is also confirmed by comparing the Ni 2p core level spectra for pure Ni and $GdNiAl_4$ (Fig.5). In the Ni 2p core level spectrum of pure Ni are present also satellites as an evidence for the d character in unoccupied states. The absence of these satellites in the Ni 2p level spectrum of $GdNiAl_4$ (similar with the Cu 2p spectrum in Cu metall [9]), shows that the 3d - band in this compound is filled.

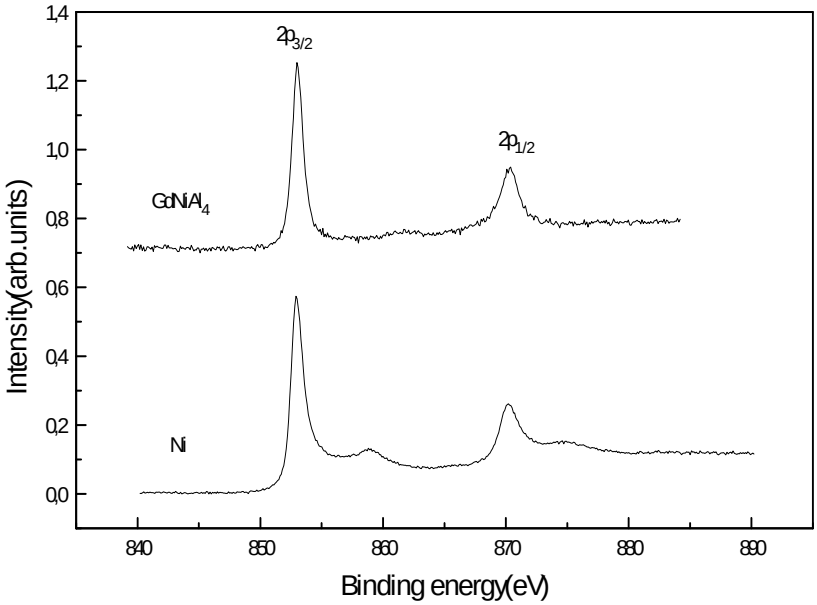

Fig. 5. Ni 2p core level spectra of Ni metall and $GdNiAl_4$

Summarizing the results, one may conclude that the Ni 3d - band in $GdNi_{5-X}Al_X$ compounds is sensitive to the local environment, showing a large variety of magnetic behaviors by partially replacing of Ni by Al atoms.

ACKNOWLEDGEMENTS

One of us (M. C.) would like to thank the Alexander von Humboldt Foundation for financial support and the University of Osnabrück for the kind hospitality.

REFERENCES

1. Villars P., Calvert L. D., Pearson's Handbook of Crystallographic Data for Intermetallic Phases, ASM Information Society, vol.1, 1994, p. 859.
2. Ginoux D., Givord D., del Moral A., Solid State Commun., **19**, 891 (1976).
3. Coldea M., Andreica D., Bitu M., Crisan V., J. Magn. Magn. Mat., **157/158**, 627 (1996).
4. Burzo E., Pop V., Costina I., J. Magn. Magn. Mat., **157/158**, 615 (1996).
5. Burzo E., Gratz E., Pop V., J. Magn. Magn. Mat., **123**, 159 (1993).
6. Crisan V., Popescu V., Andras A., Andreica D., Burda I., Cristea S., J. Alloys Comp., **223**, 147 (1995).
7. Martensson N., Johansson B., Phys. Rev. Lett., **45**, 482 (1980).
8. Steiner P., Höchst H., Hüfner S., J. Phys. F, **7**, L105 (1977).
9. Moulder J. F., Stickle W. F., Sobol P. E., Bomben K. D., Handbook of X-ray Photoelectron Spectroscopy, Perkin-Elmer Corporation, Physical Electronics Division, Eden Praire, Minnesota, 1992, p. 86.

STUDIA UNIVERSITATIS BABEŞ-BOLYAI, PHYSICA, XLIV, 2, 1999

SHORT AND LONG TIME RADIOISOTOPES CONTAMINATION AFTER CHERNOBYL ACCIDENT IN TRANSYLVANIA

C. COSMA*

ABSTRACT. After April 1986 Chernobyl disaster, the principal contributors during month of May and following 1986 year to the radioactive exposure were the short and medium half-live time radionuclides as: $^{132}Te+^{132}I$, ^{131}I, $^{140}Ba+^{140}La$, $^{103}Ru+^{103}Rh$, $^{95}Zr+^{95}Nb$, ^{136}Cs, ^{134}Cs, ^{141}Ce, ^{144}Ce and ^{125}Sb. Later, four-five years after only ^{137}Cs and ^{90}Sr presented and still present importance as radioactive contaminants. The measurements shown that some of these plants and foods (pollen, eggs, moss, and lichens) could be used as bioindicators of radioactive contamination in the case of the nuclear power plant accidents. The identification of radionuclides was made using gamma spectrometry of high resolution (GeLi) and the measurement of the cesium deposit both with GeLi and NaI(Tl) scintillation detectors. Regarding soil contamination, following the northeast-southwest direction there were measured the higher cesium deposits in Romania, some of these being above 80 kBq/m^2. This direction is the same with the cloud passage over Romania during the first week of May 1986 and it was confirmed by measurements in the former Yugoslavia, Albania and north of Italy.

This paper also presents ^{90}Sr measurements from soil and sediments using a method without chemical separation of strontium from samples. This method was used to determine the strontium content in four samples, which were collected in Cluj-Napoca and other three towns from Transylvania. The measurements were done using a Geiger-Muller proportional radiation detector of VA-Z-520 type, an RFT-20026 counter and aluminum plates of two thicknesses.

The obtained values for these samples are in 40-75 Bq/g interval of strontium-90 being in good agreement with those measured using chemical separation. The $^{90}Sr/^{137}Cs$ ratio is about 1/8 closed of the ratio 1/10 determined in samples from Bucharest area also in Japanese samples measured during 1988.

Keywords: radioactive contamination, cesium and strontium deposit, radioactive bioindicators, gamma and beta spectrometry,

* University "Babes-Bolyai", Physics Department, 3400-Cluj-Napoca, Romania

INTRODUCTION

The radioactive cloud passage over Romania beginning with the 30th of April 1986 caused fall-out of different intensities in different regions, especially where the cloud passage was accompanied with the rain appearance. [1-2]. Beginning with 1St May we started measurements for identifying the radionuclides and also to establish the gamma activity for the environmental factors. In the order of importance, the following radionuclides: ^{132}Te+^{132}I, ^{131}I, ^{140}Ba+^{140}La, ^{103}Ru+^{103}Rh, ^{95}Zr+^{95}Nb have had an essential contribution to the total activity during the month of May. The important radionuclides because having average half-life (as ^{134}Cs, ^{141}Ce, ^{144}Ce and ^{125}Sb) were also present in the first year. The ^{137}Cs and ^{90}Sr were and still remain the principal contaminants in the following years [3-7].

The grass was, at beginning, mostly affected component part of the environment and it contaminated rapidly the majority of foods, first things first all the animal products: milk, butter, cheese, meat, eggs [8-10].

After this catastrophic accident a diversity of ^{137}Cs deposits were found in different countries [11-14]. In Romania the biggest deposits were measured for the country center [15-16], some of these are higher than 80 kBq/m^2. The cesium deposits have been measured during 1986 year and some years after the disaster, for undisturbed soils, using high-resolution gamma spectrometry and cesium standards for volume sample calibration [16-17]. In a previously work [17] it was described a method for cesium measurement using volume samples and NaI(Tl) detector of large dimensions.

In this work are presented the results for isotopic composition of radioactive contaminants and some aspects of cesium deposition and cesium migration in soil from Transylvania. The measurements on pollen, eggs, lichens and moss samples proved that these materials could be used in monitoring of the soil and air contamination with fission products.

The strontium isotopes, which have chemical properties similarly to calcium, can substitute the calcium atoms in the bone metabolism. Because of his long half-live time value (28. 8 years), ^{90}Sr becomes dangerous when it is deposited in bones, especially for growing organism of young people. For this reason the evaluation of this radionuclides in foods and drinking water presents a great importance [18-19]. The estimation of the concentration of a pure beta radionuclides such as ^{90}Sr and his radioactive descendant ^{90}Y mixed with other β-γ radioactive isotopes from samples requires the chemical separation of the analyzed component [20-23].

This paper also presents data of ^{90}Sr content for deposits from four places in Transylvania region measured without separation of these radionuclides from samples.

EXPERIMENTAL METHOD

Identification of the radionuclides was done by a 512-channel analyzer of NTA-512M type, coupled to a GeLi detector of KOVO 327-type. Also, it was used a 4096 channel analyzer of Canberra type coupled to a GeLi detector of 65 cm^3 from IFIN Bucharest. The total gamma activity ($E\gamma$>80keV) was measured by a NP -424 type counter coupled to a NaI(Tl) detector of large size (75*45mm) . The measurements were done with the detector and the sample in a lead tower. Quantitative cesium determinations were made using the same device. The samples were measured either in Marinelli geometry (0. 5 l) or in cylindrical box (0. 18 l) directly seated on the NaI(Tl) scintillator[17]. For comparison some samples were re-measured using high-resolution gamma spectrometry. The soil samples were gathered from undisturbed soils in the period 1987-1995. For this a special device permitting the sampling from different soil depths was used. The pollen samples, daily gathered between 1-30 May 1986, were measured in the cylindrical boxes. In the case of eggs there were daily examined their activity and the nuclide repartition in eggshell and for yolk.

For ^{90}Sr and for short and median live-time radionuclides, the measurements were done on sediments, which were collected on May 17 from the roof of a building in Manastur district in Cluj-Napoca town, and from other three towns (Huedin, Dej, Aiud) during June 1986. The measurement of ^{90}Sr from these samples was done on May 1988. From the gamma spectrum recorded on May 10 (1988), Fig. 1., one can see that the most important radionuclides appeared at this time were Cs, Sb, Ru and Ce. Based on this observation it was used the total absorption of the β-rays less than 1500 KeV in a suitable aluminum layer. The measurement was carried out using a Geiger-Muller proportional detector, of VA-Z-520 type coupled with RFT-20026 monochanel gamma spectrometer and aluminum plates of two thicknesses. For energies higher than 1500 KeV the single contribution to the counting rate are those due to the ^{90}Y and ^{106}Rh isotopes. The beta spectra of these two radioisotopes are shown in Fig. 2. These spectra were reproduced following the data from [24] where the most important data of beta spectra of the fission products were done.

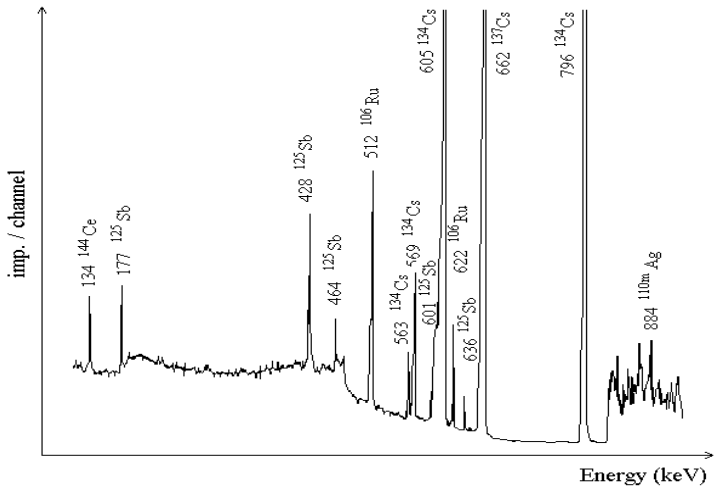

Fig. 1. Gamma spectrum of sediment sample measured in July 1988

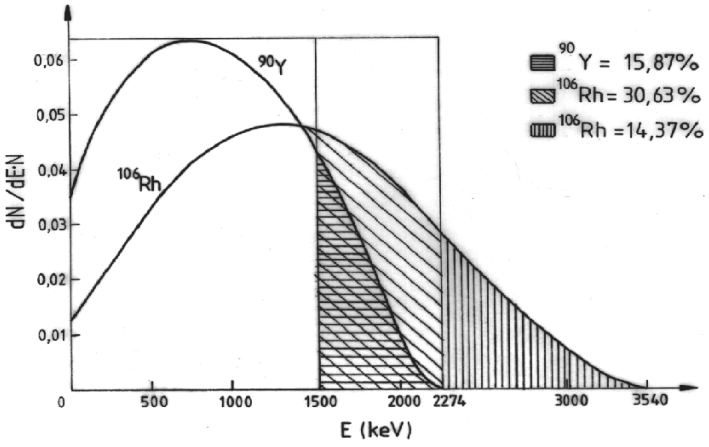

Fig. 2. Beta spectra of ^{90}Y and ^{106}Rh radioisotopes.

The mass of samples was 0. 911 g and their thickness was 2 mm. To prepare these samples, 2-3 g of sediments were pressed uniformly in the sample support from Fig. 3, which have 4-mm deepness and 22-mm diameter. The first aluminum layer (d_1) will absorb all the beta rays having energies lover 1500 KeV, therefore the beta contributions of ^{137}Cs, ^{134}Cs, ^{144}Ce, ^{125}Sb to the sample spectrum will be eliminated.

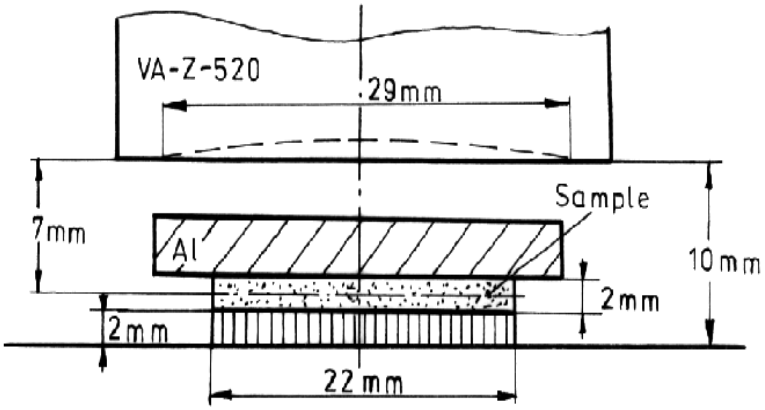

Fig. 3. The geometric disposal of beta sediment samples

The second aluminum layer (d_2) was thus calculated as to allow the measurement of beta rays having energy higher than 2, 274 KeV (beta edge for $^{90}Sr+^{90}Y$) . The measurement using this aluminum layer have revealed only the contribution of $^{106}Ru--^{106}Rh$ to the total beta spectrum of sediments. The solid angle for this measurement disposal was evaluated on the computer by solving the following triple integral:

$$\Omega = (a/\pi A^2) \int_0^A 2\pi\, x_0\, dx_0 \int_0^R r\, dr \int_0^{2\pi} d\varphi \,/\, (r^2+x_0^2+a^2-2rx_0\cos\varphi)^{3/2} \qquad (1)$$

where "a" is the distance between the sample and the entrance of detector, A is the radius of the cylindrical sample and R is the radius of the detector

RESULTS AND DISCUSSION

In Table 1 is shown the radioisotope composition of the sediment collected during April 26- May 17, 1986. This sediment is in general similarly to other samples from this region. This sample was consecutively measured on May 18, November 20, 1986, respectively March 4, 1997 and July 7, 1988. The contribution of $^{132}Te+^{132}I$, $^{140}Ba+^{140}La$ and ^{131}I respectively ^{129m}Te were recalculated for May 10 when the majority of radionuclides already were deposed. As it can be see from this table the deposits in this area contain very high quantities of radionuclides with short half life time, that is ^{132}I, ^{132}Te and ^{131}I. The ratio $^{137}Cs/^{106}Ru$ found in our sample is about 1/2 whereas in the north of Greek deposits this ratio is about 3 [13]. For $^{137}Cs/^{103}Ru$ the ratio is 1/3 and for Greek samples is 1/5. Therefore the contamination with short live time radionuclides was most important in our county that in Greece.

Table 1. Isotopic composition of Cluj-Napoca (Transylvania county) deposits

Nuclide	$T_{1/2}$	Specific activity kBq/kg	Deposits KBq/m^2
$^{132}Te+^{132}I$*	3. 2 days/23 hours	-	688
^{131}I*	8. 1 days	-	172
$^{140}Ba+^{140}La$*	12. 8 days/40	-	120
^{103}Ru	hours	1268	43. 2
$^{144}Cs+^{144}Pr$	39 days	191	10. 1
^{125}Sb	286 days	765	2
$^{106}Ru+^{103}Rh$	2, 73 years	442	24
^{95}Zr	367 days	97. 4	2. 6
^{95}Nb	65. 5 days	557	14. 8
^{134}Cs	35 days	210	5. 6
^{137}Cs	2. 06 years	482	12. 8
^{129m}Te	30 years	-	43
^{110m}Ag	-	5. 3	0. 2
^{90}Sr	250 days	49	1. 3
TOTAL	2. 86 years	-	116
	-		

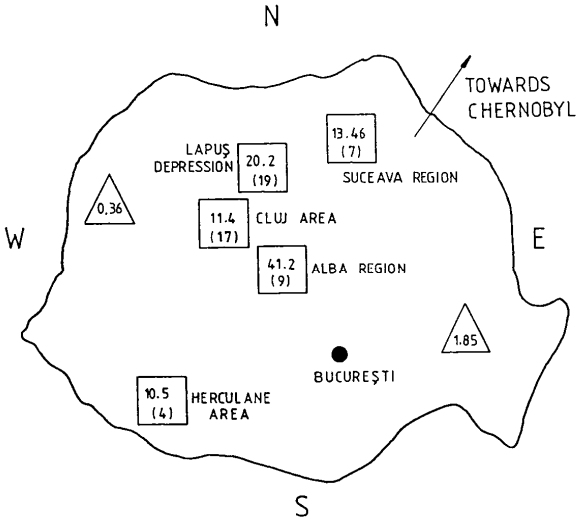

Fig.4. The ^{137}Cs deposits in Romania after Chernobyl accident.

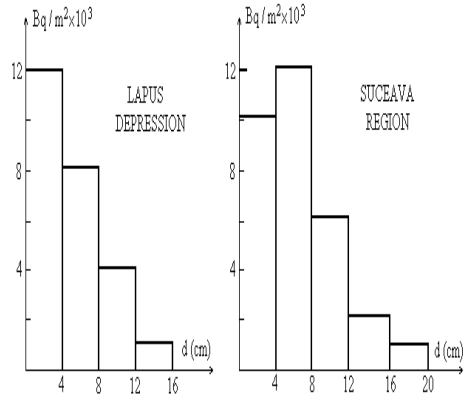

Fig.5. Profile of soil cesium content

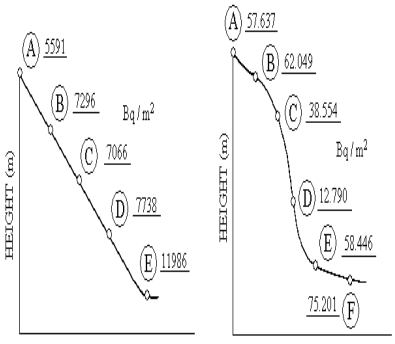

Fig.6. Cs deposition on diferent slopes for two samples

The picture from Fig. 4 presents the cesium deposit in different areas from Romania which were found on the direction of radioactive cloud passing during May 1st – May 4-th. It was remarked that at this time, there were many rainfalls. In this picture, in rectangles is shown the average value (kBq/m^2) having in brackets measurement number in this area. The values from triangles are the results reported in paper [25]. From this figure, we can remark that an important Cs deposit (especially on NE-SW direction) exists in Romania, due to the fact that this direction coincided with radioactive cloud direction (1 -4 May '96) and much rainfalls were recorded at that time. Also on this direction, in other countries, (Serbia, North of Greece, Albania, South of Italy), important radioactive fallout were measured [26]. In Fig. 5 are shown two soil depth profiles obtained in undisturbed soil (1994) in Suceava and respectively Lapus Depression. The difference between the two soil radon profiles is in connection with the local characteristics of the soil. In Fig. 6 is shown the variation of cesium deposition among slopes due to soil erosion.

Fig. 7 presents the obtained results for ^{137}Cs daily content in pollen samples measured two years later the samples were gathered. The daily evolution presents two maxims, in 1 and 7th of May, according to them of the release of radionuclides from the damaged Chernobyl station, in 26 April respectively 5 May [27]. The five days delay corresponding to the first maximum is do to the fact that the first three days after the accident the wind blew towards N and NW, then changing the direction to SW [28]. The second maxim for 7 May was registered at only two days after the maximum of radionuclides release from 5 May because, in this time, the wind blew constantly in SW direction. These maxims were rediscovered also, in air samples measured in Albania in May 3, respectively in May 9 [29]. On the other hand, these two maxims prove that the contamination of pollen grains happens during the later transport from the gather place to the beehive. The pollen acts like a filter for the radionuclides presents in the air.

This thing speaks about the fact that the pollen could be used to monitor some possible radioactive substance deliverance, in close vicinity of nuclear equipment.

Fig. 8. presents the activity evolution (count/10s) for eggs from hens fed with grass and from hens not fed with grass. In the first case, the egg activity is (between 2-10 May) 5 times greater than in the second one, where the activity is maintained at a relative low value (100imp/10s between 5-15 May) .

The activity of the eggs from the hens fed with grass presents also two peaks: the first is higher on 5 and 6 May, due to the massive deposits on May 1 and 2 (rain), and the second peak is higher on May 9 and 10,

corresponding to some new accentuated fall-out in that zone between May 6 and 7.

Fig. 9. shows the gamma spectrum of the eggshell and according to that for the egg content (8 May) . The shell concentrated a great amount of $^{140}Ba+^{140}La$ as can be seen from this spectrum. This fact can be explained if we considered that the eggshell contains mainly calcium which has a chemical analogy with barium. The fact that the maximum egg activity is reached after 2 or 3 days, later than the maximum activity of the environment, is due to the period of the egg formation in final stage. We found in the eggshell some ^{132}Te, too, due to the great contamination with this radionuclides brought in the area by the rain of May 1.

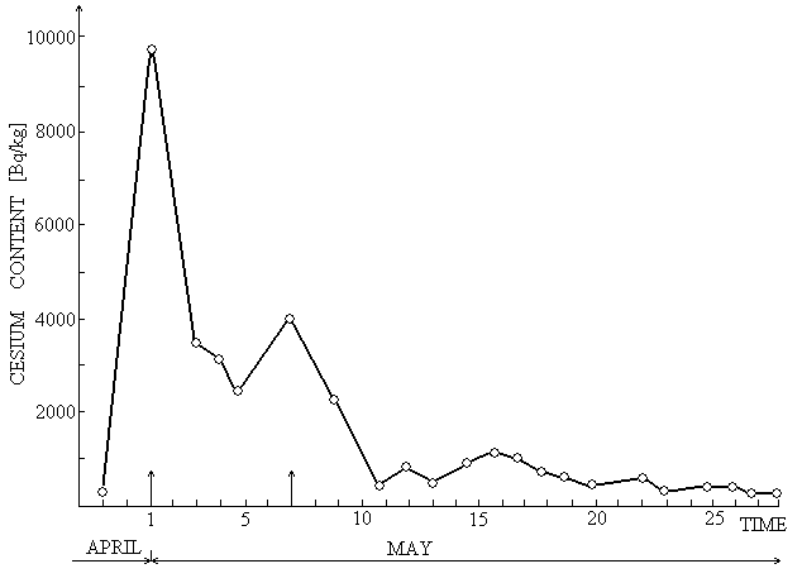

Fig.7. Daily cesium content of pollen samples gathered during May 1986

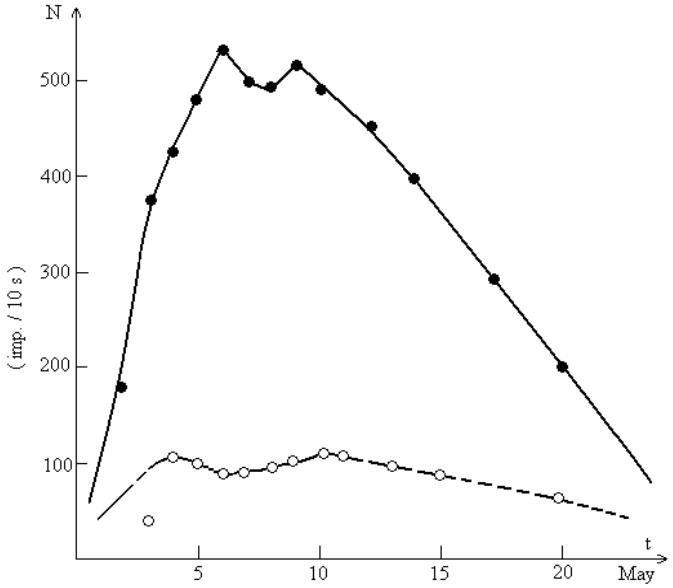

Fig.8. Gamma global activity of eggs during May 1986

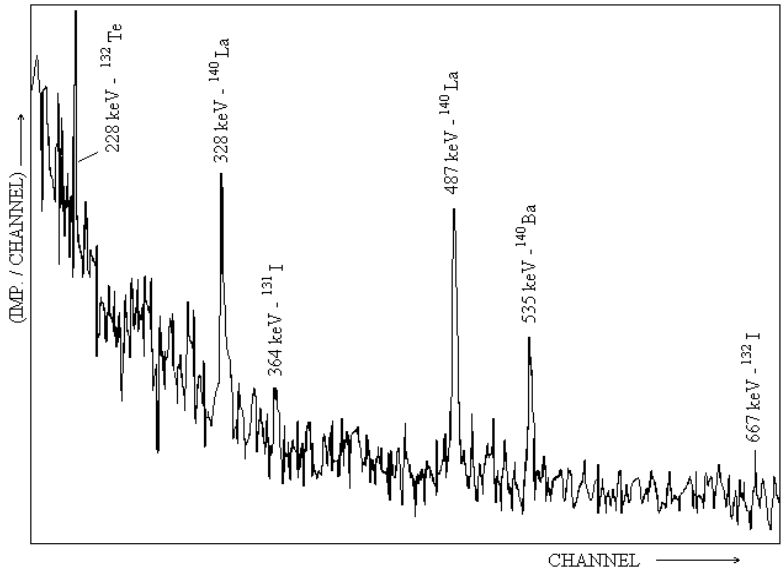

Fig. 9. Gamma spectrum of the eggshell for the sample gathered in May 10, 1986

The ^{131}I and ^{132}I radioisotopes appear in great concentration in the spectrum of egg content where ^{140}Ba and ^{149}La present very low concentration. Therefore, we can say that eggs have a behavior as of a separator.

The mosses, lichens and other plant samples were harvested from Transylvania forests or plains situated at big distances away from roads and human habitats. Preference for cesium accumulation was observed at the perennial plants (Lichen Islandicus and mosses [29]) . It is considered that inferior plants (lichens, algae, moss) presents for any kind of pollutants some morphological and physiological properties which makes them more suited for bioindicators than superior plants. These perennial inferior plants grow very slow, having a long life. This is the reason for which they store pollutants, in this case, ^{137}Cs.

The ^{90}Sr measurements in the four samples of sediment arising from: Cluj-Napoca, Huedin, Dej and Aiud are shown in Table 2 where also are inserted the measurement results obtained using the conventional chemical separation for two samples (last column) .

Table 2. Strontium and cesium content in some sediment from Cluj county.

Nr.	Place	^{90}Sr Content Bq/g	^{137}Cs Content Bq/g	$^{90}Sr/^{137}Cs$	Chem. Separat. ^{90}Sr Content Bq/g
1	Cluj-Napoca	56. 76	484. 5	1/8. 5	52. 62
2	Huedin	50. 31	397	1/7. 9	-
3	Dej	41. 25	330	1/8	-
4	Aiud	73. 52	595	1/8. 1	70. 68

The average ratio $^{90}Sr/\ ^{137}Cs$ is about 1/8. 1. Other measurement for evaluating the concentration of ^{90}Sr were done in our country in Bucharest by using the chemical separation and the ratio was found $^{90}Sr/^{137}Cs$ as being 1/10 [30]. For the deposition in Japan the above ratio was found to vary between ½ and 1/10 [31].

REFERENCES

1. S. E. Simopoulos: Int. J. Radiat. Appl. Instrum. A40 (1989) 607.
2. C. Cosma, K. Kovacs, L. Manzat, Studia UBB, Physica, 32 (1987) 160.
3. IAEA, The international Chernobyl project: Surface contamination maps. Report by an international advisory committee, Vienna, 1991.
4. A. A. Borovoy, V. F. Demin, L. D. Blinova, Nuclear Society International, 1992 pp 9-20.
5. L. E. Haugen, T. H. Garmo, F. Pedersen, H. Bjornstad, Analyst, 117 (1992) 529.
6. Z. Franic, A. Bauman, Health Physics, 64 (1993) 162.
7. N. P. Petropoulus, E. P. Hinis, S. E. Simopoulus, Environ. International, 22 (1996) 369.
8. C. Cosma, I. Mastan, V. Znamirovschi, O. Cozar, National Symposium "Methods, Models and Tehnics in Physics" Cluj Napoca, 1987, Pg. 166.
9. E. L. Cooper, V. Valkovic, V. Srachnov, R Dekner, P. R. Dancsi, Appl. Radiat. Isot. 43 (1992) 149.
10. A. Louizi, C. Proukakis, Health Physics, 61 (1991) 885.
11. C. Cosma, Internal Report, Univ. Cluj Napoca, Romania, May 1986.
12. L Monte, S. Fratarcangeli, F. Pompei, S. Quaggia and C. Battella: Radiochimica Acta 60 (1993) 219.
13. National Technical University of Athens, Radiometric Maps, http://arcas. nuclear, ntua. gr/radmaps/.
14. M. Antonopoulos-Domis, A. Clouvas, S. Xanthos, D. A. Alifrangis, Health Physics, 72 (1997) 243.
15. C. Cosma, I. Cozmuta, C. Micu and I. Chereji: in Proc. 3rd Int. Symp. on Environ. Contam. in Central and Eastern Europe Warsaw 1996. (Eds. NATO Science Committee) Warsaw, 1996, p. 736.
16. C. Cosma, M. Salagean, A. Pantelica, T. Fiat, Studia UBB, Physica, 33 (1988) 65.
17. C. Cosma, L. Daraban, D. Ristoiu, M. Todica and C. Ronneau. Czechoslovak Journal of Physics, 49, 211-216 (1999).
18. R. M. Alexakhin, I. N. Sanzharova, N. I. Fesenko, S. V. Sprin, E. V. Firaskova, Nuclear Society International, (1992) 9.
19. H. E. Bjornstad, H. N. Lien, Y. Yu-Fu, B. Salbu, J. Radioanal. Nucl. Chem., 156 (1992) 165.

20. D. H. Oughton, B. Salbu, T. L. Brand, J. P. Day, A. Aarkrog, Analyst, 118 (1993) 1101.
21. A. Tessier, P. C. Campbell, M. Bisson, Anal. Chem., 51 (1979) 844.
22. G. Kossl, W. Warburgg, PTB Mitteilungen, 96 (1986) 249.
23. E. Dycker, The Chernobyl accident and its impact, Royal Meteorological Institute of Belgium, Brussels, Belgium, 1986.
24. M. Kolobaskin, P. P. Dmitriev, Beta izlucenie productov delenia, Atomizdat, Moskva, 1986, pp. 358 (in Rusian).
25. S. Sonoc, C. Dovlete, I. Osvath, F. Baciu and G. Ruzsa: *Artificial Radioactivity in Romania*, Bucuresti, Romania, 1994, p. 22.
26. M. Kedhi, J. Radioanal. Nucl. Chem. Letters, 145 (1990) 115.
27. Abaghian, Atomnaia Energhia, 61 (1986) 301 (in Rusian).
28. International Atomic Energy Agency. Summary report on the post-accident review meeting on the Chernobyl accident. Safety Series No. 75-INSAG-1, 1986, pg. 24.
29. A. Aarkrog, J. Environ. Radioactivity, 6 (1988) 151.
30. N. Paunescu, I. Vata, J. Radioanal. Nucl. Chem., Letters, 126 (1988) 97.
31. *** Radioactivity Survey Data in Japan, 1988, 80.

STUDIA UNIVERSITATIS BABEŞ-BOLYAI, PHYSICA, XLIV, 2, 1999

STRUCTURAL AND DYNAMICAL STUDIES OF SOME MOLECULAR COMPLEXES OF BIOLOGICAL RELEVANCE

O. COZAR*, L. DAVID, G. DAMIAN, V. CHIŞ

ABSTRACT. Powder EPR spectra of some Cu(II)–complexes with antiinflammatory drugs ($[Cu_2(aspirinate)_4](H_2O)_2$, $[Cu_2(indomethacin)_4](H_2O)_2$, $[Cu(ibuprofen)_2](H_2O)_2$) show the existence of Cu(II) acetate like dimers, characterized by strong antiferromagnetic exchange interaction ($J = 300\ cm^{-1}$). The $[Cu(piroxicam)_2](DMF)_2$ compound magnetically diluted with Zn(II) shows the presence of monomeric species with d_z2 ground state ($g_{||} = 2.093$, $g_{\perp} = 2.241$, $A_{||} = 76.7$ G). In the case of $Cu(oxazepam)_2Cl_2$ there is a superposition of two nonequivalent mononuclear species, one with $d_x2_{-y}2$ ground state and another with d_z2 ground state. $Cu(theophylline)_2(NH_3)_2{\cdot}2H_2O$ has an axial spectrum ($g_{||}$=2.255, $g_{\perp}$=2.059) due to a static Jahn-Teller effect ($E_{JT} \approx 2880\ cm^{-1}$). The spectrum of $Cu(theophylline)_2(npa)_2{\cdot}2H_2O$ is a superposition of one axial ($g_{||} = 2.299$, $g_{\perp}$=2.064) and one isotropic component ($g_0 \approx 2.100$) arising from one dynamic Jahn-Teller effect. The different modes of coordination of the metallic ions with 5'-GMP and 5'-CMP nucleotides is also presented. The mobility of spin labels depends on the nature and hydroaffinity of surface supports, solvent nature and hydration degree. The γ - irradiated dose dependence of the formation kinetics and structure of the produced free radicals in some biomolecules (drugs, aminoacids) are presented too.

INTRODUCTION

Many studies about molecular structure and molecular dynamics of some complex combinations of biological relevance have been done in the last years.

We have obtained significant results about the electronic structure of these complexes, metal ion-ligand of biological interest interaction,

* "Babeş-Bolyai" University, Faculty of Physics, Cluj-Napoca, Romania

solvent effects, modification of the local symmetries by the ligand-solvent subtraction, molecular association effects with the synthesis of some dimeric (polymeric) species and the behavior of some biomolecules in nuclear radiation fields.

The main directions of the research are the following:

– Interaction between metal ions - drugs and other biomolecules (anti-inflammatory, tranquilizing, antibacterial, aminoacids, nucleotides);

– Solvent effects on the metal complexes with biologically active ligands and molecular association mechanisms;

– Molecular dynamics of nitroxidic radicals adsorbed on some surfaces and in polymeric solutions;

– Identification of the radiation products in some biomolecules, kinetics and recombination aspects in connection with adsorbed radiation dose;

– Structural investigation and interaction between metallic ion pairs in some heteropolyoxometalates compounds.

1. Metal ions - drugs and other biomolecules interaction

Many antiinflammatory agents have been developed to inhibit some component of the inflammatory process without correcting the cause of the disease or promoting tissue repair.

Copper(II)–complexes of some antiinflammatory drugs have been found to be more potent and desirable drugs than their parent drugs [1,2]. The hypothesis that copper compounds might be active as antiinflammatory agents is supported by the finding that copper complexes are effective against arthritic and other degenerative diseases of man. In addition, these metal complexes exhibit a variety of pharmacological effects such as antiulcer, antidiabetic, anticancer, anticonvulsant and radiation recovery activities [3,4]. The following Cu(II)–complexes with antiinflammatory drugs were prepared and investigated by EPR method: $[Cu_2(aspirinate)_4](H_2O)_2$, $[Cu_2(indomethacin)_4](H_2O)_2$, $[Cu(ibuprofen)_2](H_2O)_2$ and $[Cu(piroxicam)_2](DMF)_2$ [5-11].

Derivatives of 1,4-benzodiazepine have been used for many years in pharmacology as tranquilizing and sedative-hypnotic drugs [12-14]. In order to obtain further information the Cu(II)-complexes with tranquilizing drugs (diazepam, nitrazepam, oxazepam) were also investigated by EPR spectroscopy [15-19].

Transition metal complexes containing theophylline (1,3-dimethylxantine) and amine type ligands may serve as model for coordination

of metal ions to nucleic acids through their oxopurine base [20-24]. The EPR studies of Cu(theophylline)$_2$(L)$_2$·2H$_2$O (L: NH_3, npa = n-propylamine) complex showing an interesting Jahn-Teller effect will be presented.

We have also investigated the Cu(II)–complexes with nucleotide molecules [25,26], namely guanosine-5'-monophosphate, 5'-GMP, and cytidine-5'-monophosphate, 5'-CMP.

1.a. Dimeric complexes

Powder EPR spectrum of [Cu$_2$(aspirinate)$_4$](H$_2$O)$_2$ complex [7,8], measured at room temperature, exhibits absorptions typical of randomly oriented triplet state (S = 1) species having an axial symmetry with a small rhombic distortion (Fig.1).

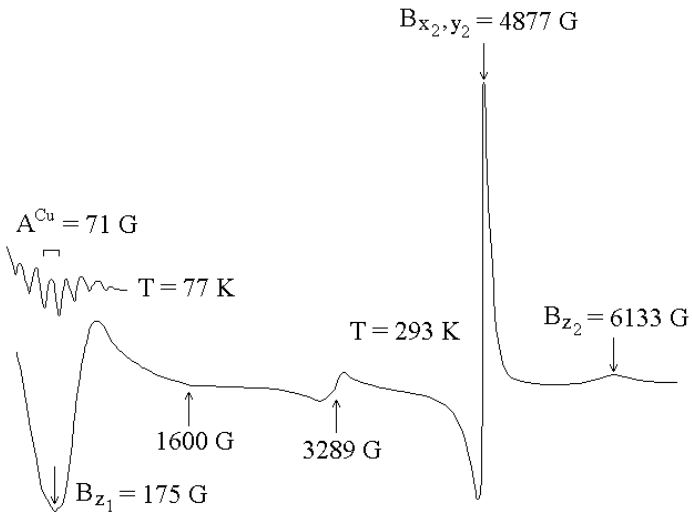

Fig.1 Powder EPR spectrum of Cu$_2$(aspirinate)$_4$·2H$_2$O complex at 293 K

These dimeric species are characterized by a short Cu–Cu distance (~ 2.7 Å) and a strong antiferromagnetic exchange coupling (J = –288 cm^{-1}) similar with those evidenced in other copper acetate like dimers [27]. The parallel (z) and perpendicular (xy) fine structure components resulting from the zero-field splitting can be readily identified in the spectrum. Also, the seven hyperfine lines due to the two equivalent copper nuclei (I_{Cu} = 3/2) are

clearly resolved on the B_{z1} signal at 77K. The obtained spectrum can be adequately described by the following spin Hamiltonian:

$$\mathbf{H} = \beta\mathbf{BgS} + D(\mathbf{S_z^2} - 2/3) + E(\mathbf{S_x^2} - \mathbf{S_y^2}) + \mathbf{SA}(\mathbf{I_1} + \mathbf{I_2})$$

where β is the Bohr magneton, **B** is the external magnetic field, **g** is the anisotropic Landé splitting tensor, **S** is the total spin vector, D and E are the zero-field splitting
parameters, A is the hyperfine tensor and I_1 and I_2 represent the individual nuclear spin operators of the two copper nuclei.

The spin Hamiltonian parameters were calculated in a relative straightforward manner from the observed spectrum according to the procedure described elsewhere [27,28]. The obtained values are: $g_{\|}$ = 2.305; $g_{\perp}$ = 2.08; D = 0.346 ; E < 0.016 cm^{-1} , and $A_{\|}$ = 71G. Besides the three fine structural signals, there are also two weak absorptions at ~ 1600 G and ~ 3200 G respectively. The half-field resonance (~ 1600 G) is due to the forbidden $\Delta M_S = \pm 2$ transition characteristic for the dimeric species in which the Cu–Cu distances is ~ 4–5 Å [7,8]. The spin-spin coupling in this little amount of dimeric species is realized by the dipole–dipole interaction. The absorption observed at 3200 G arises from the mononuclear impurities of spin S = 1/2. The intensity of this absorption increases when the temperature is lowered at 4K.

The powder EPR spectrum of $[Cu_2(indomethacin)_4](H_2O)_2$ complex (Fig.2a), suggests also the presence of two kinds of dimeric species: one of them characterized by a short Cu–Cu distance analogous to the dominant form of Cu(II)–aspirinate complex and the other type in which the metal–metal distance is bigger than in the first case [6,12].

The second dimeric species using the carbonyl for the coordination is characterized by a Cu–Cu distance of ≈ 4–5 Å [6] and the spin–spin coupling is realized here mainly by dipole–dipole interaction. The strong absorption observed at 3300 G arises from the allowed $\Delta M_S = \pm 1$ transition characteristic to the above mentioned dimeric species with a zero field splitting parameter D = 0.332 cm^{-1} and to the monomeric impurities of S = 1/2. The number of mononuclear species increases when the temperature is lowered or by a magnetically dilution with Zn(II). The powder EPR spectrum of (Cu–Zn)–indomethacin in the 3200 G region is shown in Fig.2b. The characteristic EPR parameters: $g_{\|}$ = 2.335, $g_{\perp}$ = 2.061, $A_{\|}$ = 138 G and $A_{\perp}$ = 20 G suggest a tetrahedral (T_d) coordination of Cu^{2+} ions [29]. Using the LCAO–MO scheme described in the paper [29], a mixture of $2d_{xy}$ and 2% $4p_z$ copper orbitals results for the paramagnetic electron ground state. The more intense g = 2.2 signal from the parallel band may

be attributed to a little amount of monomeric species with d_z2 ground state. A similar spectrum was reported by us for Cu^{2+} ions in water–ethanol mixtures at 77K [30]. The characteristic spin Hamiltonian parameters of the first dimeric species in which the coordination is realized by carboxyl groups and the copper ions are strongly coupled by exchange interactions are the follows: $g_{||} = 2.327$, $g_{\perp} = 2.040$, $D = 0.332\ cm^{-1}$, $E < 0.014\ cm^{-1}$, $J = -288\ cm^{-1}$.

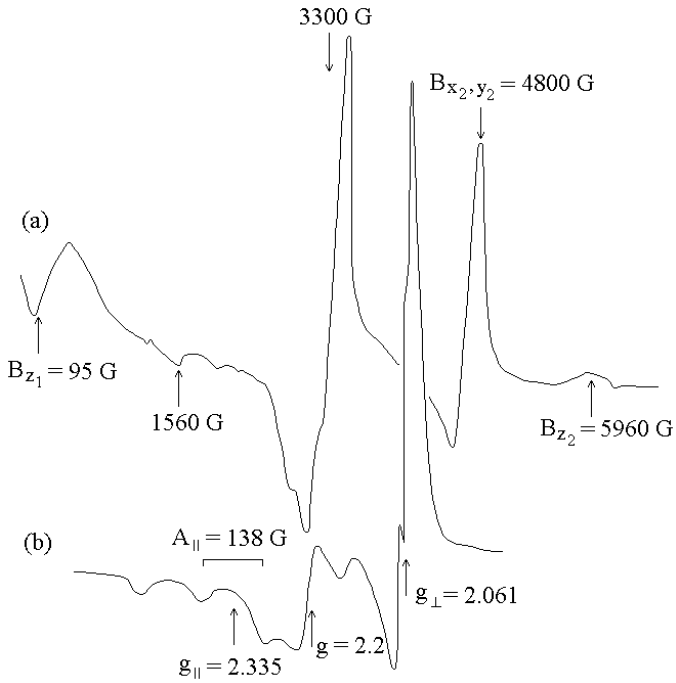

Fig.2 Powder EPR spectra of Cu(II)–indomethacin (a) and (Cu:Zn)–indomethacin (b) complexes

Powder EPR spectrum of Cu(II)–ibuprofen complex (Fig. 3) shows that in this case prevail monomeric and dimeric species characterized by a Cu–Cu distance of 4–5Å and a dipolar spin coupling. The small intensity of the absorption peaks from 161 G and 4911 G suggests the presence of a little amount of dimeric species having a short Cu–Cu distance (2.7 Å).

Copper(II) halides and sulfate complexes with 1,4-dihydrazinophtalazine (DHP) (a medical drug for blood pressure control) were also synthesized and characterized by IR, electronic, magnetic

susceptibility and EPR methods [31-33]. Powder EPR spectra and temperature dependence of magnetic susceptibility show the presence of dimeric species in which the separation between singlet and triplet state (2J) is around 100 cm^{-1}.

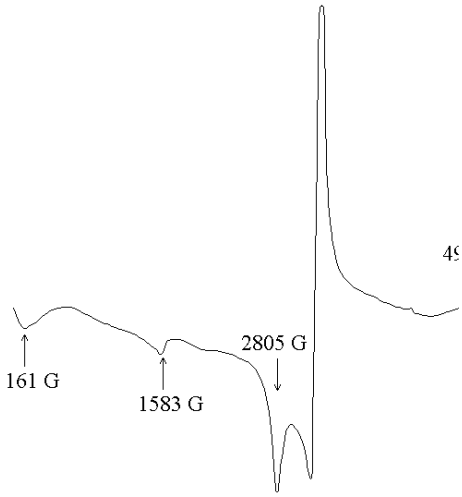

Fig.3 Powder EPR spectrum of Cu(II)-ibuprofen at 295K

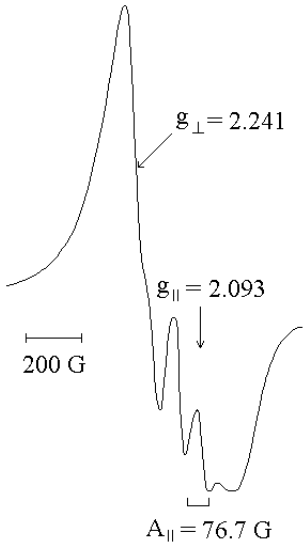

Fig.4 Powder EPR spectrum of (Cu:Zn)–piroxicam compound

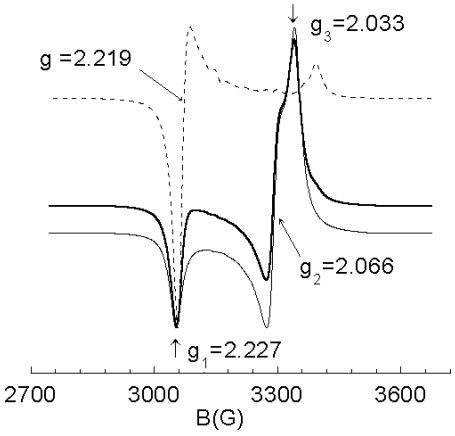

Fig.5 Powder (thick solid line) and simulated (thin solid and dashed lines, respectively) EPR spectra of $Cu(oxazepam)_2Cl_2$ complex

1.b Cu(II)–complexes with d_z2 ground state

In the case of $[Cu(piroxicam)_2](DMF)_2$ compound only the monomeric species of a distorted tetrahedral–octahedral symmetry of Cu^{2+} sites occur with d_{xy} orbital as ground state for paramagnetic electron [12].

The characteristic g-values ($g_{||}$ = 2.464, $g_{\perp}$ = 2.050) and the absence of the copper hyperfine structure indicate a $3d_{xy} + 4p_z$ admixture for the ground state of paramagnetic electron. The contribution of the $4p_z$ orbital is greater here (~ 10%) than in the case of Cu–indomethacin monomeric species. By magnetically dilution with Zn(II), the monomeric species with d_z2 ground state occurs (Fig. 4). Characteristic EPR parameters are: $g_{||}$ = 2.093, $g_{\perp}$ = 2.241, $A_{||}$ = 76.7 G. These monomeric species are comprehended along the O_z axis by a strong coordination of DMF molecules at Cu^{2+} ion on this direction.

Powder EPR spectrum of the $Cu(oxazepam)_2Br_2$ complex obtained at room temperature exhibit the absorption signals typical of randomly oriented single state (S = 1/2) species having an axial symmetry with a small rhombic distortion (g_1 = 2.201, g_2 = 2.067, g_3 = 2.028 for $Cu(oxazepam)_2Br_2$ and g_1 = 2.227, g_2 = 2.066, g_3 = 2.033 for $Cu(oxazepam)_2Cl_2$). In the case of $Cu(oxazepam)_2Cl_2$ powder spectrum the absorption signal from the $g_{||}$ region may be considered as a superposition of the absorption for two nonequivalent monomeric species, one with a $d_x2_{-y}2$ ground state and another with a d_z2 ground state for paramagnetic electron [19,34]. The presence of two monomeric species is evidenced by the simulation of the $Cu(oxazepam)_2Cl_2$ powder spectrum (thick solid line in Fig.5) by considering a superposition of the above rhombic spectrum (thin solid line in Fig.5) and one inverted spectrum ($g_{\perp}$ = 2.219, $g_{||}$ = 2.002) (dashed line in Fig.5). The proportion of these components at the whole spectrum is 4:1.

1.c Jahn-Teller effect in theophylline and nucleotide compounds with Cu(II)

The axial powder EPR spectrum of $Cu(theophylline)_2(NH_3)_2{\cdot}2H_2O$ compound with $g_{||}$ =2.255 and $g_{\perp}$ = 2.059 values suggests a compressed pseudotetrahedral symmetry around the metallic ion and a CuN_4 chromophore.

Powder EPR spectrum of $Cu_2(theophylline)_2(npa)_2{\cdot}2H_2O$ complex (Fig.6, thick solid line) is very large and quasiisotropic (g_{II} = 2.299, $g_{\perp}$ = 2.073). The simulation of the spectrum was made by considering a superposition in the same amount of one axial component (g_{II} = 2.299, $g_{\perp}$ = 2.081) and one isotropic component (g_0 = 2.089). The axial and isotropic spectra correspond to statical and dynamical compressed species through a Jahn-Teller effects, respectively.

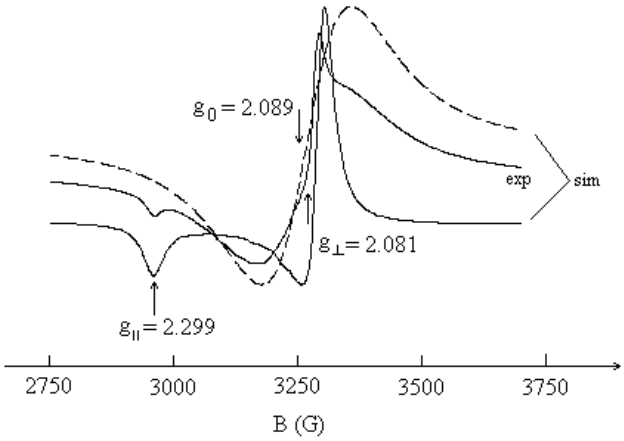

Fig.6 Powder EPR spectrum of pseudotetrahedral Cu(theophylline)$_2$(npa)$_2$·2H$_2$O complex at room temperature. The experimental spectrum (thick solid line - exp) and simulated spectra (thin solid line and dashed line, respectively - sim)

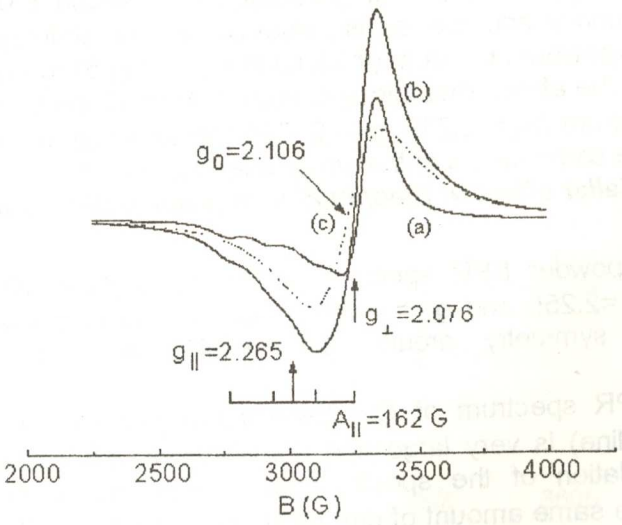

Fig.7. Powder EPR spectrum of Cu(II)–5'-CMP (a) the experimental spectrum, (b) the axial component, (c) the isotropic component

In DMF solutions adsorbed on NaY zeolite, both complexes of $CuN_2N^*_2$ chromophore present strong compressed pseudotetrahedral symmetries. (Table 1). The degree of the pseudotetrahedral compression was evaluated using the R(ω) dependence reported in [35] for CuN_4 chromophore, where R(cm) = $g_{\|}/|A_{\|}|$ and ω is the dihedral angle between each of the two coordination planes defined by a CuN_2 moiety.

Table 1. EPR parameters of DMF Cu(II)-theophylline solutions adsorbed on NaY zeolite at room temperature

Compound	$g_{\|}$	$g_{\perp}$	$\|A_{\|}\|$ (G)	R(cm)	ω(°)	α^2	β^2	δ^2
$CuT_2(NH_3)_2$	2.254	2.060	178	121	30	0.83	0.61	0.60
$CuT_2(npa)_2$	2.246	2.057	174	124	36	0.81	0.61	0.60

The distortion ω angle shows only a small deviation (≈15°) of the Cu-N bonds out of the xy plane. The Jahn-Teller energy (E_{JT} ≈ 2880 cm^{-1}) was calculated using the following expression [35,36]:

$$2E_{JT} = \frac{1}{3}e_{\sigma}(5-18\cos^2\theta+9\cos^4\theta) - \frac{9}{4}e_{\pi}(2-9\cos^2\theta+9\cos^4\theta)$$

where the energy values e_{σ} = 13400 cm^{-1} and e_{π} = 15400 cm^{-1} in the Angular Overlap Model (hole formalism) were determined from the diffuse reflectance spectra and the angle θ ≈73° between one Cu-N bond and the Oz axis with the same procedure like ω [35].

Powder EPR spectra of the Cu(II)–5'-CMP and Cu(II)–5'-GMP complexes obtained at room temperature suggest different local symmetries around Cu(II) ions.

The simulation of the Cu(II)–5'-CMP experimental spectrum (Fig.7a) indicates a superposition in the same amount between an axial spectrum ($g_{\|}$ = 2.265, $A_{\|}$ = 162 G, $g_{\perp}$ = 2.076) (Fig.7b) and an isotropic spectrum (g_0 = 2.106) (Fig.7c).

The axial spectrum corresponds to a penta-coordinated square-pyramidal (C_{4v}) species in which the Cu(II) ion is coordinated by three oxygen atoms (from cytosine base and phosphate groups) and one nitrogen atom (N3) in the xy plane and a water molecule along the Oz axis. The isotropic spectrum (instable in time) corresponds to a high symmetry species (octahedral) distorted by a dynamic Jahn-Teller effect [36], in which the Cu(II) ion interacts with the cytosine base, the phosphate group and two water molecules.

2. Spin labels dynamics in various environments

EPR studies of spin labels at liquid-solid interfaces, give valuable informations on the structure and dynamics of molecular interactions occurring in colloid systems. Two aspects were taken in consideration in our studies: liquid-inorganic surface support and liquid-organic surface support.

The adsorption of spin labels on inorganic support was studied using nitroxide radicals and hydrophilic (NaY zeolites and SiO_2 - Merck), hydrophobic(HY zeolites and SiO_2 -Arcc) and neutral (Al_2O_3 neutral) porous materials. The behavior of spin labels depends on the nature and hydroaffinity of surfaces, solvent nature and degree of hydration. For hydrophilic surfaces, the mobility of molecules decrease monotonically with decreasing of number of water molecules (Fig.8). In case of hydrophobic surfaces, due to the hydrophobic forces, the molecular mobility are strongly dependent on the first layer of water molecules on the surface. Thus, the molecular mobility is suddenly changed when only one water layer remains (Fig.9) [37,38]. Also, in the first layer of the hydrophobic surfaces the concentration of the paramagnetic centers increase and as result, spin-spin interactions are involved in dynamically processes [39]. The motion of the nitroxide radicals on porous surfaces is determinated by the existence of the strength of acidic sites, too. This effect was evidentiated using organic solutions with nitroxidic radicals and adsorbed on the inorganic supports with different strength and concentrations of the acidic sites [40-42].

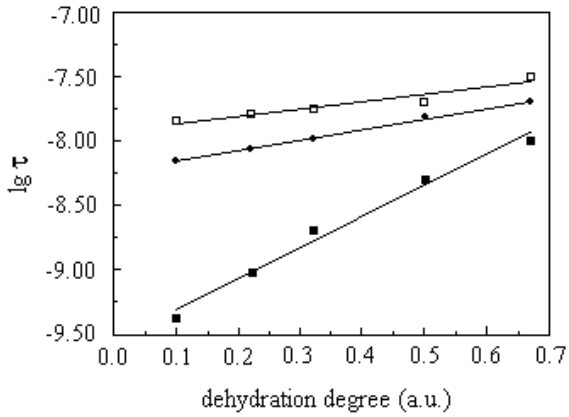

Fig.8 Correlation times vs. dehydration degree for nitroxide radicals adsorbed on SiO_2 hydrophilic (•, Tempyo; □, acetamide-Tempo; ■, oxo-Tempo; —, Cd linear fit)

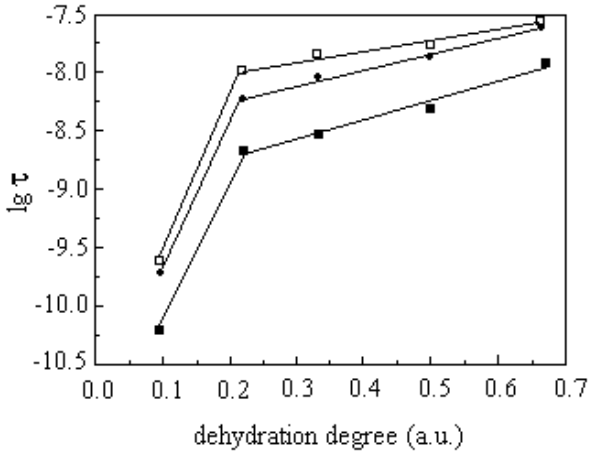

Fig.9 Correlation times vs. dehydration degree for nitroxide radicals adsorbed on SiO_2 hydrophobic (●, Tempyo; □, acetamide-Tempo; ■, oxo-Tempo; —, Q linear fit)

The EPR of nitroxide spin labeled biological molecules have been extensively used in the last decades for the study of their interactions, mobility and microenvironment in biological systems. The study of molecular processes at liquid-organic surface supports was perform using nitroxide radicals and new nicotinic acid derivatives spin label, as molecular probes, and organic polymers [43] (i.e. human blood plasma, bovine serum albumin and multilamelar liposomes) [44,45]. Two types of molecular interaction, corresponding to two paramagnetic species, were observed. One of the two species has an unusual low hyperfine constant and is due to the delocalization of the nitrogen unpaired electron, probably caused by a dipolar interaction. This interaction may be due either to a local association of two or more labeled molecules or to the presence of a biradical structure [46,47]. The rotational correlation time calculated from the magnetic data, assuming a Brownian diffusion model, correspond to a weakly increased viscosity of the environment.

3. The free radicals produced in γ - irradiated biomolecules

Part of our studies were focused on the free radicals produced in γ-irradiated biomolecules particularly since these radicals are key intermediates in the processes leading to biological damage of cellular

components. Among the investigated biomolecules we mention some antiinflammatory drugs and some aminoacids [48-55].

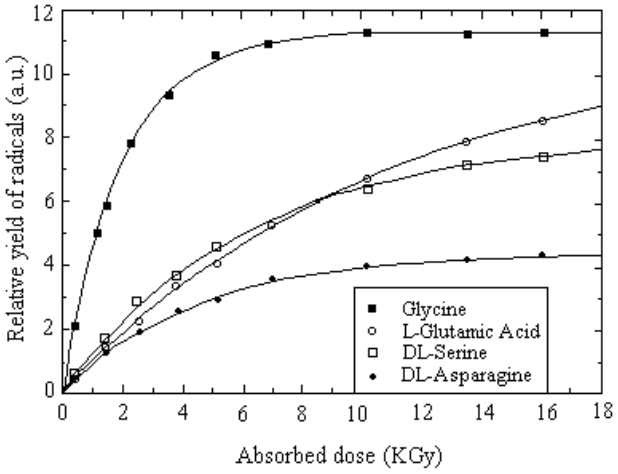

Fig.10 The relative yield of radicals in four γ-irradiated aminoacids as a function of dose. The continuous line represents the best-fit calculated values.

3.a The formation kinetics dependence of γ-irradiated dose

Some works have been done in order to study the formation kinetics in some γ-irradiated aminoacids and antiinflammatory drugs [48,49]. This kind of studies could provide very useful information about the possibility to use this type of biological samples for radiation control purposes. The number of the generated free radicals in γ-irradiated aminoacids increases almost linear for low values of doses, while for higher doses they approaches a limiting value over 8KGy (Fig.10). However, the dose response of the investigated γ-irradiated drugs is almost linear for low values of dose for all the samples while at higher values the intensity of the EPR signal tends slowly to saturate. Experimental data in Fig.10 were fitted by a function describing a first order kinetics and the constant of destroying the free radicals by the radiation were obtained for all the sample investigated. These constants are of the order 10^{-1} for the aminoacids and 10^{-2} for the irradiated drugs .

3.b The structure of the produced free radicals

An other important task in this field of high energy irradiation of biomolecules is to determine the structure of the produced free radicals. Using several advanced EPR techniques we were able to identify a new radical in a room temperature γ-irradiated single crystal of glycine [52]. This radical, CH_2NH_2, is produced by decarboxylation of the primary anion radicals and it is formed together the other two, $^{+}NH_3CHCOO^{-}$ and CH_2COO^{-}, observed by other authors in the past. The high field EPR (HF-EPR) spectra for a freshly and an aged γ-irradiated single crystal of glycine are shown in Fig.11. As it can be seen the hyperfine splitting of the low field triplet is about 11G and it is attributed to the new radical whereas that of the triplet indicated by the arrows is of 21G being associated to the radical CH_2COO^{-}.

ENDOR investigations have been done in the frequency interval 5-35MHz and three hyperfine tensors were obtained for the unknown radical CH_2NH_2.

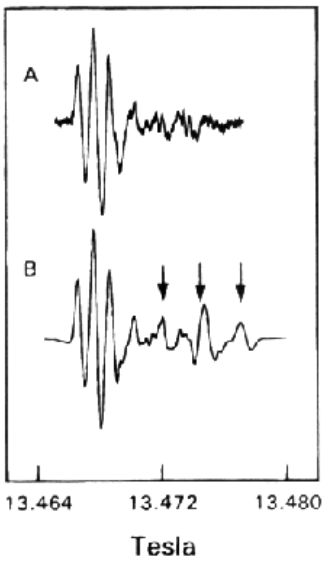

Fig.11 HF-EPR spectra with B||c. a) an aged glycine crystal and b) a freshly irradiated one.

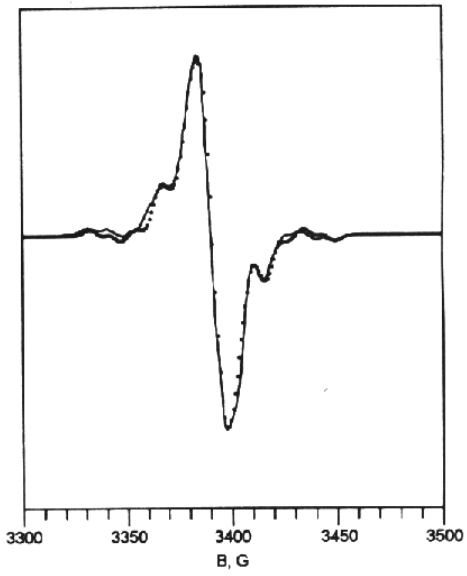

Fig.12 Experimental (continuous line) and simulated (dotted line) EPR spectra of γ-irradiated Aspirin at 159KGy.

An Electron Spin Echo Envelope Modulation (ESEEM) study has been also performed on this system confirming the ENDOR results. In addition, by a two-dimensional Hyperfine Sublevel Correlation (HYSCORE) experiment we observed that weak correlation peaks are present between the ν_+ frequencies of two protons of the radical CH_2NH_2, concluding that the two corresponding hyperfine couplings have different signs.

By a careful examination of the hyperfine tensors obtained by ENDOR spectroscopy it has been established that the radical CH_2NH_2 is not planar at the C site. The lengths of C-H_α bonds are R=1.061Å and 1.095Å for the two α-protons, respectively and the angle between the corresponding directions is 109.7^o. This structure has been also confirmed by semiempirical and *Ab Initio* calculations at UHF6-31G* level of theory [53].

Electron spin lattice relaxation time of radical $^+NH_3$-CH-COO^- has been determined by using the *Saturation Recovery* (SR) method in the temperature range 190-290K [53]. We have obtained the corresponding times lying in the range T_1=60-140μs. Fitting the dependence of T_1 versus temperature a value of 2.8KJ/mol has been obtained for the activation energy. This small value suggests an essentially free rotation of the NH_3 group around the C-N bond in the temperature range investigated.

Due to the fact that rather few attempts to identify the free radicals in γ-irradiated drugs were made we performed also a study of the γ-irradiated Aspirin [48]. EPR spectrum of this sample has changed by increasing the radiation dose suggesting that different radicals are formed depending on the absorbed dose. For low values of the doses the EPR spectrum consists of a triplet assigned to a radical of the form R-CH_2, produced by removal of a hydrogen atom from the methyl group, superimposed on a unique central line attributed to a radical of the type ROO^-, formed by hydrogen abstraction from the carboxyl group. As the radiation dose increases, besides the signals above mentioned a new signal having some hyperfine structure appears on its wings. This signal detected only over about 85KGy has little contribution to the total intensity of the spectrum and it is also saturated by increasing the microwave power level in the EPR cavity. We have attributed this signal to another radical produced by hydrogen addition at one of the carbons of the aromatic ring. The spectrum in Fig.12 is simulated assuming a mixture of the three radicals identified and the ratio 130:30:17 was found between their concentrations.

Our results are in very good agreement with the situation of the γ-irradiated cytosine were the yield of the free radicals produced by hydrogen abstraction is about ten times that of the addition radicals.

REFERENCES

1. J.R.J. Sorenson, "Metal Ions in Biological Systems", (H. Sigel, ed.), Marcel Dekker, New York, vol.14, 77 (1982).
2. J.R.J. Sorenson, V. Kishore, A. Pezeshk, L.W. Oberley, S.W.C. Leuthauser, T.D. Oberley, Inorg. Chim. Acta, 91, 285 (1984).
3. R.P. Ferrari, L. Paradisi, M. Torrielli, Anticancer Res., 9, 771 (1989).
4. R.G. Bhirud, T.S. Srivastava, Inorg. Chim. Acta, 173, 121 (1990).
5. O.Cozar, I.Bratu, I. Ardelean, S. Simon, V. Znamirovschi, Gh. Bora, Ext. Abstr. Congress Ampere, Stuttgart, 1990, p.590.
6. L. David, O. Cozar, V. Chiş, A. Negoiescu, I. Vlaşin, Appl. Magn. Res., 6, 521 (1994).
7. O. Cozar, L. David, V. Chiş, C. Cosma, V. Znamirovschi, G. Damian, Appl. Magn. Res., 8, 235 (1995).
8. O. Cozar, L. David, "Rezonanță electronică de spin pe sisteme paramagnetice cuplate", Ed. Presa Univ. Clujeană, 1999.
9. O. Cozar, I.Bratu, J.P. Huvenne, P. Legrand, Spectroscopy of Biological Molecules (J.C. Merlin, S. Turrel, J.P. Huvenne, Eds.) Kluwer Acad. Publ., London, 1995, p.553.
10. I.Bratu, V. Chiş, L. David, O. Cozar, Gh. Bora, P. Legrand, J.P. Huvenne, Spectroscopy of Biological Molecules (J.C. Merlin, S. Turrel, J.P. Huvenne, Eds.) Kluwer Acad. Publ., London, 1995, p.557.
11. L. David, O. Cozar, I.Bratu, V. Chiş, Gh. Bora, Studia UBB, ser. Physica, 40, 25 (1995).
12. O. Cozar, I.Bratu, L. David, V. Chiş, J.P. Huvenne, P. Legrand, Conference on Isotopic and Molecular Processes, Cluj-Napoca, 1999, p.91.
13. C. Preti, G. Tosi, Transition Met. Chem., 3, 246 (1978).
14. M.A. Cinellu, M.L. Ganadu, G. Minghetti, F. Cariati, F. Demartin, M. Manassero, Inorg.Chim.Acta, 143, 197 (1988).
15. O. Cozar, L. David, V. Chiş, E. Forisz, C. Cosma, G. Damian, Fressenius Journal of Analyt. Chemistry, 355, 701 (1996).
16. O. Cozar, L. David, V. Chiş, Balkan Phys. Letters, 6, 220 (1998).
17. O. Cozar, L. David, A. Hernanz, R. Navarro, E. Forizs, I. Bratu, Spectroscopy of Biological Molecules; Modern Trends (P. Carmona, R. Navarro, A. Hernanz, Eds.) Kluwer Acad. Publ., London, 1997, p.625.
18. E. Forizs, L. David, O. Cozar, C. Crăciun, M. Venter, M. Kilyen, J. Molec. Structure, 408, 195 (1997).
19. E. Forizs, L. David, O. Cozar, V. Chiş, R. Tetean, M. Todică, Appl. Mag. Resonance, 16, 499 (1999).

20. E. Forizs, O. Cozar, L. David, D. Ristoiu, C. Crăciun, C. Bălan, Studia UBB, ser. Physica, 42, 31 (1997).
21. L. David, O. Cozar, E. Forizs, V. Chiş, C. Crăciun, Balkan Phys. Letters, 5, 219 (1997).
22. O. Cozar, L. David, C. Crăciun, Roum. J. Physics, 43, 561 (1998).
23. E. Forizs, L. David, O. Cozar, V. Chiş, G. Damian, J. Molec. Structure, 482, 143 (1999).
24. L. David, O. Cozar, E. Forizs, C. Crăciun, D. Ristoiu, C. Bălan, Molec. And Biomolec. Spect., Spectrochimica Acta, Part A, 55, 2559 (1999).
25. M. de la Fuente, O. Cozar, L. David, R. Navarro, A. Hernanz, I. Bratu, Molec. And Biomolec. Spect., Spectrochimica Acta, Part A, 53, 637 (1997).
26. O. Cozar, I. Bratu, L. David, A. Hernanz, M. de la Fuente, C. Bălan, Conference on Isotopic and Molecular Processes, Cluj-Napoca, 1999, p.93.
27. C.J. Doumit, G.L. McPherson, R.L. Belford, S.B. Lanoux, H.B. Jonassen, Inorg. Chem., 16, 565 (1977).
28. N.D. Chasteen, Inorg. Chem., 10, 2339 (1971).
29. O. Cozar, I. Ardelean, J. Non Cryst. Solids, 92, 278 (1987).
30. O. Cozar, V. Znamirovschi, Rev. Roum. Phys., 23, 87 (1978).
31. R.M. Semeniuc, O.Cozar, L.David, V. Chiş, R. Semeniuc, Rev. Roum. Chimie, 42, 627 (1997).
32. L. David, O. Cozar, V. Chiş, D. Ristoiu, C. Bălan, Studia UBB, ser. Physica, 42, 49 (1997).
33. R.M. Semeniuc, R. Semeniuc, O.Cozar, L.David, Synthesis and Reactivity in Inorganic and Metal-Organic Chemistry, 28, 501 (1998).
34. Z. Lu, C. Duan, Y.X. Tian, X. Huang, Inorg. Chem. 35, 2253 (1996).
35. J. Gouteron, S. Jeannin, Y. Jeannin, J. Livage, C. Sanchez, Inorg. Chem., 23, 3387 (1984).
36. D. Reinen, Comments Inorg. Chem., 2, 227 (1983).
37. G. Damian, O. Cozar, V. Miclăuş, Cs. Paizs, V. Znamirovschi, V. Chiş, L. David, Colloids and Surfaces A: Physicochemical and Engineering Aspects 137, 1 (1998).
38. G. Damian, V. Miclăuş, O. Cozar, V. Znamirovschi, R. Salomir, Abstract "Conferința Națională de Biofizică", Cluj-Napoca16-18 oct. 1997, p.7.
39. G. Damian, O. Cozar, V. Miclăuş, Cs. Paizs, M. Todică, V. Chiş, Balkan. Phys. Lett., 5, 289 (1997).
40. G. Damian, V. Znamirovschi, O. Cozar, V. Miclăuş, Cs. Paizs, V. Chiş, L. David, M. Todică, Abstract "VIIth Interanational Symposium on Magnetic Resonance in Colloid and Interface Science, ISMRCIS VII" Madrid, Spain, 11-15 sept. 1995, p.121.

41. G. Damian, V. Znamirovschi, O. Cozar, M. Todică, V. Chiş, L. David, R. Salomir, Studia UBB, ser. Physica, XLI, 1, 49 (1996).
42. G. Damian, V. Miclăuş, V. Znamirovschi, O. Cozar, N. Dulamita, V. Chiş, L. David, Progress in Catalysis, 7 (2), 61 (1998).
43. M. Todică, O. Cozar, G. Damian, L. David, J. Molec. Structure, 482, 355 (1999).
44. G. Damian, S. Bossman, V. Miclăuş, C.M. Lucaciu, Abstract "Specialized Colloque Ampere", 14-18 June, 1999, Pisa, p.153.
45. G. Damian, S. Bossman, V. Miclăuş, C.M. Lucaciu, Abstract on Colloquium Spectroscopicum Internationale XXXI, sept. 5-10, 1999, Ankara, p.445.
46. C.M. Lucaciu, S. Bossman, V. Miclăuş, G. Damian, Abstract on Colloquium Spectroscopicum Internationale XXXI, sept. 5-10, 1999, Ankara, p.344.
47. V. Miclăuş, G. Damian, S. Cavalu, C.M. Lucaciu, Abstract "Vth National Byophysics Conference", Târgu Mureş, 5-6 nov. 1999, p.84.
48. O.Cozar, V.Chiş, L.David, G.Damian, I.Barbur, J.Radioanal.Nucl.Chem., 220, 241 (1977).
49. V.Chiş, G.Damian, L.David, O.Cozar, V.Znamirovschi, L.Kazimirski, Studia UBB Ser.Physica, 42, 33 (1997).
50. V.Chiş , O.Cozar, G.Damian, L.David, C.Cosma, R.Semeniuc, T.Drăgoiu, Studia UBB, Ser.Physica, 39, 17 (1994).
51. V.Chiş, PhD Thesis, Babeş-Bolyai University, 1998.
52. M.Brustolon, V.Chiş, A.L.Maniero, L.C.Brunel, J.Phys.Chem., 101, 4887 (1997).
53. V.Chiş, M.Brustolon, C.Morari, O.Cozar and L.David, J.Molec.Struct., 482, 283 (1999).
54. V.Chiş, M.Brustolon, A.L.Maniero, L.David, O.Cozar, D.Ristoiu, Balkan Phys.Lett.Suppl., 5, 227 (1997).
55.
55. V.Chiş, M.Brustolon, O.Cozar, L.David, S.Simon, A.Darabont, Balkan Phys.Lett.Suppl, 5, 223 (1997).

STUDIA UNIVERSITATIS BABEŞ-BOLYAI, PHYSICA, XLIV, 2, 1999

METALLIC NANOSTRUCTURES IN SURFACE ENHANCED RAMAN SPECTROSCOPY

T. ILIESCU*, S. CÎNTĂ*, D. MANIU*, S. ASTILEAN*

ABSTRACT. In this paper an introduction to surface-enhanced Raman scattering (SERS) is presented. The main enhancement mechanisms are discussed. A very recent fundamental development, as single-molecule spectroscopy is reviewed. SERS of some biological interest molecules (drugs), studied in our department in the last years, are presented.

1. Introduction

Nanometer scale structures represent an exciting, challenging, and rapidly expanding area of research that crosses the borders between many areas of the physical science and engineering [1].

Surface metallic nanostructure obtained in different ways allow to observe surface enhanced spectroscopy which include: surface enhanced Raman scattering (SERS), enhanced absorption, enhanced fluorescence, enhanced photochemistry and enhanced second harmonic generation.

The present discussion is restricted to the enhancement of the Raman signal. SERS has been discovered twenty five years ago being a very exciting field, firstly, in explaining the mechanisms of the enhancement and secondly, for many applications in various fields which include electrochemistry, chemical physics, solid state physics, biophysics, environment and even medicine.

In last years a new direction of SERS is developed, the single molecule vibrational spectroscopy, which promises to be a very interesting area for both theoretical and experimental study.

2. History and fundamentals

SERS phenomenon was firstly observed by Fleischmann et al [2]. They observed intense Raman scattering from pyridine adsorbed onto a roughened silver electrode surface from aqueous solution. Fleischmann's

* "Babes-Bolyai" University, Physics Faculty, Optics and Spectroscopy Department, Kogalniceanu 1, RO 3400 Cluj-Napoca, Romania

approach was to roughen the electrode to increase its surface aria and, hence, the number of adsorbed molecules available for study.

Independently Jeanmaire and Van Duyne [3] and Albert and Creighton [4], recognized that the large intensity observed could not be accounted for simply increasing the number of present scatterers. They suggested that an enhancement of the scattered intensity could occur in the adsorbed state.

SERS has been observed for a very large number of molecules adsorbed on the metal surface. Silver, gold and copper were mostly used as SERS substrates but works have been reported on the alkali metals and some few others.

The largest enhancements occur for the surfaces, which have rough on the nanoscale (10-100 nm). These include electrode surfaces roughened by oxidation-reduction cycles, island films deposited on the glass surface, colloids (especially aggregated colloids).

The irregularly roughened substrates generally exhibit poor reproducibility.

Electron-beam lithography offers the possibility to obtain a very reproducible nanoscale structured surface as the gratings and crossed gratings with independent varying period, width and depth [5].

Differences between SERS and ordinary Raman spectroscopy of molecules and solids could be largely. The intensity of the observed bands fall off with increasing vibrational frequency, overtones and combination bands are not commonly, selection rules are relaxed resulting in the appearance of normally forbidden Raman modes in the surface spectra.

It is now widely accepted that SERS is due to enhanced electromagnetic fields at or very near the metal surface (electromagnetic mechanism) and for increasing of the molecular polarizability of the new molecular species, so called molecule-metal complex, obtained by chemisorption (chemical mechanism).

3. Electromagnetic mechanism

The electromagnetic field at the surface can be greatly enhanced under condition of surface plasmon excitation.

Nonradiative plasmon specific to that surface, cannot transforms into the light because its momentum is larger than that of light of the same energy. Surface roughness can help to change the momentum of nonradiative plasmons allowing transformation of nonradiative modes into radiative and thereby enhancing the scattering process.

Full electrodynamics calculations have been carried out for the simple systems as the metal spheres, whose radius are much smaller than

the wavelength of the light, the electric field being uniform across the particle (Rayleigh approximation)[6].

The induced electric field at the surface of the sphere is related to the applied external (laser) field by eq. (1) where $\varepsilon_1(\omega)$ is the complex "dielectric" function of the metal, and ε_2 is the relative permittivity of the ambient phase:

$$E_{induced} = \{[\varepsilon_1(\omega) - \varepsilon_2(\omega)]/[\varepsilon_1(\omega) - 2\varepsilon_2(\omega)]\}E_{laser} \quad (1)$$

By changing the frequency the resonance can be obtained for $Re(\varepsilon_1) = -2\varepsilon_2$.

In this case, the sphere can be considered as a time dependent dipole.

Different metals have their surface plasmon resonance in different spectral regions.

The plasmon excitation can occur either from incident light or from Raman (stokes) scattered light which is nearly resonant with surface plasmon, the enhanced signal being proportional to $E^2_{Laser}.E^2_{Raman}$.

This fact explains the decrease in observed intensity of the high wavenumbers vibrational bands, when the surface plasmons are excited by the laser field **or** the Raman field but not both.

The electromagnetic mechanism provides a long-range enhancement. The Raman spectrum of the molecule, which is physisorbed on the metal surface is similar to Raman spectrum of unadsorbed molecule. This is the key for the differences of this mechanism from other mechanisms.

4. Chemical mechanism

Electromagnetic enhancement should be a nonselective amplifier in surface enhanced Raman scattering for all molecules adsorbed on a particular surface. However, in the same experimental conditions, the SERS intensity is different for different molecules.

A surface potential dependence of SERS intensity is another fact that can not be explained by electromagnetic mechanism. These observations can be explained by a resonant Raman mechanism in which either **(a)** the electronic state at the adsorbed is shifted and broadened by their interaction with the surface or **(b)** new electronic states which arise from chemisorption serve as resonant intermediate states in Raman scattering (chemical mechanism provides a short range enhancement).

It is very difficult to select the contributions of electromagnetic and chemical mechanisms in the enhancement factor. However when the band

positions are the same as in the spectrum of free molecules, we have a physisorption, when the electromagnetic mechanism is responsible for SERS signal. When the chemical mechanism is present, a change in peak positions is observed because new species, molecule-metal complex, is formed.

5. Single molecule spectroscopy

Recently, Kneipp et al [7] and Nie and Emory [8] observed extremely large Raman cross section on the order of 10^{-17} –10^{-16} cm^{-2} per molecule in SERS experiment using near-infrared excitation for dyes adsorbed on colloidal silver. These enormous cross section provided the hope of using SERS for single molecule detection as a complementary method to fluorescence [9], which can offer exciting new aspects: **(1)** A SERS vibrational spectrum provides a high degree of structural informations about molecule. **(2)** Because of the shorter vibrational relaxation time compared to electronic relaxation time, the number of Raman photons per time unity that can be emitted by a molecule under saturation condition, will be higher than the number of fluorescence photons whit about a factor of 10^3. This allows shorter integration time for detecting a molecule or higher rates for counting single molecule. **(3)** SERS avoids photodecomposition of the probed molecules because the excitation energy is not in resonance with molecular transitions.

The single molecule spectroscopy opens new horizons for research into basic questions related to both dynamics and function of molecule, which might be completely marked by the inhomogeneous distribution of environments that usually surround these molecules in solids and liquids. For the molecules adsorbed on a surface, the environment of each molecule will dictate its exactly physical behavior, such as its absorption or emission spectrum. An optical measurement involves the whole assembly, which entails an average over the distribution of environments, sampled by different molecules.

A measurement on a single molecule overcomes this overseeing problem, and allows much more delicate informations on the interaction of each molecule with its surroundings to be collected [10].

6. SERS studies in Optics and Spectroscopy department

Our SERS studies are focused on two directions.

First direction is related to the vibrational analysis of some molecules of biological interest in order to establish the possibility of adsorption on the metal (especially silver) surface and to verify if the

biological properties of adsorbed molecules are the same as the free molecules.

The molecules of biological interest were chosen because many of them present a large fluorescence in visible excitation and after adsorption on silver surface, the fluorescence is quenched. In this way, SERS offers the possibility to obtain vibrational informations on these molecules.

Outstanding to the high sensibility of SERS, we can also obtain the information about the absorption of these molecular species in human body. Infrared spectroscopy is not usually in this study owing to the high absorption of water contained in the human tissue.

The molecular species studied by SERS are 9-phenylacridine (9PA) [12], 9-methylacridine (9MA) [13], PP vitamin (nicotinamide, PPV) [14-16], B_6 vitamin (B6V) [17], 2,4-diamino-6-phenyl-1,3,5-triazine (DTP) [18], triazenido complexes (TAC) [19] and 1,4-benzodiazepine drugs (BOA) [20].

In most cases the SERS support was silver colloid prepared in usual way [4].

For 9PA, 9MA and PPV, the influence of pH values on SERS spectra was studied. In all cases SERS spectra were compared to the ordinary Raman and IR spectra. Visible absorption spectra of silver sol after addition of 9PA, 9MA and PPV present besides the band at ~400 nm specific to plasma resonance absorption of silver sphere in water, a new broad band at longer wavelength. This new band is an indication of the aggregation of sol, which is very important for SERS observation, confirming the contribution of the electromagnetic mechanism to the enhancement.

The change in frequency and relative intensity of 9PA, 9MA bands after adsorption are consistent with 9PA and 9MA adsorption via nitrogen lone pair electrons. At low pH values, $9PAH^+$ $9MAH^+$ (phenylacridinium and 9-methylacridinium ions) were adsorbed via chloride ions. At large pH values neutral form of 9PA and 9MA are adsorbed on the silver surface.

According to electromagnetic surface selection rules, a vibrational mode with its perpendicular component to the metal surface is likely to become more enhanced than the parallel one. Because the ring stretching modes of 9PA, 9MA in their protonated form are more enhanced compared to the other, we assume all these species to be perpendicular or, at least tilted with respect to the silver surface.

The PPV was found to adsorb onto the silver surface in neutral form at large pH values and in protonated form at low pH values. It was found that a strong interacting amide-metal group is present in protonated form. The ring nitrogen-metal interaction has an important role in the adsorption process at neutral form.

SERS spectra of PPV in aqueous gold colloid as well as on thermal evaporated and laser ablate silver island films were recorded and compared to the corresponding FT-Raman spectrum of free species. The enhancement on different surfaces was compared through the relative intensities I_1/I_{12} of the SERS bands assigned to the symmetric ν_1 and ν_{12} mode of PPV. Interaction between the N ring and each metal surface was confirmed based on the near coincidence both in wavenumbers and relative intensities of the SERS fingerprint bands assigned to the ν_1 and ν_{12} modes. Both mechanisms, the electromagnetic and the chemical one, give the contribution in enhancement factor.

The PPV–Au colloidal system was found to be the most efficient SERS complex .

Theoretical ab-initio (3-STO) and semiempiric (PM3) IR spectra of isolated B_6 vitamin (B6V) molecule have been obtained and found in good agreement with the experimental IR spectrum. FT-Raman spectrum of the B_6 vitamin in solid polycrystalline state, polarized Raman as well as the Raman and SERS spectra on Ag colloidal surface at different pH values, have been recorded and discussed. The protonated and deprotonated form of the B_6 molecule was evidenced from the pH dependence Raman spectra. SERS bands associated to the chemical interaction between the deprotonated N ring atom and Ag colloidal particles were absent compared to the related polysubstituted pyridine molecules, a different SERS behavior of molecule was concluded.

Raman and IR vibrational studies of 2,4-diamino-6-phenyl-1,3,5-triazine (DTP) proved the existence of only one protonated form of the DPT molecule.

Neutral DPT is adsorbed on the Ag surface through one N atom from triazinic skeletal plane resulting in a perpendicular orientation of the molecule on the metal surface. The adsorption of the DPT ion is more favorable through the N atom of the $–NH_2$ group which remains after protonation of the other one. The orientation of the skeletal plane of the DPT ion on the Ag surface is more or less vertical.

The reaction of neutral 1,3-diphenil triazenide derivatives PhNHNNPh with $[(PPh_3)_2Cu(CH_3COO)]$ leads to a mixture of different coordinated Cu(I) complexes (TPPC) in contrast to the homologue complexes containing bidentate triazenido ligands $[(PPh_3)Cu(TolNNNTol)]_2$ and $[(PPH_3)_2Cu(XC_6H_4NNNC_6H_4Y)]$, with X = H, Y = Me. The SERS spectrum of the reaction product reveals the strong enhancement of the ν(N=N) mode, characteristic to the monodentate ligand, in contrast to the commonly enhanced band ν(NNN) of the related studied complexes with bidentate triazenido ligands. The complete analysis of the SERS spectrum

elucidates the nature of the mixed Cu(I) triazenido complexes in the reaction product and strongly suggests the presence of the main complex with monodentate coordinated Cu(I) adsorbed on the Ag surface.

From the SERS spectrum of diazepam and nitrazepam we concluded that the C=N bond vibration of 1,4-benzodiazepine is strongly affected by adsorption and enhanced. The SERS system of Ag colloid with diazepam and nitrazepam allow the recognition of the drug sample at concentration of 10^{-7} mol l^{-1}.

The second direction of our SERS studies is focused on the possibility to obtain the new stable and reproducible SERS support.

We are currently interesting in this direction and our approach combines the rigorous coupled-wave analysis with several lithographic technologies in order to produce high quality optimized silver structures at nanometric scale [21]. It is for the first time that this computational approach is used to study the electromagnetic enhancement in SERS. From the magnitude of the local field enhancement, a silver grating-structure has been optimized as o function of their geometrical parameters and the excitation wavelength in order to be used as spectroscopic enhancers for the Raman signal.

Conclusions and perspectives

Together with the new detecting equipment and data analysis, a strong branch of vibrational spectroscopy –*Surface Enhanced Vibrational Spectroscopy*- has reached maturity and has become a very active area of basic research with a broad range of analytical applications.

The ability of SERS for in-situ detection of hazardous chemical substances in different biological or environmental samples, the sensitivity and the benefit of fluorescence quenching, the molecular specificity of these surface enhanced techniques are suitable for lowering detection limits of vibrational spectroscopy even to one molecule detection. Changing the statistic spectral response into one molecule spectral signal, turns into a new light the theoretical and experimental aspects of molecular spectroscopy.

An entire challenge field of analytical applications involving from two-dimensional infrared methods, infrared and Raman microscopy and vibrational imaging, combined with surface enhanced techniques is broad open.

Getting insight into the molecule-surface interaction and the mechanisms at the interface leads to a new approach in the interface phenomena, like corrosion, lubricates, catalysis.

REFERENCES

1. Nanostructure and Mesoscopic Systems (Ed. by M. A. Reed, W. Kirk) Academic Press, San Diego, (1992).
2. M. Fleischmann, P. J. Hendra, A. J. Mc-Quillan, Chem. Phys. Lett., **26**, 163, (1974).
3. D. L. Jeanmaire, R. P. Van Duyne, J. Electroanal. Chem., **84**, 1, (1977).
4. M. G. Albert, J. A. Creighton, J. Am. Chem. Soc., **99**, 5215, (1977).
5. M. Kohl, E. Voges, W. Hill, Spectroscopy Europe, **10**, 8, (1998).
6. M. Moskovits, Rev. Mod. Phys., **57**, 783, 91985).
7. K. Kneipp, Y. Wang, H. Kneipp, L. Perchman, I. Itzkan, R. R. Dasari, M. S. Feld, Phys. Rev. Lett., **78**, 1667, (1997).
8. S. Nie, S. R. Emory, Science, **275**, 1102, (1997).
9. R. A. Mathies, K. Peck, Anal. Chem. **62**, 1786, (1990).
10. T. Ha, T. Enderle, D. S. Chemla, P. R. Selvin. S. Weis, Phys. Rev. Lett., **77**, 979, (1996).
11. G. Pryhusest, Electrochemistryy of Biological Molecules, Academic Press, New York, p.473, (1977).
12. T. Iliescu, I. Marian, R. Misca, v. Smarandache, Analyst, **119**, 567, (1994).
13. T. Iliescu, M. Vlassa, M. Caragiu, I. Marian, S. Astilean, Vibrational Spectr., **8**, 451, (1995).
14. T. Iliescu, S. Cinta, S. Astilean, I. Bratu, J. Mol. Struct., **410-411**, 193, (1997).
15. T. Iliescu, S. Cinta, S. Astilean, I. Bratu, Studia Univ. Babes-Bolyai, Seria Physica, **39**, 39, (1994).
16. S. Cinta, E. Vogel, D. Maniu, M. Aluas, T. Iliescu, O. Cozar, W. Kiefer, J. Mol. Struct., **482-483**, 679, (1999).
17. S. Cinta, C. Morari, E. Vogel, D. Maniu, M. Aluas, T. Iliescu, O. Cozar, W. Kiefer, Vibrational Spectr., **19**, 329, (1999).
18. S. Cinta, T. Iliescu, M. Venter, O. Cozar, J. Mol. Struct., **410-411**, 189, (1997).
19. S. Cinta, M. Venter, T. Iliescu, O. Cozar, I. Haiduc, W. Kiefer, Vibrational Spectr., **19**, 679, (1999).
20. S. Cinta, T. Iliescu, S. Astilean, L. David, O. Cozar, W. Kiefer, J. Mol. Struct., **482-483**, 685, (1999).
21. S. Astilean, Ph. Lalanne, P. Chavel, E. Cambril and H. Launois, Opt. Lett. **23**, 552, (1998).

STUDIA UNIVERSITATIS BABEŞ-BOLYAI, PHYSICA, XLIV, 2, 1999

TRANSPORT PHENOMENA AND MAGNETIC PROPERTIES IN Bi:2223 BULK SUPERCONDUCTORS DOPED WITH Cr

**G. ILONCA*, A. V. POP*, C. LUNG*, G. TARTA*,
N. DULAMITA*, M. MATEI* AND R. DELTOUR****

We had performed a study on magnetoresistivity Hall, Nernst, Seebeck effects in the mixed and normal state for Bi:2223 bulk with Cr $0 \le x \le 0.07$ doped, prepared by the conventional solid state reaction method in magnetic fields between 0 and 5 T and in the temperature range 5-300 K. The critical temperatures, ac susceptibility, Hall concentration, Nernst and Seebeck coefficients depend strongly on the Cr content in the samples. The linear dependence of intergranular temperature T_P on ac field amplitude aggress with the Muller critical state model. The anomalies oh Hall concentration $n_H(T)$ and inverse mobility $\mu_H^{-1}(T^2)$ around 240 K, are discussed in the framework of phase separation theory. The experimental data in the mixed state are in agreement with the prediction of the time dependent Ginsburg-Landau theory.

1. Introduction

In the mixed state of high temperature superconductors the motion of the flux lines leads to Hall effect and magnetoresistivity due to an applied current that induce Lorentz force and to the occurrence of variety of large thermomagnetic effects, when a thermal gradient is applied to the flux-line lattice. Also, high – T_C cuprates are characterized by a large number of anomalous "normal – state" properties observed in resistivity, Hall effect, thermoelectric power, magnetic susceptibility, etc.

As for the transport, several reports have been published for $La_{2-x-y}RE_ySr_xCuO_4$ (RE rare earth elements), for $Bi_2Sr_2Ca_n(Cu_{1-x}M_x)_{n+1}O_y$ and $YBa_2(Cu_{1-x}M_x)_3O_{7-\delta}$ families, with M = Zn, Fe, Ni, Al, Ga, Co [1-14].

In this paper, we report the effect of the partial states of the galvanomagnetic effects for $(Bi_{1.6}Pb_{0.4})(Sr_{1.8}Ba_{0.2})Ca_2(Cu_{1-x}Cr_x)_3O_y$ bulk doped with Cr, $0 \le x \le 0.7$

* Babes Bolyai University, 3400 Cluj - Napoca
** Universite Libre Bruxelles, Physique des Solides CP 233, 1050 Bruxelles, Belgium

2. Experimental Details

Sintered samples of $(Bi_{1.6}Pb_{0.4})(Sr_{1.8}Ba_{0.2})Ca_2(Cu_{1-x}Cr_x)_3O_y$ samples were prepared by the conventional solid state reaction method. The high purity materials of Bi_2O_3, $SrCO_3$, $CaCO_3$, $BaCO_3$, CuO and Cr_2O_3 powders, were used. The powders were mixed and prefired at 800 ^oC for 15h in air. Then they reground, pressed into pellets and sintered for 30h at temperature of 860 ^oC in controlled oxygen atmosphere. In order to increase the oxygen content, the samples were annealed in situ for 4h at 450 ^oC in oxygen atmosphere and cooled down to room temperature at 10K min^{-1} rate. This sintering process was carried out once again so as to obtain homogeneous samples. The examination by X ray diffraction, X ray analysis (EDAS) and optical microscopy revealed a single phase, with impurity level being less than 1-2%. The electrical resistivity and Hall voltage were measured by the standard DC method, using a Keithly 220 programmable current source and the Keithly 182 sensitive digital voltmeter.

The Seebeck coefficients were measured by the standard method using a temperature gradient as small as possible in order to minimize the temperature difference between the two voltage leads. The Seebeck coefficient of the samples was obtained by substituting the cooper thermopower from the measured thermopower.

Cylindrical specimens were cut from the sintered samples and used for ac susceptibility measurements. The real (χ') and imaginary (χ'') parts of the ac susceptibility were simultaneously collected with a Lake Shore Model 7000 ac susceptometer. The measurements were performed at a frequency of 666.7 Hz as a function of temperature at fixed ac magnetic field amplitude (H_{ac}) in a range from 0.4 to 800 Am^{-1}. The ac field was applied parallel to the cylindrical axis.

3. Results and Discussions

The temperature dependence of the magnetoresistivity, Hall, Nernst and Seebeck coefficients, in the temperature range 50-130 K, at different magnetic fields up to 5T, for Bi 2223 doped with Cr were investigated. Figure 1 shows the results for the sample with x=0.04 Cr.

The Nernst electric field begins to increase up to the thermal energy fluctuations pass through a maximum, with shifts toward lower temperature with the increasing of the magnetic field and becomes immeasurable small at the same temperature as the resistivity. The tails of the temperature dependence curves of the R_HB,NB, S and magnetoresistivity are caused by fluctuation effects which increasing magnetic field, in agreement with others

data [10-19], and valid of the theories [15,19] based on the dependent of Ginsburg – Landau theory.

The Hall data show in the normal state that the Hall coefficient is positive and independent of applied field. In the mixed state the samples shown a sign anomaly of the Hall coefficient at low magnetic field just below the transition temperature. This behavior is the standard – one observed in HTSC. Based on our experimental data, we have calculated following parameters: $\xi \approx 14\,\mathring{A}$, $\lambda_L \approx 2650 - 2750\,\mathring{A}$, $\frac{dB_{C2}}{dT} \cong -2.50\,T/K$ and $B_{C2}(T = 0K) = 162T - 118T$. These values are dependent of the Cr content.

All samples, in the normal state above the paraconductive region a linear temperature dependence on the resistivity $\rho_n = \rho_0 + aT$. The increase in the residual resistivity, $\rho(0)$ from 15 $\mu\Omega cm$ to 65 $\mu\Omega cm$ with increasing x from 0 to 0.07 Cr is accompanied by the depression of the critical transition temperature T_C from 108 to 65 K [14]. The decrease of the critical temperature with $\Delta T_C = 43K$ in our x=0.07 Cr sample, agrees with the value of the slope $\frac{dT_c}{dx} = -6K/at\%$ Cr. This results suggests that Cr atoms substitute partial Cu in the Cu-O pyramids in our (Bi,Pb):2223 superconductor. These results are in accord with the results provided by the ac magnetic susceptibility.

Figures 2 (a), (b) show the $\chi''(T)$ behavior x=0.00 Cr and x=0.02 Cr samples. If H_{ac} is lower than the Josephson lower critical field H_{C1J}, at low temperature, the real part $\chi'(T)$ saturates corresponding to full diamagnetic shielding (χ'=-1). The imaginary part χ'' approaches the value zero in the absence of any losses. By increasing temperature, the diamagnetic contribution to the χ' value decrease because of the flux penetration in the intergranular Josephson junction regions.

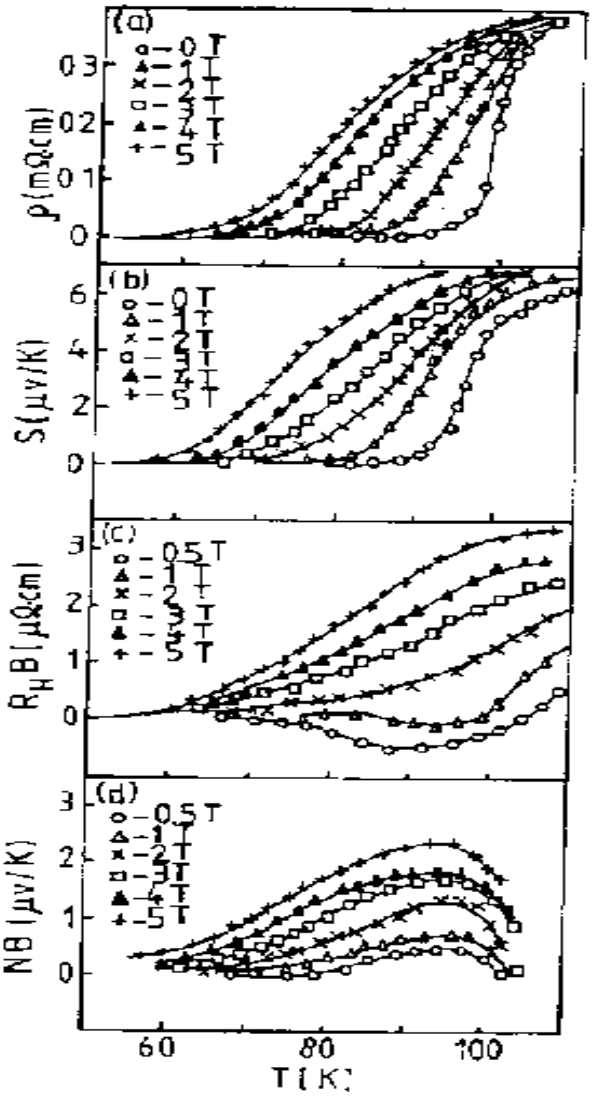

Fig. 1. The temperature dependence of the electrical resistivity, Hall, Seebeck and Nernst coefficients for x=0.02 Cr in the magnetic field B=0-5T

The real $\chi'(T)$ shows a two-step behavior characterizing the flux penetration in the intergranular matrix and in the grains respectively. The inflection point in the lower drop in the $\chi'(T)$ curve may be assigned to the intergrain critical temperature T_{CJ} while the end of the upper step (the end of the superconductor diamagnetism) corresponds to the intragrain critical temperature T_{CG}. The T_{CG} values are 108 K in x=0.00 Cr and 99K in x=0.02

Cr. The decrease of T_{CG} in our x=0.02 Cr bulk samples agrees with that found in Fe ad Ni doped Bi 2212 single crystals [20].
For x=0.00 and x=0.02 Cr samples, imaginary part of the ac susceptibility, $\chi''(T)$, exhibits two peaks at T_P and T_G, which indicates inter- and intragranular dissipation [21].

The loss peaks shift to lower temperature by increasing H_{ac}. In our samples T_{CG} are very close to the inflection point temperatures T_C in the resistivity measurements, and T_P temperatures are nearly the same as the resistivity temperatures $T_C(\rho = 0)$ [22].

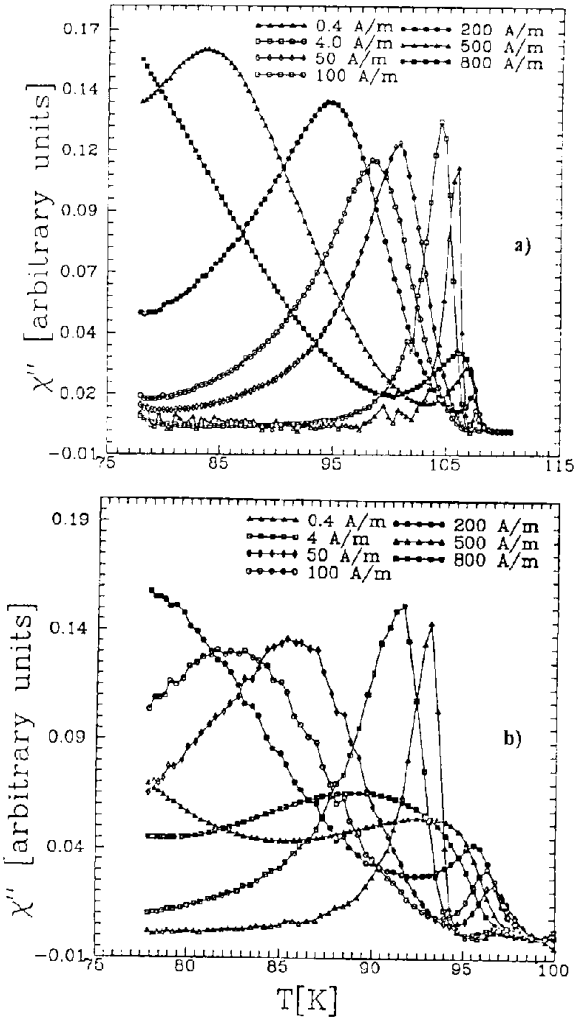

Fig.2. Temperature dependance of the imaginary part X'' of ac susceptibility for (a) x=0.00 and x=0.02Cr samples at different ac field amplitudes Hac ranging from 42 to 800 am^{-1}.

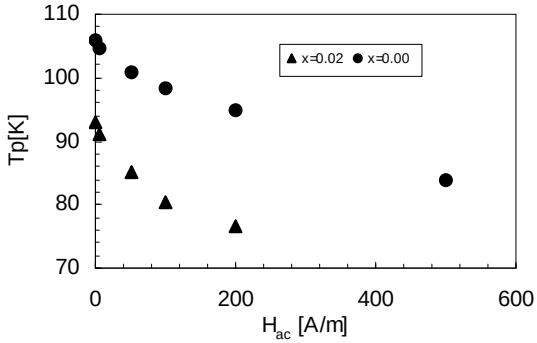

Fig.3. Intergranular X"-peak temperature T_p versus ac field amplitude for x=0.00(circles) and x=0.02 Cr (dark triangles)

In order to investigate the effect for partial substitution of Cu with Cr on the intergranular pinning force, we studied the T_P dependence as a function of H_{ac}. As can see from figure 3, we obtain a linear dependence of T_P as a function of H_{ac} in the ac amplitude range $50\mathrm{A\,m^{-1}} \le \mathrm{H_{ac}} \le 500\mathrm{A\,m^{-1}}$.

The linear fits are:$T_{p=}$a-bH_{ac}[K] which is in agreement with the relation of Muller critical state model for the intergranular critical temperature.

$\mathrm{T_p = T_{p0} - T_{p0}}\left[\mu_0\mu_{\mathrm{eff}}(0)/(2\mathrm{d}\alpha_J(0))\right]^{1/2}\mathrm{Hac}$, where d is the height of a cylindrical sample, $\mu_{\mathrm{eff}}(0)$ the effective permeability of the ceramic and $\alpha_{J(0)}$ is the intergranular pinning force density.

The temperature dependence of the Hall concentrations n_H for the Cr doped samples is shown in Fig 4. A linear decrease of n_H can be seen with increases of x, with a change of the slope around T=240K,and this is in agreement with data reported in Refs. 1 and 2. The square of the temperature dependence, of the inverse Hall mobility for x=0.02 Cr is shown in the inset of Fig 4.The straight lines represent the fit in the temperature range 160-240K according to Anderson's theory 23.The change in the mobility of the carriers around 240K is the most probably related to the chemical phase separation process[24].

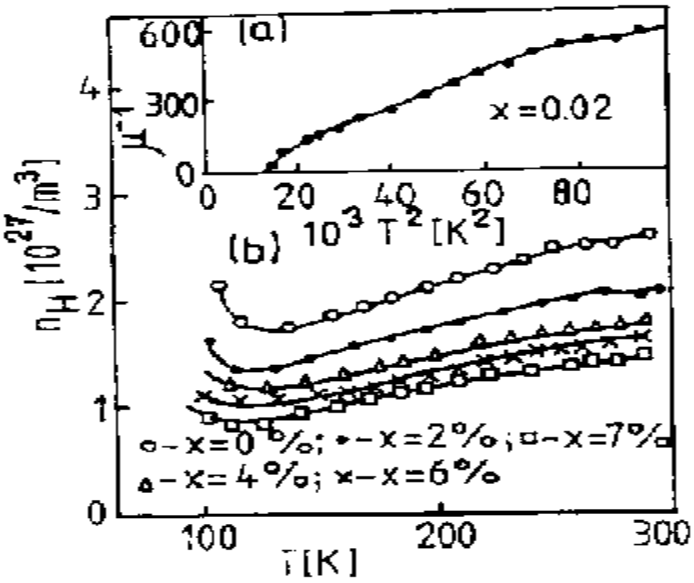

Fig. 4. (a) The square of the temperature dependence of the inverse Hall mobility for x=0.02 Cr;(b)The temperature dependence of the Hall concentrations in $(Bi_{1.6}Pb_{0.4})(Sr_{1.8}Ba_{0.2})Ca_2(Cu_{1-x}Cr_x)_3O_y$ bulk.

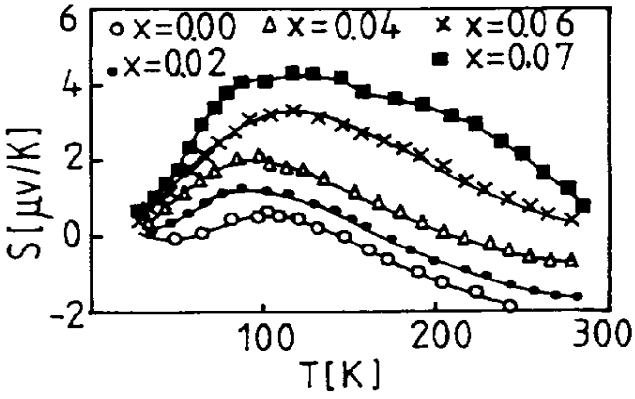

Fig. 5. Thermopower for $(Bi_{1.6}Pb_{0.4})(Sr_{1.8}Ba_{0.2})Ca_2(Cu_{1-x}Cr_x)_3O_y$

The Nernst electrical field in the normal state is immeasurable for the system. The temperature dependence of the Seebeck coefficient S(T) are shown in Fig. 5.

The value of S(T) at T=290K rises with increasing the Cr content up to x=0.07, i.e. it becomes more pronounced at high doping level. For $x \leq 0.03$,S(T) increases linearly as the temperature decreases and this is typical for Bi-based systems. These data are in agreement with a phenomena spectrum logical model [25].

4. Conclusion

In conclusion, we have reported simultaneous measurements of the resistivity, Seebeck, Nernst, Hall effects and ac susceptibility on Bi-2223 doped with Cr. The intergrain critical temperatures T_p are liner as a function of the ac field amplitude for x=o.oo Cr and x=0.02Cr and agree with the Muller critical state model. In the mixed state, the transport phenomena can be explained by the two fluid Ginsburg-Landau theory [15].In the normal state, the derivations form linear dependence of $\mu_H^{-1} = f(T^2)$ and n_H(T) can be interpreted by the percolative phase separations theory [24]and the temperature dependence of the Seebeck coefficient S(T), by asymmetric narrow-band model[25].

REFERENCES

1. See e.g., Proc.Int.Conf.Materials and Mechanisms of Superconductivity (1989-Stanford), eds. R. N. Shelton et al., Physica C162-164; (1991-Kanazawa), eds. M. Tachiki et al., Physica C185-189; (1994-Grenoble) ed. P. Wyder, Physica C235-240; (1997-Beijing) eds.Yu-Sheng et al., Physica C282-287.
2. C. Hohn, M. Galffy and A. Freimuth, Phys.Rev. E50, 5875 (1994).
3. G. Ilonca, M. Mehbod, A. Lanckbeen and R. Deltour, Phys. Rev. B47, 15265 (1993).
4. G. Ilonca, M. Mehbod, A. Lanckbeen and R. Deltour, Journal of Alloys and Compounds 195, 347 (1993).
5. G. Ilonca, A. V. Pop, M. Ye,M. Mehbod, G. Debrue, D. Ciurchea and R. Deltour, Supercond. Science and Technol. 8, 642 (1995).
6. G. Ilonca, A. V. Pop, C. Corega, M. Rusu, M. Ilonca and R. Deltour, Czech. Journ. Phys. 46, S2, 1881 (1996).
7. G. Ilonca, A. V. Pop, C. Corega, I. I. Geru, V. G. Kantser, L. A. Konopko, Y. Min and R. Deltour, Physica C235-240, 1391 (1994).
8. E. Ozdas and T. Firat, Phys. Rev. B48, 9754 (1993)

9. M. A. Koshima, T. Naji, I. Ono and Y. Koike, Phys. Rev. B57, 7491 (1998).
10. G. Ilonca, A. V. Pop, D. Benea, C. Lung, M. Lachescu and R. Deltour, Mod. Phys. Lett. B12, 1081 (1998).
11. A. V. Pop, G. Ilonca, D. Ciurchea, M. Ye and V. I. Geru, Int. J. Mod. Phys. B18, 967 (1996).
12. A. V. Pop, G. Ilonca, V. Pop, C. Lung and R. Deltour, Mod. Phys. Lett. B12, 419 (1998).
13. G. Ilonca. A. V. Pop and G. Tarta, T. Jurcuß and R. Deltour, Int. Journal. of Modern Phys. B vol. 13. no. 21&22, 2767 (1999).
14. G. Ilonca. A. V. Pop, I. G. Deac, T. Jurcut, R. Redac, N. Dulamita and R. Deltour, Modern Phys. Lett. B vol. 13. no. 15, 523 (1999).
15. H. C. Ri, R. Gross, F. Gollnick, A. Beck and R. P. Huebener, Phys. Rev. B50, 3312 (1994).
16. G. Ilonca, A. V. Pop, C. Corega, D. Benea, M. Rusu, M. Ilonca and R. Deltour, Czech. J. Phys. 46, 52, 1181 (1996).
17. V. Calzona, M. R. Cimberle, C. Ferdeghini, D. Marre and M. Putti, Physica C246, 169 (1995).
18. M. Gallfy, A. Freimuth and U. Murek, Phys. Rev. B 11 029 (1990).
19. R. P. Huebener, A. V. Ustinov and V. K. Kapluenko, Phys. Rev. B 42, 605 (1990).
20. Von B. Haedt, W. Lissek, K. Westerholt and H. Bach, Phys. Rev. B 49, 9898 (1994).
21. A. V. Pop., R. Deltour, A. Harabor, D. Ciurchea and G. Ilonca, Int. J. Mod. Phys. B 11, 3461 (1997).
22. A. V. Pop, R. Deltour, A. Harabor, D. Ciurchea, Gh. Ilonca, V. Pop and M. Todica, Supercond. Sci. Techn. 10, 843 (1997).
23. P. W. Anderson, Physica C. 185-189, 11 (1991).
24. R. K. Kremer, E. Sigmund, V. Hiznyakov, F. Kentsch, A. Simon, K. A. Muller and M. Mehning, Zeit Fur Phys. B 86, 319 (1992).
25. V. E. Gasumyants, V. I. Kaidanov and E. V. Vladimirskaya, Physica C 248, 255 (1995).

STUDIA UNIVERSITATIS BABEŞ-BOLYAI, PHYSICA, XLIV, 2, 1999

STRUCTURAL AND MAGNETIC PROPERTIES OF THE $Y_{1-x}Bi_xBa_2Cu_3O_{7-\delta}$ SYSTEM

S. SIMON*, M. POP*, GH. BORODI, A. HARABOR*****

ABSTRACT. The Bi doped Y-123 superconducting system synthesised through a solid-state reaction route is studied by X-ray diffraction (XRD) and A.C. susceptibility measurements.

XRD results indicate the formation of the Y-123 phase as the main phase for the samples with up to x = 0.1 Bi content, while for x > 0.1 it is evidenced the decrease of the Y-123 phase fraction and the increase of the $BaBiO_{3-x}$ phase.

The A.C. susceptibility measurements reveal the increase of the intergranular critical temperature with the yttrium substitution by bismuth in the not-fully oxygenated $Y_{1-x}Bi_xBa_2Cu_3O_{7-\delta}$ samples for a low level of substitution (x < 0.1), which denotes the improvement of the intergranular coupling. This behaviour is assigned to the formation of the $BaBiO_{3-x}$ phase at the surface of the Y-123 grains, detected from the XRD patterns. When the substitution degree exceeds x = 0.1 the intergranular coupling becomes weaker because of the Y-123 phase fraction diminishing.

Introduction

The first member of the $Y_2Ba_4Cu_{6+n}O_{14+n-\delta}$ system of high-T_C compounds, Y-123 (n = 0), with T_C = 92 K is one of the most investigated high-T_C superconductor [1-5]. An exciting feature of the $YBa_2Cu_3O_{7-\delta}$ superconductors consists in their ability to extensive elemental substitutions in the search to obtain superconducting materials with desired physical properties. A large number of studies have been carried out for the case of isoelectronic substitutions at Y site with lanthanides [6]. These substitutions have a small effect on the superconducting properties despite the large magnetic moment of some rare-earth ions [7-9]. The superconducting transition temperature remains nearly constant with the

* Babes-Bolyai University, Faculty of Physics, 3400, Cluj-Napoca, Romania
** Institute of Molecular and Isotopic Technologies, 3400, Cluj-Napoca, Romania
*** University of Craiova, 1100, Craiova, Romania

substitution level excepting the case of the substitution with Pr when T_C rapidly decreases and the compound becomes non-metallic [10]. Other authors reported that by increasing the substituent concentration in $Y_{1-x}Pr_xBa_2Cu_3O_{7-\delta}$, the transition temperature of the samples is diminished and they finally become semiconducting when x is greater than about 0.56 [11].

Plenty of works [12-18] were devoted to the Ca substitution at the Y site in the Y-123 system. This substitution leads to the decrease of the T_C of fully oxygenated Y-123 samples (T_C = 90 K) [12-14] but it determines the increase of the critical temperature for the oxygen-deficient systems [15-18].

This paper reports the results obtained by XRD analyses and A.C. susceptibility measurements on Y(Bi)-123 superconducting system. By the replacement of yttrium with bismuth is intended to obtain an improvement of the intergranular coupling between the superconducting grains in polycrystalline samples.

Experimental

The samples of the series $Y_{1-x}Bi_xBa_2Cu_3O_{7-\delta}$ (x=0; 0.05; 0.1; 0.2; 0.3) were synthesised through a solid-state reaction route, using as starting chemicals Y_2O_3, Bi_2O_3, CuO and $BaCO_3$, of reagent grade purity (p.a). The corresponding mixtures were calcinated for 10 h at 860℃. After calcination the samples were subjected to a heat treatment in flowing oxygen for 24 h as follows: 18 h at 930℃ and other 6 h at 940℃. A fter the heat treatment the samples were slowly cooled to 400℃ and further they were treated in flowing oxygen for 24 h at this temperature. The cooling velocity was less than 3℃/min.

X-Ray diffraction patterns of the samples were recorded with a Dron 2 type diffractometer (Cr-K_α radiation). A.C. magnetic susceptibility measurements were carried out using a 7130 A.C. susceptometer. The complex susceptibility was measured at 666.7 Hz as function of temperature in the range 78-90 K at a field amplitude H_{AC} = 0.4 A/m.

Results

1. X-Ray Diffraction

The X-Ray diffraction patterns (Fig. 1) of $Y_{1-x}Bi_xBa_2Cu_3O_{7-\delta}$ with x=0.0; 0.05; 0.1; 0.2; 0.3 allow to establish the formation of the Y-123 phase for the undoped sample and the appearance of a small amount of the $BaCuO_2$ impurity phase ($2\theta \cong 42°, 44°, 45°$). In the case of the samples with bismuth, one observes from the XRD patterns the formation in addition of the $BaBiO_{3-x}$ phase suggested by the appearance of two additional

peaks which become stronger with increasing Bi content ($2\theta \cong 45°$ and 64°).

For the samples with a replacement of yttrium by bismuth up to x = 0.1 one remarks from the XRD patterns the formation of the Y-123 phase as main phase, the appearance of a small, constant amount of the $BaCuO_2$ impurity phase and the formation of $BaBiO_{3-x}$ phase, whose fraction increases with the substitution level. When the substitution degree exceeds x = 0.1, one observes the decrease of the Y-123 phase and the increase of the $BaBiO_{3-x}$ phase.

2. A.C. susceptibility

The A.C. susceptibility of $Y_{1-x}Bi_xBa_2Cu_3O_{7-\delta}$ samples with x = 0.0; 0.05; 0.1; 0.2; 0.3, are shown in Fig. 2 as a function of temperature.

In the resistivity measurements the critical temperature is the temperature at which a percolation path is established. This occurs at the critical temperature of the coupling component, in particular at the onset of coupling. Thus the zero resistivity temperature is nearly the same as the intergrain coupling temperature. The intragrain transition and the intergranular phase locking temperatures from the A.C. susceptibility measurements, are denoted by T_C and T_j, respectively. The critical temperature T_C is sometimes taken as the midpoint of the diamagnetic transition. There are several problems with this. First there are two transitions, second the widths of the transitions are field dependent, third a large part of the transition to full diamagnetism is due to coupling, fourth the complete intrinsic transition is often obscured by the coupling transition. Therefore is more useful to define the critical temperatures as the onset temperatures, although the precise onset temperatures are uncertain, particularly due to fluctuation effects.

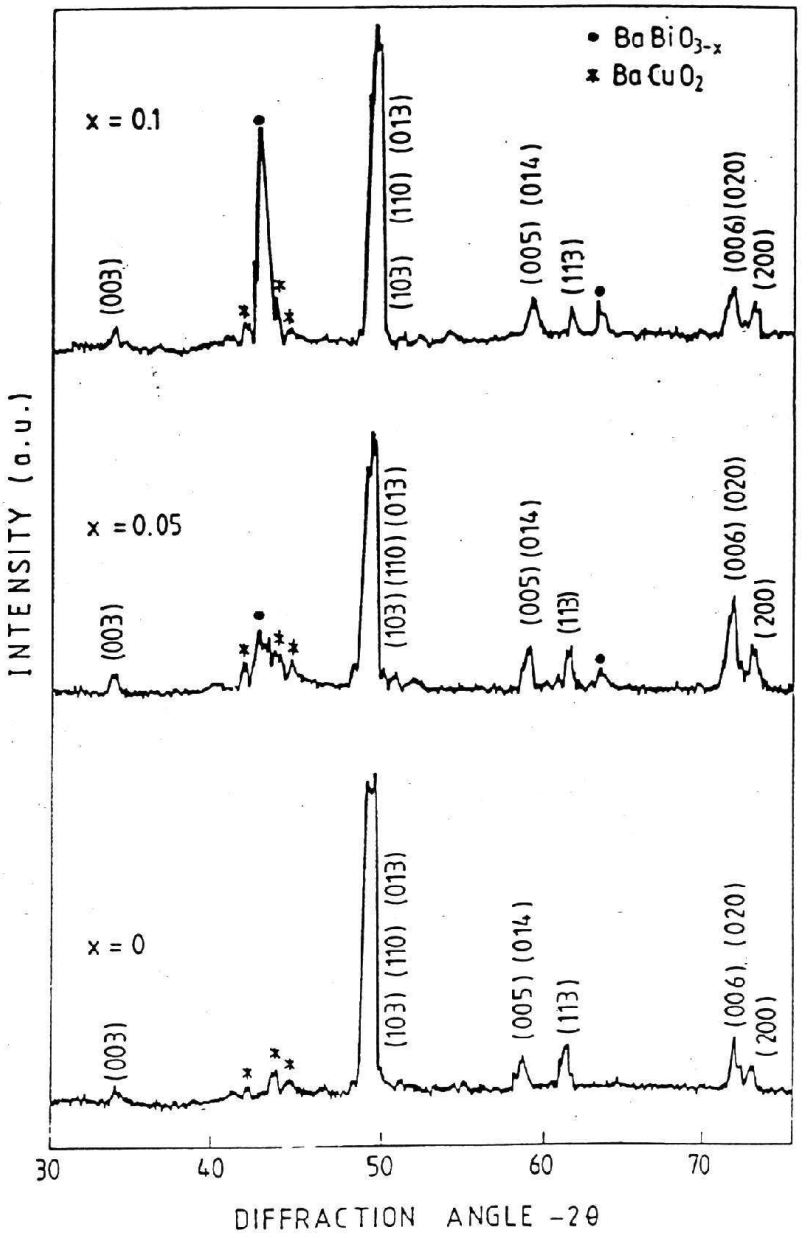

Fig.1 XRD patterns of $Y_{1-x}Bi_xBa_2Cu_3O_{7-\delta}$ samples

In the case of the investigated system as is seen from the Fig. 2a, the intergranular coupling is improved up to x = 0.1 of yttrium substitution by bismuth, by comparison with the undoped sample. This improvement occurs because the intergranular peak associated with T_j is shifted to higher temperatures. One also observes a small increase of the critical temperature T_C up to x = 0.1 substitution degree, by comparison with the undoped sample. The critical temperature values (about 88 K for the undoped sample and about 89 K for the samples with $x = 0.05$ and $x = 0.1$) show an oxygen deficiency in the samples corresponding to about $\delta = 0.19$ and 0.17, respectively [6].

The improvement of the intergranular coupling evidenced by the A.C. susceptibility measurements is assigned to the formation of the $BaBiO_{3-x}$ phase at the surface of the Y-123 grains, detected from the XRD patterns. This phase determines a better connection between the Y-123 grains and raises the intergranular critical temperature (T_j) at grain boundaries. The improvement of the intragrain critical temperature at low substitution levels, as reflected by the slight decrease of δ is correlated with the fact that the $BaBiO_{3-x}$ phase favourites the oxygen diffusion into the Y-123 grains. As a consequence, the oxygen content has a slight increase into the deficiently oxygenated grains, resulting in a corresponding increase of the T_C.

When the yttrium replacement by bismuth exceeds x = 0.1 (Fig. 2b.) the intergranular peak is shifted to lower temperatures, hence the intergranular coupling temperature T_j is decreasing. This behaviour can be explained by the significant increase of the $BaBiO_{3-x}$ phase in the region between the grains. Consequently, the amount of the Y-123 phase decreases with the Bi content and the intergranular coupling decreases too.

Conclusions

The yttrium partial substitution by bismuth in Y-123 superconducting system influences both its structure and magnetic properties. The X-ray diffraction and A.C. susceptibility results indicate that this replacement improves the intergranular coupling of the $Y_{1-x}Bi_xBa_2Cu_3O_{7-\delta}$ not fully oxygenated samples, for the low level of substitution (up to x = 0.1). The substitution in the $0.05 \leq x \leq 0.1$ range leads to the formation of the $BaBiO_{3-x}$ phase in small amount, which improves the connection between the grains.

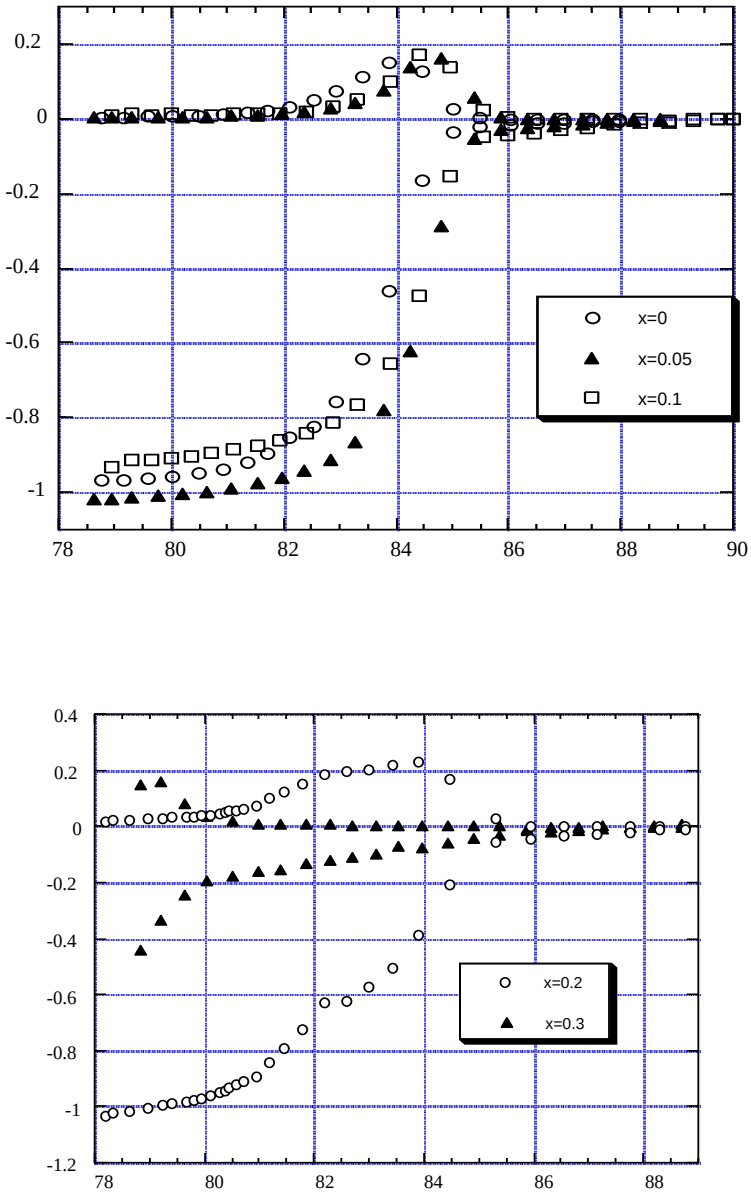

Fig. 2. Temperature dependence of A.C. susceptibility

For higher substitution levels (x > 0.1) the intergranular coupling is diminished due to the significant growth of the $BaBiO_{3-x}$ phase at the Y-123 grain boundaries and due to the corresponding decrease of the Y-123 phase by yttrium replacement with bismuth.

REFERENCES

1. S. Hosoya, M. Onoda, S. Shamoto and M. Sato, Jpn. J. Appl. Phys. 26 (1987) L456.
2. W. Guan, Y. Xu, S. R. Sheen, Y. C. Chen, J. Y. T. Wei, H. F. Lai, M. K. Wu and J. C. Ho, Phys. Rev. B 49 (1994) 15993.
3. J. G. Lin, C. Y. Huang, Y. Y. Xue, C. W. Chu, X. W. Cao and J. C. Ho, Phys. Rev. B 51 (1995) 12900.
4. V. P. S. Awana, S. K. Malik and W. B. Yelon, Physica C 262 (1996) 272.
5. P. Berastegui, S. G. Eriksson, L. G. Johansson, M. Kall, L. Borjesson, M. Kakihana and H. Mazaki, Physica C 259 (1996) 97.
6. S. Simon, M. Crisan, “Supraconductibilitate la temperaturi inalte", Ed. Presa Univ. Clujeana (1999) p. 93-96.
7. P. H. Hor, R. L. Meng, Y. Q. Wang, L. Gao, Z. J. Huang, J. Bechtold, K. Foster and C. W. Chu, Phys. Rev. Lett. 58 (1987) 1891.
8. D. E. Morris, J. H. Nickel, J. Y. T. Wei, N. G. Asmar, J. S. Scott, U. M. Scheven, C. T. Hultgren, A. G. Markelz, J. E. Post, P. J. Heany, D. R. Veblen and R. M. Hazen, Phys. Rev. B 39 (1989) 7347.
9. D. B. Currie, M. T. Weller, P. C. Lanchester and R. Walia, Physica C 244 (1994) 43.
10. H. B. Radousky, J. Mater. Res. 7 (1992) 1917.
11. Y. Dalichaouch, M. S. Torikachvili, E. A. Early, B. W. Lee, C. L. Seaman, K. N. Yang, H. Zhou and M. B. Maple, Solid State Commun. 65 (1988).
12. A. Manthiram, S. J. Lee and J. B. Goodenough, J. Solid State Chem. 73 (1989) 278.
13. V. P. S. Awana and A. V. Narlikar, Phys. Rev. B 49 (1994) 6353.
14. V. P. S. Awana and A. V. Narlikar, Phys. Rev. Lett. 71 (1993) 303.
15. V. P. S. Awana, Ashwin Tulapurkar, S. K. Malik and A. V. Narlikar, Phys. Rev. B 50 (1994) 594.
16. E. M. McCarron III, M. K. Crawford and J. B. Parise, J. Solid State Chem. 78 (1989) 192.
17. A. Manthiram and J. B. Goodenough, Physica C 159 (1989) 760.
18. V. P. S. Awana, S. K. Malik and W. B. Yelon, Physica C 262 (1996) 272.

STUDIA UNIVERSITATIS BABEŞ-BOLYAI, PHYSICA, XLIV, 2, 1999

MARGINAL FERMI LIQUID MODEL FOR HIGH - T_C SUPERCONDUCTORS

D. BODEA*, I. TIFREA*, I. GROSU* AND M. CRISAN*

We analyse the phenomenological model of the Marginal – Fermi Liquid used to explain the normal state in high – T_c superconductors. The microscopic models have been proposed based on the realistic recent data obtained from relevant experiments.

1. Fermi Liquid

It is well known that the normal metals, as well as normal ^{3}He, follow the same type of low energy behavior described by Fermi liquid theory [1]. This originally purely phenomenological theory makes specific predictions on low energy scaling behavior of thermodinamic and transport properties as functions of temperature, frequency or momentum scales. In metals the anysotropy of the Fermi surface, the impurities generate any complications but the theory is robust with respect to such complications. The most important properties of the model are: the existence of the Fermi surface, a specific heat $C_v \sim T$, a susceptibility χ = constant, a metalic conductivity increasing with decreasing the temperature, implying the eistence of gapless excitations. These proprieties are very symilar with the proprieties of the non-interacting Fermi gas. In Fermi – liquid theory the properties are described by the "quasiparticles" that are fermionic elementary excitations described by the propagator

$$G(k,\omega) = \frac{Z_k}{\omega - v_F(k - k_F) + i\gamma} \tag{1}$$

where the renormalization constant Z_k satisfies

$$0 < Z_{k_F} \leq 1 \tag{2}$$

$v_F(k_F)$ are the Fermi velocity (momentum) and γ is related o the life-time of quasiparticles by

$$\gamma = \frac{1}{\tau_\omega} \sim (\omega - E_F)^2 \tag{3}$$

* Department of Theoretical Physics "Babeş-Bolyai" University of Cluj

The interaction with a Bosonic mode with energy scale $\omega_D/E_F<<1$ (E_F – Fermi energy) and the sistem can be treated using the theory of perturbation, neglecting the vertex corrections.

The parameter characterizing these almost free excitations are very different for different metals. A tipical exemple is the effective mass of quasiparticles which is so-called heary fermion systems can be $m^*=10^2\ m_e$ (m_e electronic mass). The energy (temperature) scale is also strongly material dependent. Usually three distinct scales have to be considered: the Fermi temperature T_F (associated with E_F), a coherence temperature T^* below which Fermi – liquid behavior sets in, and a transition temperature T_c associated with an instability of the normal Fermi liquid towards some sort of symmetry breaking.

Until recently, Fermi – liquid theory seemed universally applicable at least to all suficiently pure interacting Fermi system, and its general features even to quite dirty sistems (Kondo systems). This situation has changed after the discovery of high-temperature superconductors. These materials have the normal state ($T > T_c$) very different to the standard metalic state described by the Fermi – liquid theory. The most proeminent quantities which presents an esential difference is the electrical resistivity whose temperature dependence deviates from T^2 at low temperatures and is liniar in T. The proximity of an antiferromagnetic Mott insulating phase reveals the importance of electron-electron interaction even in the normal phase. The specific heat $C_v \sim T\ln T$ showed also the strong deviations from the Fermi – liquid theory.

2. Model for Non-Fermi Liquid: Marginal Fermi Liquid

Before starting the discussion on the models for the non-Fermi liquid we will define a "non-Fermi liquid".

A normal metalic phase of interacting fermions with low-energy behavior that is not described by Fermi – liquid theory is generally called a "non-Fermi liquid". Metalic behavior implies that these are gapless charge fluctuations in these systems but recent experiments showed that the coupling to the electrons to such charge fluctuations can give a "pseudogap" and the occurrence of it is again associated to the non –Fermi behavior of these is not a microscopic model for the non-Fermi liquid and the most important experimental data have been used to elaborate a phenomenological model. Let us now present the main of them:

- Photoemission, optical absortion and paramagnetic susceptibility show the state is metalic.
- The quasiparticle scattering rate varies as

$$\frac{1}{\tau} = \alpha T + \beta\omega$$

where $\alpha \cong \beta \cong 1$.

- All the response functions have a polarizability well aproximated by

$$\mathrm{Im}\prod(q,\omega,T) = \begin{cases} -\dfrac{\omega}{T}N(0); \omega << T \\ -N(0); T < \omega < \omega_c \end{cases} \tag{4}$$

where N(0) is the density of states.

3. Marginal Fermi Liquid: A Phenomenological approach

The Green function for the interacting quasiparticles is expressed as:

$$G^{-1}(\omega,k) = G_0^{-1}(\omega,k) - \sum(\omega,k) \tag{5}$$

In the Born approximation the self-energy is given by

$$\sum(k,\omega) = g^2 \int dq \int dz \int dz' \frac{A(\vec{p}-\vec{q},z)B(q,z')}{\omega - z - z'}\left[n_B(z') + 1 - f_F(z)\right] \tag{6}$$

where $n_B(z)$ is the Fermi function.

In this point we consider that the electronic excitations describe by the spectral function A(k, ω) are coupled to he bosonic mode describe by the spectral function:

$$B(q\omega) = \frac{\tanh\dfrac{\omega}{T}}{1 + \left(\dfrac{\omega}{\omega_c}\right)^2} \tag{7}$$

The microscopic nature of this bosonic mode is not specified but it can be given by the spin fluctuations or by the proximity of a quantitum critical point. Taking for A(k, ω) a δ- form expression and performing another important approximations which consist in neglecting of momentum dependence in Eq.(6) the imaginary part of the self-energy is

$$\mathrm{Im}\sum(\omega) = \begin{cases} \pi^2 \lambda T, \omega << T \\ \pi\lambda\omega; T << \omega << \omega_c \end{cases} \tag{8}$$

where λ is dimensionless coupling constant.

Using Kramers-Kroning relations we calculate also $\mathrm{Re}\sum(\omega)$ and the general form is

$$\sum(\omega,T)=\lambda\pi\left[\frac{2\omega}{\pi}\ln\left(\frac{\pi T+i\omega}{\omega_c}\right)+\frac{i\pi T}{2}\right] \tag{9}$$

Performing the Matsubara analitical continuation $i\omega_n\rightarrow\omega$ the self-energy given by Eq.(9) becomes

$$\sum(i\omega_n)=-i\lambda T\arctan\frac{T}{\omega_n}-\frac{i\lambda\omega_n}{2}\ln\frac{\omega_n^2+\omega_c^2}{\omega_n^2+T^2} \tag{10}$$

As a consequnce of this self-energy the quasiparticle residue vanishes logaritmically:

$$Z^{-1}=1+\lambda\ln\frac{\omega_c}{x} \tag{11}$$

x = max (ω, T), and this property generated the name: marginal Fermi liquid.

This model has been proposed by Varma et al [2] and is in fact a phenomenological model. In the next sections we will show that it is possible to give microscopie mechanismus for this behavior.

4.Microscopic theory of the Marginal Fermi – Liquid; Coupling to a Bosonic Mode [3]

We consider the coupling to a bosonic mode of the electronic excitations with the self-energy

$$\sum(\vec{k},\omega)=ig^2\int\frac{d^3\vec{k}}{(2\pi)^2}\int\frac{d\omega'}{2\pi}\prod(\vec{k}-\vec{k}',z)G(\vec{k}',\omega) \tag{12}$$

where $\prod(k,\omega)$ is the bosonic polarization and $G(\vec{k},\omega)$ is the electronic Green function.

If we introduce for bosonic polarization the spectral representation:

$$\prod(\vec{k}-\vec{k}';\omega-\omega')=\int_{-\infty}^{+\infty}dz\frac{B(\vec{k}-\vec{k}',z)}{\omega-\omega'-z+i\delta} \tag{13}$$

In agreement with the hypotessis from the MFL the wave – vector dependence in $\prod(\vec{k}-\vec{k}';\omega-\omega')$ and using for the electronic Green function, the free-electron Green function we obtained from Eqs.(12) and (13) the imaginary part of the self-energy $\gamma(\omega)=\mathrm{Im}\sum(\omega)$ as

$$\frac{d\gamma(\omega)}{d\omega}=-N(\upsilon)g^2\int_{-\infty}^{+\infty}d\omega\delta(\omega-\omega')\mathrm{sgn}(\omega')B(\omega')-\pi N(\upsilon)g^2\,\mathrm{sgn}(\omega)B(\omega) \tag{14}$$

where the spectral density $B(\omega) = -\frac{1}{\pi}\mathrm{Im}\prod(\omega)$ and using Eq.(4) it has the form

$$B(\omega) = \begin{cases} \frac{N(0)}{\pi T}(\omega); |\omega| << T \\ \frac{N(0)}{\pi}; \quad |\omega| >> T \end{cases} \tag{15}$$

and $B(\omega) = 0 \quad |\omega| > \omega_c$ (16)

The Eqs.(15-16) gives

$$\frac{d\gamma(\omega)}{d\omega} = \begin{cases} -N(0)g^2\frac{\omega}{T}; \quad |\omega| << T \\ -N(0)g^2\,\mathrm{sgn}(\omega); \quad |\omega| >> T \end{cases} \tag{17}$$

This equation will be taken in the asymptotic regims:

$$\frac{d\gamma(\omega)}{d\omega} = -N^2(0)g^2\begin{cases} 0; \quad |\omega| << T \\ \mathrm{sgn}(\omega); \quad |\omega| >> T \end{cases} \tag{18}$$

which gives

$$\gamma(\omega) = -N^2(0)g^2\begin{cases} C; \quad |\omega| << T \\ |\omega|; \quad |\omega| >> T \end{cases} \tag{19}$$

The constant C can be determined from the condition $\gamma(\omega = T+0) = \gamma(\omega = T-0)$ we get

$$\gamma(\omega) = -N^2(0)g^2\begin{cases} T; \quad |\omega| << T \\ |\omega|; \quad |\omega| >> T \end{cases} \tag{20}$$

which is in fact the marginal behavior predicted in Ref.[1].
From Eq.(14) we can calculate the scattering time $\tau^{-1} = \gamma(\upsilon)$ as

$$\gamma(\upsilon) = \frac{\pi}{2}g^2\int_{-\infty}^{+\infty} d\omega' B(\omega') \tag{21}$$

and using the asymptotic form of Eq.(15)

$$B(\omega) = \begin{cases} 0; \quad |\omega| << T \\ \frac{N(0)}{\pi}; \quad |\omega| >> T \end{cases} \tag{22}$$

we obtain

$$\gamma(\upsilon) = N^2(0)g^2\omega_c - N^2(0)g^2T \tag{23}$$

Using the Kramers-Kroning relation:

$$\mathrm{Re}\prod(\omega)=\frac{1}{\pi}\int_{-\infty}^{+\infty}\frac{\mathrm{Im}\prod(z)dz}{z-\omega} \tag{24}$$

we calculate

$$\mathrm{Re}\prod(\omega)=-\frac{N(0)}{\pi}\left\{\frac{\omega}{T}\ln\left|\frac{T-\omega}{T+\omega}\right|+\ln\left|\frac{\omega_c-\omega}{T-\omega}\right|-\ln\left|\frac{T+\omega}{\omega_c+\omega}\right|+2\right\}$$

which will be approximated as:

$$\mathrm{Re}\prod(\omega)=-\frac{N(0)}{\pi}\left\{2\left(\frac{\omega}{T}\right)^2+2\ln\frac{\omega_c}{T}\right\} \qquad \text{if } |\omega|<<T \qquad \text{and}$$

$$\mathrm{Re}\prod(\omega)=-\frac{N(0)}{3\pi}\left\{\left(\frac{\omega}{T}\right)^2+3\ln\left(\frac{\omega_c}{T}-1\right)\right\} \quad \text{if } |\omega|>>T\,.$$

These results will be used in the asymptotic form:

$$\mathrm{Re}\prod(\omega)=-N(0)\begin{cases}\dfrac{2}{\pi}\left[2-\left(\dfrac{\omega}{T}\right)^2\right] & |\omega|<<T\\[2ex] \dfrac{1}{3\pi}\left(\dfrac{T}{\omega}\right)^2 & |\omega|>>T\end{cases} \tag{25}$$

and using this result we obtain form Eq.(12)

$$\mathrm{Re}\sum(\omega)=2N^2(\upsilon)g^2\omega\ln\frac{x}{\omega_c} \tag{26}$$

$$Z^{-1}=1-\frac{\partial}{\partial\omega}\mathrm{Re}\sum(\omega)=\ln\frac{\omega_c}{\omega} \tag{23}$$

5. Proximity of a Quantum Phase Transition

Consider the electrons near a Quantum Phase Transition point. In this situation the critical bosons will couple to the electrons and this interaction change drastically the energy of the electronic excitation.

For this system we write the self-energy simulator to Eq.6, using for the critical bosons the propagator $D(\vec{k},\omega)$. In the same approximation the electronic self-energy is:

$$\sum(\vec{k}\omega)=-g^2\sum_{\vec{k}}\int_{-\infty}^{+\infty}\frac{dz}{2\pi}\int_{-\infty}^{+\infty}\frac{dz'}{2\pi}\frac{\mathrm{Im}G(\vec{p}+\vec{k},z')\mathrm{Im}D(\vec{k},z)}{z+z'-\omega-i\delta} \tag{24}$$

where we will take for $G(\vec{k}\omega)$ the Green function for the free electrons. For a 3D system we calculate from Eq.(24)

$$\mathrm{Im}\sum[\varepsilon(\vec{k})] \cong \frac{g^2}{2(2\pi)^2}\int_0^{2p_F} p^2 dp \int_0^{\varepsilon(k)-E_F} \frac{d(\cos\theta)[g^2 D(\vec{p},z')]}{\left[D^{-1}(\vec{p},z')+g^2\prod'(\vec{p},z')\right]^2+\left[g^2\prod''(\vec{p},z')\right]^2} \quad (25)$$

where we defined $D(\vec{p},\omega)$ by the equation

$$D^{-1}(\vec{p},\omega) = D_0^{-1}(\vec{p},\omega) + g^2 D_0(\vec{p},\omega) \qquad \prod' = \mathrm{Re}\prod \quad \text{and}$$

$$\prod'' = \mathrm{Im}\prod \quad (26)$$

The proimity of a QPT will be expressed in Eq.(25) by the condition:

$$D_0^{-1}(\vec{p},\omega) + g^2 D_0(\vec{p},\omega) \quad (27)$$

This equation gives the "instability root" ω_c(p) as

$$\omega_c(p) \cong \omega_+ \cdot \omega_- \left(\frac{\Omega^2(p)}{g^2 N(0)} - 1\right) \quad (28)$$

where $\Omega(p) = a(\vec{p})$ is the energy of the "base" bosons. The Eq.(28) defines a critical mode vector p_c by

$$p_c^2 > \frac{g^2 N(0)}{d^2}$$

and we will consider that the critical mode appears in a domain of small frequency around $\omega_c(p) \cong \overline{\omega}$. Performing an expresion

$$\overline{\omega} - \omega_c(p) = \alpha(p^2 - p_c^2)$$

we calculate the imaginary part of electronic self-energy from Eq.(25) as

$$\mathrm{Im}\sum[\varepsilon(k)] = const[\varepsilon(k) - E_F]I_{3D} \quad (29)$$

where $I_{3D} = \int_0^{2p_F} \frac{pdp\prod''(p_c\overline{\omega})}{(p-p_c)^2 + g^4\left[\prod''(p_c\overline{\omega})\right]^2} \cong \frac{\pi}{2}$

This mode was developed by Crisan and Tataru [4-5] and confirmed by RNG calculations [6b].

6. Proximity of the hot spots.

We consider (see Ref. 6a) now a simple electronic system with the enery

$$\varepsilon(k) = k_x k_y \quad (30)$$

The polarizability for this system has been calculated as:

$$\mathrm{Im}\prod\left(\vec{k},z\right)=\frac{2}{\pi\varepsilon\left(\vec{k}\right)}\left\{\left|z+\varepsilon\left(\vec{k}\right)\right|-\left|z-\varepsilon\left(\vec{k}\right)\right|\right\} \tag{31}$$

$$\mathrm{Re}\prod\left(\vec{k},z\right)=\frac{1}{2\pi}\left\{\ln\left|\frac{4E_c\varepsilon\left(\vec{k}\right)}{z^2-\varepsilon^2(k)}\right|-\frac{z}{\varepsilon\left(\vec{k}\right)}\ln\left|\frac{z+\varepsilon\left(\vec{k}\right)}{z-\varepsilon\left(\vec{k}\right)}\right|+2\right\}$$

and the imaginary part of the electronic self-energy is

$$\mathrm{Im}\sum(p,z)=\frac{2g^2}{\pi}\int\frac{d^2\vec{k}}{(2\pi)^2}\int_0^\infty dz\,\mathrm{Im}\prod\left(\vec{p}-\vec{k},z\right)\mathrm{Im}G\left(\vec{k},z+\omega\right) \tag{32}$$

We mention that the dispersion $\varepsilon(k)=\frac{1}{2}\left(k_x^2-k_y^2\right)$ is equivalent to the parabolic band-model described by Eq.30. Performing the transforms

$$k_x=\frac{k}{2}\left(\lambda+\frac{1}{\lambda}\right)\quad,\quad k_y=\frac{k}{2}\left(\lambda-\frac{1}{\lambda}\right)$$

we calculate the imaginary part of self-energy (32) as

$$\mathrm{Im}\sum\left(\vec{p},\omega\right)=\frac{g}{\pi^3}\int_0^\infty kdk\int_{-\infty}^{+\infty}\frac{d\lambda}{\lambda}\frac{1}{\varepsilon\left(\vec{p}-\vec{k}\right)}$$
$$\left\{\left|\varepsilon\left(\vec{k}\right)-\omega+\varepsilon\left(\vec{p}-\vec{k}\right)\right|-\left|\varepsilon\left(\vec{k}\right)-\omega-\varepsilon\left(\vec{p}-\vec{k}\right)\right|\right\} \tag{33}$$

which can be calculated as:

$$\mathrm{Im}\sum\left(\vec{p},\omega\right)=\frac{2mg^2}{\pi^3p^2}\int_0^p\left(\varepsilon(k)-\omega\right)kdk \tag{34}$$

and for $p\cong p_F$ we get

$$\mathrm{Im}\sum(\omega)=-3N(0)\left(\frac{g}{\pi}\right)^2\left(\omega-\frac{E_F}{2}\right) \tag{35}$$

This results shows that this electronic system is marginal as we showed [6a] using the RNG method. [6b]

7. Conclusions and Results.

The phenomenological model of the marginal-Fermi liquid has been formulated in terms of different microscopic models insirated from the experimental data.

We can conclude that the 2D caracther of the Fermi surface and the proximity of a quantum phase transition are the most posible scenarios for this behavior.

The authors would like to express thanks to A. E. Ruckenstein (Rutgers), A. J. Millis (Rutgers), A-M. E. Trenblaky (Sherbrooke), C. Strinati (Camerino), M. Lavagna (Grenoble), A. Perali (Roma), for valuable discussions concerning the concept of marginal Fermi liquid. They also thank H. von Löhneysen (Karlsruhe), A. Schröder (Karlsruhe), H. Julien (Cambridge), for valuable coments concerning experimental results.

REFRENCES

1. D. Pines and P. Nozieres, The Theory of Quantum Liquids (Cap.I) Benjamin, New York (1966).
2. C.M. Varma, P. B. Littlewood, S. Scmitt-Rink, E. Abrahams and A. E. Ruchenstein, Phys. Rev. Lett. 63, 1996 (1989).
3. M. Crisan and L.Tataru J., Supercond. 6, 312 (1993).
4. M. Crisan and L.Tataru J., Supercond. 8, 341 (1995).
5. M. Crisan and L.Tataru, Phys. Rev. B 54, 3597 (1996).
6. a) C. P. Moca and M. Crisan J., Supercond. 10, 3 (1997).
   b) M. Crisan and C. P. Moca, Modern. Phys. Lett. B9, 1953 (1995).
7. C. P. Moca, I. Tifrea and M. Crisan Phys. Rev. B 61, 3247 (2000).
8. C. P. Moca, I. Tifrea and M. Crisan, Physica C (in press).

STUDIA UNIVERSITATIS BABEŞ-BOLYAI, PHYSICA, XLIV, 2, 1999

HUMAN BRAIN AS A RANDOM GENERATOR. PART III. WHITE, COLOURED NOISE AND NOISY PERIODICITY IN HUMAN BRAIN BEHAVIOUR

V. V. MORARIU[1], ALLOUETTE-MINERVA CHIS[2], LAURA C. MORARIU[3]

***ABSTRACT*.** Can human brain purposely generate randomness? Conscious activity is generally consistent with a deterministic mode of action, however some activities may involve randomness. This work presents evidence that mind can generate sequences of events which are either random (white noise), correlated noise (red noise i. e. $1/f^a$ type of noise) and noisy periodicity, depending on the task and design of the experiment. Shannon informational entropy was calculated for noisy periodicity data: while computer generated random series revealed an average informational content of I_2 = 2. 8 bites, mental series show values as low as I_2 = 2. 25 bites per pair of terms in the series for an embedding step T=1. Return maps suggest that the deterministic chaos is not involved in these phenomena. The white noise produced by the mind does not seem to correspond to a true random series of data and some short-range correlation seems to persist.

1. Introduction.

It is generally admitted that mind or consciousness is a product of the human brain activity. Conscious activity has always been regarded as having a purpose and therefore represents a deterministic action. On the other hand in the every day life one encounters with actions which are regarded as random. This is represented by expressions such as: "picking at random", "chance", "due to the chance", doing randomly" etc [1]. Acting in a deterministic way implies a rule or an algorithm. Complete randomness involves the absence of any rule or algorithm i. e. a non-deterministic process. This work further attempts to answer to the basic question on

[1] Department of Biophysics, National Institute of R&D for Isotopic and Molecular Technologies, P.O.Box 700, 3400 Cluj-Napoca, Romania; vvm@L40.itim-cj.ro, and Faculty of Physics, Babes-Bolyai University, Cluj-Napoca

[2] The American University in Cairo, 113 Sharia Kasr El Aini, Cairo, Egypt

[3] Department of Psychology, Institute of Social Sciences, Cluj-Napoca, Romania

whether mind can produce random events. It is a fundamental question as far as the mechanism of the consciousness is concerned. This has been for the first time approached in these series of articles [2-3]. The problem of consciousness has attracted much interest during the last decade from the part of an interdisciplinary effort of mathematics, physics, biology, psychology and philosophy, as remarkably shown by Tucson (University of Arizona) Conferences entitled "Toward a science of consciousness" in 1994, 1996, 1998.

The goal of this work is to answer whether mind can generate time series having a purely random or non-algorithmic character. Penrose reasoned that consciousness must involve a non-algorithmic i. e. a non-deterministic component [4]. On the other hand the only non-deterministic phenomena in the Universe are a few random phenomena. Later, Penrose speculated that such a component is not related to randomness [5]. Our work is certainly not on the line of Penrose's hypothesis where the non-algorithmic character of the consciousness is not understood in the sense of randomness. However, we may simply address this question as to the best of our knowledge there has been no attempt to answer such an elementary question, except in these series of articles.

The problem could have, at least two answers: one is that the generation of a random series of data is implicitly based on a rule in respect with the random character. The output is pseudorandom and the problem is reduced to establishing the validity of this rule. If the mental algorithm is not valid, the result will illustrate the image of the subject about randomness. Another theoretically possibility is that the generation is performed with no preimposed algorithm. The subject generates the series of events, without making use of a preconceived rule. Again all what we can do is to evaluate the degree of the randomness of the output and find if it fulfills such a condition. Clearly, to know which of the two alternatives is operative is hard to control in an experiment and at the best what we can do is to establish the character of the output.

Our research was started on an "empty ground" in 1995. To the best of our knowledge no similar attempts have been done previously.

2. Consciousness and randomness: design of the experiment

A subject is asked to verbally produce a series of integers within a preimposed range of values and the data are recorded by a second person. The series are subsequently analyzed by different mathematical procedures, which aim to distinguish the mental data from random series produced by the computer. In a strict sense the latter represent pseudorandom data, as the computer generation is in fact algorithmic. However they satisfy the characteristic for random series.

Experiment A: The first experiments consisted of series of 200 data with integers ranging in the [0, 1, . . . 9] interval. The subject, in sitting position, was allowed for a while to relax in a quiet room. Then it was asked to produce verbally a series of integers at regular time intervals of about one second. This type of experiment was done with many subjects such as university students and gymnasium children. No special reasons led to the choice of integers as objects of the mental "picking up". However it was considered that number ten is something odd as it is represented by two successive symbols and therefore it was excluded from the experiment. It was preferred to include in the experiment the first nine integers and zero as all are represented by a single symbol and therefore the subject of choice is a relatively homogeneous range of items.

Experiment B: The subjects have been asked to mentally produce longer series of events consisting of 512 or even 1024 data within the same range of values [0, 1,. . . . 9]. This was more convenient from a statistical point of view but at the same time produced some concern on the psychological state of the subject. Prolonged and monotonous dictating of the numbers produced sleepiness or possibly slight hypnosis. At this stage of investigation, it was not possible to decide which state was involved and whether they affected the outcome of the experiment.

Experiment C: The range of "random" choice was extended to larger intervals such as [0-20] but also to 1000 values between [0,1, 2,. . . . 999]. The "random" choice was performed either mentally or visually. To our surprise the outcome of the experiment was entirely different compared to other types of experiments.

The data have been subjected to various types of analysis: Fast Fourier Transform, data distribution, return maps and Shannon information entropy.

The presentation of the data in the next sections is done according to the three different characteristics of the series which resulted from spectral analysis: 1) noisy periodic series, 2) red noisy series represented by $1/f^a$ spectra and, 3) white noise series which represent quasi-random data.

3. Results

3. 1 Noisy periodic series. The most numerous experiments belong to category A. They have systematically produced results of the kind shown in fig. 1. A high level of noise characterizes the spectrum but an average broad maximum centered at about 0.15Hz can be easily identified. This corresponds to the repetition of an event after occurrence of about six to seven other different events on average. However the broadness of the maximum suggests that such a repetition may vary within several events

limits. It was an important revelation that such an average figure is equivalent to the so-called "magic number" of the short memory. This represents the maximum average number of independent events, which can be dealt by the brain. The short memory or the work memory cannot go beyond this figure, at least on average.

3. 2 Correlated noise

The C type of experiment produced time series, which have a $1/f^a$ type of spectrum (fig. 2). Such a type of power law spectrum is known to represent a fractal dynamics. This is revealed by the linear fit of the amplitude spectrum represented on a double logarithmic scale (fig. 3). The slope of the fitting line is -0. 36. The slope is double for the corresponding power law spectrum, therefore we have a $1/f^{0.72}$ type of spectrum. Such a spectrum is also termed as a red noise spectrum as the power increases toward lower frequencies.

3. 3 White noise

The spectrum of such a series of events is illustrated in fig. 4. It has been rarely noticed for some series produced in conditions B. The fitting line of the spectrum as represented on a double logarithmic plot has a slope of -0. 089 which is clearly a zero slope. Such a value is suggesting that we deal with a white spectrum, which corresponds to a random series of events. Figure 5 illustrates the spectrum for a random series produced by the computer. The slope of the linear fit is -0. 0584 which is also close to zero as it should be for a random series. Further, the return maps $x_{i+1}=f(x_i)$, of the two kind of series are shown in fig. 6. They show two important facts: first, the mental series do not have any particular location of the trajectories, i. e. no chaotic attractor is possibly involved and second, the mental and random series have qualitative common features. A particular feature is the presence of rectangular trajectories. These are equivalent to a repetition of events in the series. The repetition of a number is equivalent to a horizontal trajectory, followed by a vertically one, on the return map. For mind generated time series, such trajectories are very rarely observed as the "algorithm" of producing randomness is generally thought by most of the subjects to involve, at contrary, total lack of successive repetition of the events. Series of the type shown in fig. 1 lack such type of succession of events. On the other hand randomness does not exclude occasional repetition of events. We further found that in a few isolated cases, subjects produced such type of series, which included occasional repetition of events. These proved to have white spectra, and obviously qualitative similar return maps with the random series, as shown in fig. 6.

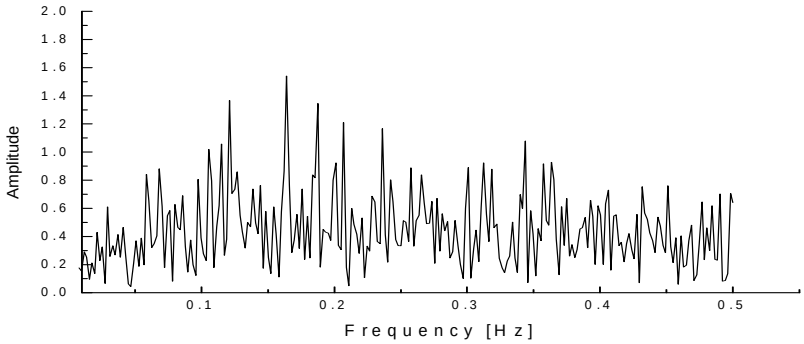

Fig.1. Fourier transform of a series consisting of 512 data produced as a mentally "random" series; numbers fall within the [1-20] range. It can be noticed that a maximum occurs around 0.16 Hz frequency which is equivalent to a periodic repetition of about 6 items.

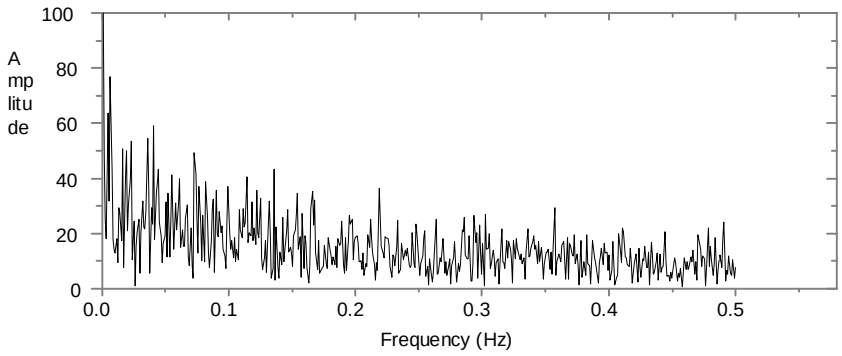

Fig. 2. Spectrum of a mental series of data with values ranging within the [1-1000] interval. It can be noticed the increasing amplitude at lower frequencies which is a feature of a $1/f^a$ type of spectrum (f is frequency) or correlated noise, colored noise or red noise.

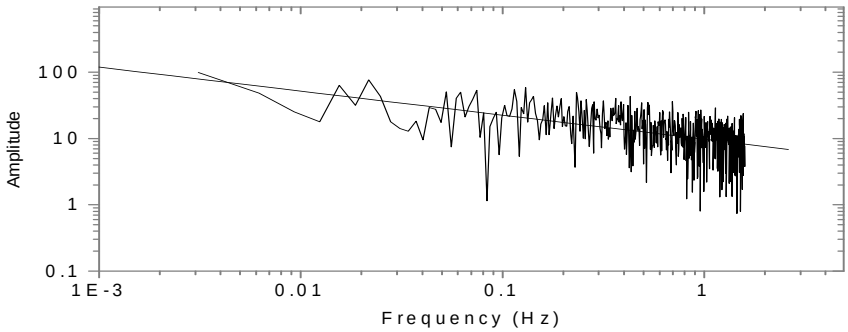

Fig.3. Double logarithmic plot of the spectrum in fig. 2. The linear fit of the spectrum reveals a fractal type of dynamics with no characteristic time of the process. The slope of the fitting line gives the power law index of the power spectrum. In our case the spectrum is for amplitude, and the slope equals -0.36.

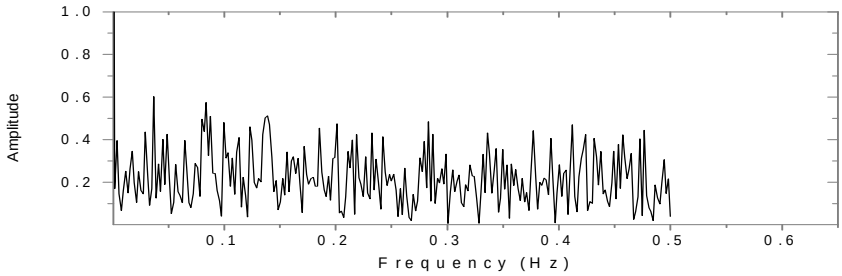

Fig. 4. Spectrum of a mentally produced series of data based on the [1-10] range of values. It shows that there are no preferential frequencies, a fact, which is similar to random series. The slope of the fitting line of the double logarithmic plot is -0.089 which is within very close limits to fig.5 for a random series.

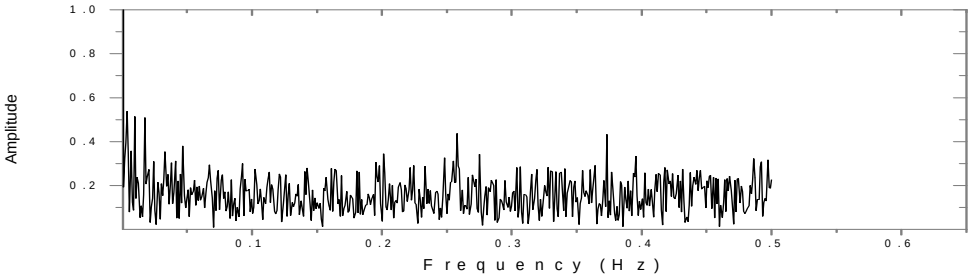

Fig. 5. Spectrum of a random series: the slope of the fitting line of the double logarithmic plot is -0.0584.

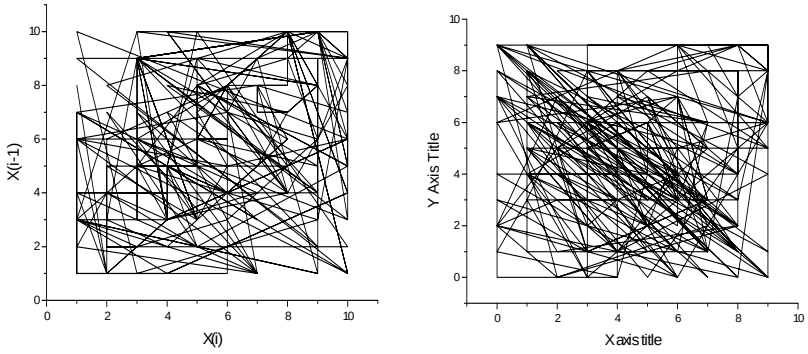

Fig.6. Phase diagrams of the first 200 of data of the series whose spectra are shown in fig.4 and 5. (Left: mental series and right: random data). They show that that the two different series have common features, mainly rectangular trajectories.

At this stage of investigation we should clarify whether knowing of the "correct algorithm" (i. e. producing events according to a non-repetition rule mixed with occasional repetition) can automatically produce randomness. Consequently the series of mental data which produced the results shown in fig. 4 and 6 respectively have been subsequently subjected to a change such as to randomly substitute the repetition of a

number with a different one. This produced a series with non-repetitive values. The outcome was possibly expected to be equivalent to figure 1, i. e. a noisy periodic spectrum. However to the greatest surprise it did not so. The actual spectrum is shown in fig. 7, which is practically a white spectrum. The slope of the fitting line of the spectrum in a double logarithmic plot was -0. 022 which is in the range of the slopes for spectra shown in fig. 4 and 5.

Further, the value of the standard deviation, SD was 2. 865 for the series of data corresponding to fig. 7.

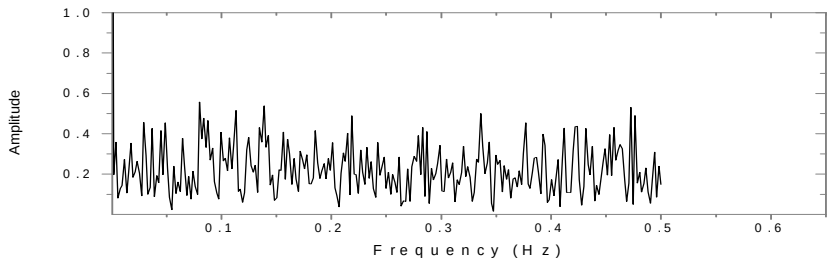

Fig.7. Spectrum of a modified series of data, which produced fig.4: Repetitive values in the original series have been randomly replaced with different values such as to result in a series with non-repetitive data. The outcome of this modification persisted in a white spectrum.

This is much the same as for the series having the spectrum shown in fig. 4 where SD=2. 8733. Therefore the two series show practically similar magnitude of fluctuation.

Despite of the fact that the appearance of the spectra in fig. 4,5 and 7 is that of a white spectrum, slight differences can still be noticed between mental and computer random series. Both mental series (fig. 4 and fig. 7) show somewhat broader peaks than the random series (fig. 5) and correspondingly higher amplitude. These is why we can only possibly label the result as being a quasi-random series and further analysis of data should be carried out in order to characterize such series.

3. 4 Analysis of the data in terms of Shannon informational entropy

Let as suppose that in an experiment there are R_0 different results that are possible and equally probable. The larger R_0, the greater the uncertainty before receiving the message and the quantity of information

after receiving the message will be greater. Therefore we could proceed as follows: at the beginning we have no information, $I_0=0$, and R_0 results are equally probable. Finally, we have $I_1\neq 0$ and $R_1=1$, only one result. So, we could introduce a measure of quantity of information, I, which will be connected with R_0. In the theory of information I is summed for independent events and it is showed that this requirement is satisfied only if:

$$I = k\ln R_0$$

where k is a convenient constant. If the information content is evaluated in bites therefore, we obtain:

$$I=\log_2 R_0$$

Let as suppose now that the message is transmitted by means of an alphabet with two symbols. Let be N the length of the message, and N_1, N_2 numbers of apparition of symbols "1", respectively "2". In this conditions:

$$N = N_1 + N_2$$

and the total number of occurrences is:

$$R = \frac{N!}{N_1!N_2!} \text{ Then:}$$

$$I = k\ln R = k\left[\ln N! - \ln N_1! - \ln N_2!\right]$$

This expression is transformed, by using Stirling's formula, in:

$$I = kN\left[\frac{N_1}{N}\ln\frac{N_1}{N} + \frac{N_2}{N}\ln\frac{N_2}{N}\right]$$

Next we introduce the probability of apparition of each symbol:

$$p_i = \frac{N_i}{N},\ i = \overline{1,2}$$

We obtain for i=I/N, the expression:

$$i = k\left[p_1\ln p_1 + p_2\ln p_2\right]$$

where i is the averaged quantity of information for each symbol from the message.

For a message transmitted by means of an alphabet with n symbols, the relations above can be generalized:

$$R = \frac{N!}{\prod_{j=1}^{n} N_j!}$$

$$i = k\sum_{j=1}^{n} p_j \ln p_j \ - Shannon's\ formula$$

The value of i calculated with the Shannon's formula give information only about the frequencies of apparition of single symbols, with no indication on their succession. To consider this problem too, we have to look at the way of emergence of successive events. Consider the same alphabet with n symbols, by means of which the message is transmitted. Let us suppose that the symbol "l" appears N_l times, followed by different symbols "k", by N_{kl} times. Consequently:

$$N_l = \sum_{k=1}^{n} N_{kl}$$

These symbols can possibly be arranged in:

$$R_l = \frac{N_l!}{\prod_{k=1}^{n} N_{kl}!}$$

different ways. Supposing that the arrangement of symbols for "m" is independent from that for "l", we can say that the number of different arrangements is:

$$R_2 = \prod_{l=1}^{n} R_l = \prod_{l=1}^{n} \frac{N_l!}{\prod_{k=1}^{n} N_{kl}!}$$

This formula is the most convenient for data processing in our experiment, taking account that:

$$i_2 = \frac{\log_2 R_2}{\sum_{l=1}^{n} N_l}$$

For the processing of the series of data the time series are embedded with a given embedding step (T). Each event is now considered as a bidimensional vector $x_i \rightarrow (x_i, x_{i+T})$. The number of apparition for each vector is calculated (N_{kl} values) for a given embedding step. Then N_l is evaluated as the sum of N_{kl} values for all the possible values of the index k. The averaged quantity of information transmitted by means of each pair of

events is calculated with the above formula for R_2. The dependence $i_2=f(T)$ is also evaluated. The result for a series, which is characterized by a noisy periodicity, is illustrated in fig. 8 (marked as pseudorandom).

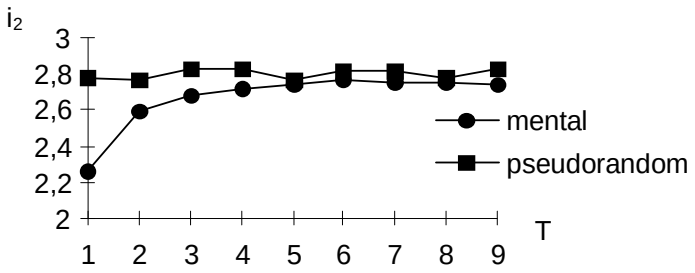

Fig. 8. Typical dependence of informational content on the embedding step for mental and random series generated by computer (pseudorandom).

For the computer generated time series only fluctuation (<1%) with respect to an average value of 2,8 bites are observed, while the mind generated time series reveals a monotonous growth which reach the random value asymptotically. Practically it is impossible to make distinction beyond T>6. These results clearly shows that the mind generated data as such are not pure random. At contrary, there is correlation, which decrease the informational entropy of the mind-generated data.

Further we can see that beyond 6-7 steps in the series the correlation becomes very weak and in fact disappears. These results can be simply understood in terms of the role of the short term or working memory in the generation of the series. The general implicit assumption made by subjects about randomness seems to be lack of repetition. However this algorithm is limited by memory which is in turn limited to 6-7 independent objects, also known as the magic number of the short-term memory [6]. We may regard this magic number as representing the limit between stochastic and deterministic processes at the human brain level.

Although these results show that the series of data as such do not have a random character they show that randomness is "embedded" in non-random series. In other words we could produce random series from mental series if embed in the mental series beyond the first six or seven embedding steps. If for example we consider an embedding order of n = 7 than such a series is constructed from the original one by considering for

example the first and the seventh term, the second and the eighth term etc: x_1, x_7, x_2, x_8, . . . x_i, x_{i+n-1}. This is a nice example of how to extract from a mental algorithmic generation of a purposely-random series a non-algorithmic series of data.

4. Discussion

The previous two parts of these series of articles showed that practically all the experiments produced series of events, which represented a highly noisy periodicity (2-3). The periodicity coincides with the magic number of the short-term memory, which is corresponding to about 6-7 independent events, which can be memorized by our brain [6]. The results have been obtained on a large number of subjects over several years of investigation and on subjects of variable age. However in some isolated cases, experiments performed on longer series produced white spectra which can be interpreted at most as a result of a quasi-random series as some short range correlation seem to persist. If the experiment is performed with a wide range of values [0-999] instead of [0-9] the outcome is a colored noise i. e. a $1/f^a$ type of spectrum. Although the mental algorithm is apparently similar ("avoid repetition of values"), the outcome is an increasing long range correlation of the data or in other words the lower the frequency the greater the amplitude or the number of events. This clearly suggests that the mental algorithm is acting in a more complex manner than when dealing with few events. While the latter remains under some control of the short memory, the former proceeds through a complex correlation procedure. This further shows that mind is not simply concentrated on the first integer of the number in the case of dealing with the [0-999] range, in other words is not equivalent to the experiment with a reduced range of events [0-9]. In fact mind seems to be distributed over the wide range of data "preferring" long-range correlation such as to produce higher amplitudes at lower frequencies. Colored noise or $1/f^a$ type of spectra is widely known in Universe in all natural processes.

According to Penrose a significant part of the conscious activity of the brain proceeds according to rules which cannot be described by any algorithm. This is contrary to the common belief, which assumes that the conscious activity involves perfect logical reasoning and therefore it can be described by algorithms. Penrose's idea has a connection with Gödel's theorem. It means that we can never produce a truth by using an algorithmic method. It is necessary to have an exterior possibility to decide whether an algorithm is correct or not. Such a capacity is the distinct sign of consciousness (4). Let us imagine a computer program. It is obviously that it cannot appear as a result of the natural selection. It is in fact a product of the human consciousness. Further the mathematical reasoning is non-

algorithmic but "there is no suggestion here that there is anything special about mathematical as opposed to any other kind of understanding. The conclusion is that whatever brain activity is responsible for consciousness… it must depend upon a physics that lies beyond computational simulation" (5).

Consciousness is, almost certainly, a property of physical brain (7). The experimental physiological data have been analyzed in terms of two different ways: either the consciousness is the result of effects at the neural network level, or it emerges from quantum mechanisms that appear at subneural level (8-9).

In the first context this is a result of the fact that the analysis of neuronal tissues revealed chaotic, and therefore deterministic character of the electrophysiological signals (10-12). At the same time chaos appear to be a very attractive concept in psychology (13). This fact represents a basically algorithmic aspect of the psyche. Although there are great difficulties to predict the human behavior (13), on the other hand, the human behavior is consistent with a complete determinism. From this point of view, a sequence of actions do not represent "chance" but a deterministic behavior whose features could be evaluated with the chaos theory.

In the second context, human thought is considered to be, at least in some special situations, non-algorithmic. At present, the only non-algorithmic processes known in the Universe are a few random phenomena. However, Penrose considers that pure chance does not represent itself a source for the non-algorithmic character of thought. What kind of actions could be non-computational? According to Penrose "it is hard to see what advantage to a system there might be in having a genuinely *random* input, as opposed to a merely *pseudo-random* one that can be generated entirely computationally (5). This is because the differences between random and pseudorandom would seem to be of no real relevance to the issues of artificial intelligence. In fact Penrose brings strong arguments that pure randomness does nothing useful for us and it would be better to stay with the pseudorandomness of chaotic behavior which is computational.

So, at least in some situations, human thought is based on principles that are now across of current physical understanding, but not out of any scientifically understanding. According to Penrose (5), it is possible that subsequent theories could include non-algorithmic processes, (but not randomness), probably exemplified by physical structures seemingly with quasicrystals. .

REFERENCES

1. S. Pincus, B. H. Singer, Proc. Natl. Acad. Sci. USA, *93,* 2083, (1996).
2. V. V. Morariu, S. I. Morariu, Romanian J. Biophys. , *5*,1,(1995).
3. A. Negreanu-Maior, V. V. Morariu, Romanian J. Biophys. (in print).
4. R. Penrose, The Emperor's New Mind. Concerning Computers, Minds, and the Laws of Physics, Oxford University Press, 1989.
5. R. Penrose, Shadows of the mind: A search for the missing science of consciousness,Oxford University Press, 1994.
6. K. H. Norwich, Information, Sensation, and Perception, Academic Press, San Diego, New York, Boston, 1993, pp 247.
7. R. Grush, P. Churchland, J. Consc. Studies *2*,10 (1995).
8. S. R. Hameroff, J. Consc. Studies. *1,* 98 (1994).
9. S. R. Hameroff, R. Penrose, in Toward a science of consciousness: contribution from the 1994 Tucson conference eds. S. R. Hameroff, A. Kaszniak and A. Scott (Cambridge,MA. MIT Press,1996).
10. T. Chang, S. J. Schiff, T. Sauer, J. P. Gossard, R. E. Burke, Biophys. J. *67*,671 (1994).
11. S. J. Schiff, K. Jerger, T. Chang, T. Sauer, P. Aitken, Biophys. J. *67*, 684 (1994).
12. D. A. Scott, S. J. Schiff, Biophys. J. 69, 684 (1995).
13. L. M. Ward, R. L. West, Psychological Science,5, 232 (1994).